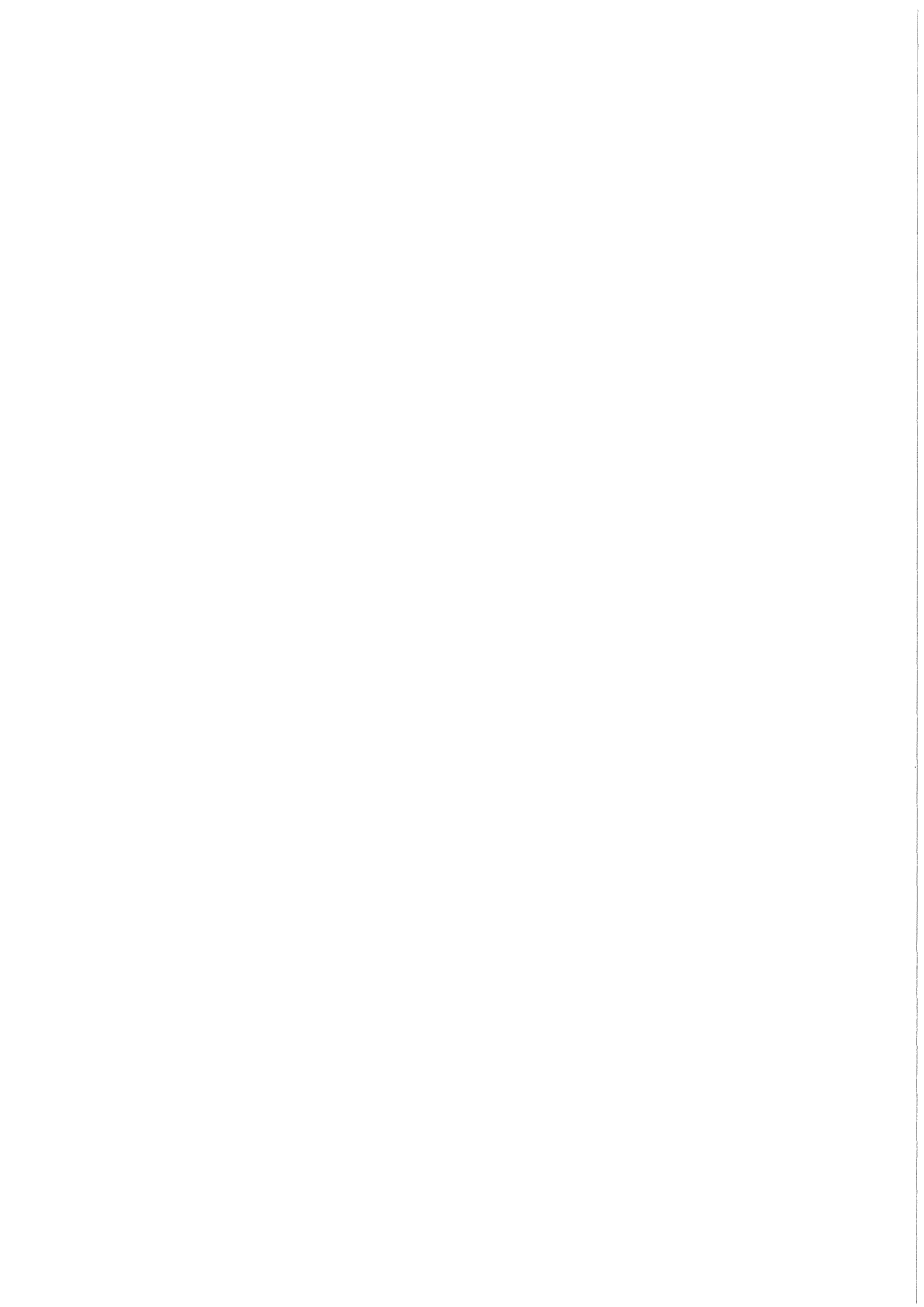


KfK 3557
März 1985

**Temperature Escalation in
PWR Fuel Rod Simulators
due to the
Zircaloy/Steam Reaction:
ESSI-4 to ESSI-11
Test Results Report**

**S. Hagen, H. Kapulla, H. Malauschek,
K. P. Wallenfels, B. J. Buescher**
**Hauptabteilung Ingenieurtechnik
Projekt Nukleare Sicherheit**

Kernforschungszentrum Karlsruhe



KERNFORSCHUNGSZENTRUM KARLSRUHE
HAUPTABTEILUNG INGENIEURTECHNIK
PROJEKT NUKLEARE SICHERHEIT

KfK 3557

Temperature Escalation in PWR Fuel Rod Simulators due to the
Zircaloy/Steam Reaction: ESSI-4 to ESSI-11
Test Results Report

S. Hagen, H. Kapulla, H. Malauschek, K.P. Wallenfels,
B.J. Buescher⁺)

⁺) EG&G Idaho, Inc., P.O. Box 1625, Idaho Falls, Idaho 83415,
presently the NRC Sponsored Delegate to the
Kernforschungszentrum Karlsruhe.

KERNFORSCHUNGSZENTRUM KARLSRUHE GMBH, KARLSRUHE

Als Manuskript vervielfältigt
Für diesen Bericht behalten wir uns alle Rechte vor

Kernforschungszentrum Karlsruhe GmbH
ISSN 0303-4003

Temperatureskalation infolge der Zirkon/Wasserdampf-Reaktion an DWR-Brennstabsimulatoren: Versuche ESSI 4 - ESSI-11.

Kurzfassung

Dieser KfK-Bericht beschreibt die Versuchsführung und die Ergebnisse der Versuchsreihe von Einzelstabexperimenten ESSI 4 - ESSI 11. Das Versuchsziel war die Untersuchung der Temperatureskalation infolge der Zirkon/Wasserdampf-Reaktion. Als Parameter wurde die anfängliche Aufheizrate, die Dicke der Keramikfaser-Isolierung und die Spaltbreite zwischen Dampf-führungsrohr und Isolation variiert. Diese Versuche sind Bestandteil des CORA-Out-of-Pile Programmes und werden im Rahmen des PNS Programmes zur Untersuchung schwerer Kernschäden durch-geführt.

Der Brennstabsimulator bestand aus einem zentralen Wolframheizer, den UO₂-Ringpellets und dem Zirkaloy Hüllrohr. Das den Simulator umgebende Dampf-führungsrohr bestand ebenfalls aus Zirkaloy und war wiederum mit einer Keramikfaser-Isolationsschicht umgeben. Am unteren Ende des Stabes wurde ca. 20 g/min Dampf eingespeist. In allen Versuchen konnte eine Temperatur-escalation beobachtet werden. Hierbei wurde aber in keinem Experiment eine Temperatur von 2200 °C überschritten. Die Eskalation begann im oberen Bereich des Brennstabsimulators und pflanzte sich nach unten fort, entgegengesetzt zur Richtung des Dampf-flusses. Die Beschränkung der maximalen Temperatur wird durch inhärente Prozesse hervorgerufen. Für anfänglich steile Temperaturanstiege hat das Abfließen des geschmolzenen Zirkaloy aus der Reaktionszone in kalte Bereiche eine beschränkende Wirkung. Für anfänglich langsame Temperaturanstiegsraten spielt die sich ausbildende Oxidschicht eine Rolle.

Die Versuche mit dünnem Isolationsmantel zeigen eine Verringerung der Eskalation. Das Fehlen eines Spaltes zwischen Dampfleitungsrohr und Isolation bewirkt eine deutlich schnellere Eskalation.

Die Nachuntersuchung der Brennstabsimulatoren zeigt für langsame Aufheizraten, eine nahezu vollständige Oxidation. Dadurch wird eine Wechselwirkung zwischen Hülle und Pellet weitgehend vermieden. Bei schnellen Aufheizraten dagegen kann nur eine dünne Schicht der Hülle oxidieren. Das beim Erreichen seiner Schmelztemperatur flüssige Zirkaloy löst weite Bereiche des Pellets auf. Es kommt zum Abfließen der Schmelze.

Summary

This report describes the test conduct and results of a series of single rod tests, ESSI 4 - ESSI 11. The test objective was the investigation of temperature escalation of zircaloy clad fuel rods. Tests ESSI 4 - ESSI 8 had the initial heatup rate as main parameter. The influence of the insulation thickness and the gap between insulation and shroud was investigated in tests ESSI 9 - ESSI 11. The investigation of the temperature escalation is part of the CORA out-of-pile experiments performed within the framework of the PNS Severe Fuel Damage Program.

The experimental arrangement consisted of a fuel rod simulator (central tungsten heater, UO₂ ring pellets and zircaloy cladding), a zircaloy shroud and the fiber ceramic insulation. A steam flow of ca. 20 g/min was introduced at the lower end of the bundle.

A temperature escalation was observed in every test. The maximum cladding surface temperature in the single rod tests never exceeded 2200 °C. The escalation began in the upper region of the rods and moved down the rods, opposite to the direction of steam flow. For fast initial heatup rates, the runoff of molten zircaloy was a limiting process for the escalation. For slow heatup rates, the formation of a protective oxide layer reduced the reaction rate.

The test with less insulation thickness showed a reduction of the escalation. A stronger influence was found for the gap between shroud and insulation. This is caused by convection heat losses to the steam circulating in this gap by natural convection. Removal of the gap between shroud and insulation in essentially the same experimental arrangement produced a faster escalation.

The posttest appearance of the fuel rod simulators showed that, at slow heatup rates oxidation of the cladding was complete, and the fuel rod was relatively intact. Conversely, at fast heatup rates, relatively little cladding oxidation with extensive dissolution of the UO₂ pellets and runoff of molten cladding was observed.

Contents

	Page
Introduction	1
Experiment Configuration	2
Test Conduct	4
Test Rod Temperatures	6
Shroud Temperatures	8
Tests with Increasing Initial Heatup Rates	8
Repeated Heatup Test ESSI-4/5	11
Tests with 6 mm and 12 mm Insulation	13
Post Test Examination	15
Conclusions	18
Acknowledgements	19
Literature	20
List of Figures	21

Introduction

As part of the Severe Fuel Damage Programm /1/ within the German Nuclear Safety Project, a series of out-of-pile severe fuel damage experiments using electrically heated fuel rod simulators are being conducted at the Kernforschungszentrum Karlsruhe. These tests are being performed to investigate the mechanisms causing damage to PWR fuel rods at temperatures of up to 2200 °C. The experiments directly complement the internationally conducted program of integral in-reactor bundle tests.

The objective of the out-of-pile test series is to obtain data for the following 6 major areas:

- dissolution of UO₂ by liquid Zircaloy competing with cladding oxidation.
- fragmentation of fuel rods by embrittlement due to oxygen uptake.
- influence of spacers, absorber materials and control rod guide tubes on the fuel element behaviour.
- influence of the zircaloy-steam reaction on temperature escalation.
- behaviour of liquified phases in the fuel rod bundle and their interaction with steam.
- out-of-pile reference tests for the internationally sponsored inpile test program.

The strong influence of different boundary conditions on fuel element behaviour requires a realistic simulation of these conditions in the experiments. To do this, the CORA facility is being built at the Hauptabteilung Ingenieurtechnik. In this facility fuel rod internal pressures and system pressures as well as quenching can be simulated. CORA will be ready for operation in 1985. In the meantime, experiments are being run in the existing NIELS facility for that part of the program which does not need pressure or quenching simulation.

The test program was begun with a series of single rod and bundle tests. These tests were made to investigate the temperature escalation which may occur because of the exothermal zirconium/steam reaction. This report describes the single rod tests, ESSI-4 to ESSI-11.

The introductory tests, ESSI 1-3, are described in /2/ and the bundle tests in /3 - 5/. A combined description of single rod and bundle tests is given in /6/.

The test program was started with experiments on escalation behavior for the following reasons:

1. A principal parameter for SFD fuel rod behavior is the degree of oxidation. The amount of dissolution of UO_2 by zircaloy on one hand, and the fragmentation of the fuel rod on the other hand, depend decisively on the oxidation. The degree of oxidation depends on the temperature rise rate, which may be dominated by the escalation.
2. In-reactor bundle experiments on Severe Fuel Damage are now being conducted by EG&G in the Power Burst Facility at the Idaho National Engineering Laboratory. In these tests, a 32 rod bundle (a 6x6 array without the corner rods) surrounded by a zircaloy shroud is heated in a steam atmosphere. Preliminary temperature calculations /7/, which did not take into account any limiting effects (e.g. zircaloy runoff) had predicted temperature escalation to over 3000 °C. The out-of-pile experiments tested the escalation behaviour before the in-reactor experiments were performed.

Experiment Configuration

The experiment configurations for tests ESSI-4 to ESSI-11 are shown in figures 1-4. The tests are conducted in the NIELS facility with electrically heated fuel rod simulators inside of a zircaloy flow shroud. The fuel rod simulators are constructed using zircaloy cladding and annular pellets which are as close as possible to German PWR fuel rod dimensions. The simulators contain a tungsten heater element to provide electrical heating for the tests.

A zircaloy flow shroud is installed around the test rod simulator to better simulate the effect of the surrounding rods which would be present in a PWR fuel bundle. To minimize heat losses, the test rod and shroud assemblies are insulated with ceramic fiber insulation. The nominal design parameters for the fuel rod simulators, the shroud and the insulation are given in Table 1.

For tests ESSI-4 through ESSI-8, the total insulation thickness is 101.6 mm (Fig. 41). The insulation is fabricated in two layers, an inside layer of ZrO_2 fiberboard (25.4 mm thick), and an outer layer of Al_2O_3/SiO_2 fiberboard (76.2 mm thick). The ceramic fiber material has a density of only about 8% T.D. making it a very effective insulator. The zirconia fiberboard has a conductivity of only 0.24 W/m-K at 1650 °C and the alumina-silica fiberboard has a conductivity of 0.2 W/m-K at 1100 °C.

ESSI-9 is insulated by a cylinder of 12.7 thick ZrO_2 machined from zirconia fiberboard (Fig. 60). In the tests ESSI-4 to ESSI-9 there is a gap between the insulation and the zircaloy flow shroud. This results in a direct heat loss from the flow shroud to the surrounding atmosphere by natural convection. For tests ESSI-10 and ESSI-11, an insulating blanket of zirconia felt is wrapped directly onto the zircaloy flow shroud (Fig. 62). Consequently, for these last two tests, there is no gap between the insulator and the flow shroud, eliminating the direct heat loss from the shroud to the outer atmosphere.

During the tests, steam is fed into the test rod and shroud assembly by a double tube manifold as shown in figures 1,3 and 4. An even delivery of steam into the test assembly is assured by the four holes in the double tube manifold.

The primary temperature measurement of the simulator rods and the zircaloy shroud is made using two color pyrometry. The pyrometers were used to measure the temperature of the outer surface of the test rod cladding and the temperature of the outside wall of the flow shroud. The surface temperature of the test rod is measured at an axial position 104 mm down from the upper end of the shroud. The temperature of the shroud is measured at two axial positions, 140 mm and 190 mm from the top of the shroud. For the shroud wall temperature measurements, holes are cut into the insulator so that the pyrometer can view the outer surface of the shroud. For the test rod temperature measurement, a hole is cut through the insulation and the shroud wall so that the cladding surface of the test rod can be seen by the pyrometer.

In addition to the pyrometer measurements, temperatures are also measured near the upper and lower ends of the test rods by means of inconel sheathed NiCrNi thermocouples. Inconel sheathed NiCrNi thermocouples are also used to measure the temperatures in the insulating region 140 mm from the top of the shroud. The location of the thermocouples on the test rods and in the insulation is given in Table 2.

Test Conduct

The single rod tests, ESSI-4 to ESSI-11 are all run in a flowing steam atmosphere. The steam supply for all of these tests is high enough to preclude steam starvation during the transient. The steam flow is set at a constant rate during each of these tests and the pressure in the NIELS facility is controlled by adjusting the outlet flow of steam from the test chamber. The pressure is maintained at about 1 bar for each of these tests. To prevent condensation in the test chamber during the tests, the outer walls of the test chamber were heated to 150 °C before beginning each of the test runs. The general test conditions for tests ESSI-4 to ESSI-11 are given in Table 3.

In all of these tests, the test rods are heated by resistance heating of the tungsten heater rods. The heatup is performed by applying a linear voltage ramp to the heater rods. Once a sufficiently high temperature is reached, the reaction between the zircaloy and steam causes a rapid temperature escalation. Then a constant voltage is maintained until the heating from the metal water reaction has decreased substantially.

The tests ESSI-4 to ESSI-8 investigate the influence of the oxide thickness on the temperature escalation behaviour. In these tests; the oxide layer thickness on the zircaloy is varied by changing the initial heatup rate. Starting with ESSI-4, the initial heatup rate is 0.3 °C/min. The initial heating rate then increases with each succeeding test through test ESSI-8, which has an initial heatup rate of 3.6 °C/min. The different heatup rates are achieved by applying different linear voltage ramps to

the tungsten heaters in the test rods. Figures 5-10 show the linear ramps applied during these tests. These figures also show the current through the test rods, the power and the calculated resistance of the tungsten heaters.

Test ESSI-4/5 is run at a heatup rate which falls between ESSI-4 and ESSI-5. This test investigates directly how strongly the metal water reaction affects the temperature escalation. In this test the same voltage ramp was run two times in steam (the zircaloy was oxidized during the first heatup, therefore the reaction energy is strongly reduced) and then repeated in argon and in an evacuated vessel. Between the heatups the test rod was cooled to 1200 °C, the measuring lower limit of the two color pyrometer. The first heatup in steam shows the escalation peak, the second does not. The heatup in argon and in the empty vessel should give the influence of the test atmosphere. A detailed description of test ESSI-4/5 will be given in a separate KfK-report.

The influence of the insulation on the thermal response of the system is investigated in tests ESSI-9, ESSI-10 and ESSI-11. In test ESSI-9, a 12.7 mm thick cylinder of insulation is used instead of the 100 mm block of insulation used in the earlier tests. In ESSI-10 and ESSI-11, the insulation thickness is only 6.35 mm. In these last two tests however, the insulation is wrapped directly on the zircaloy flow shroud, eliminating heat losses by convection from the outside of the shroud.

Figures 11, 12 and 13 show the power histories for these three tests along with voltage, current and calculated resistance. Tests ESSI-9 and ESSI-10 are both run at the same voltage ramp rate as ESSI-6. This can be seen in figure 14 which compares the voltage and electric current history of test ESSI-9 to ESSI-10 and in figure 15 which shows the same comparison for tests ESSI-10 and ESSI-6. Test ESSI-11 was run at the same nominal heatup rate as ESSI-5. As can be seen in figure 16, the voltage ramp rate of the two tests is quite similar.

Test Rod Temperatures

Temperature measurements on the surface of the test rods and shrouds are given in figures 17 to 26A. In figure 17, the temperatures at 140 mm from the upper end of the shroud are compared for the tests ESSI-4 to ESSI-7. The electric power input for these tests are given as dotted lines for comparison. The increase of power rise rate from ESSI-4 to ESSI-7 causes an increase of the initial temperature rise rate. Figure 18 compares the temperatures on the rod to the temperatures at two elevations on the shroud. The full line and the dashed line are the temperatures on rod and shroud at the same elevations. This comparison shows that the shroud is reasonably well simulating the surrounding rods of a bundle.

Figure 19 and 20 gives the temperatures of ESSI-8 as measured by pyrometry. Figures 21 to 25 show comparisons of ESSI-11 to ESSI-5 and ESSI-10 and ESSI-9 to ESSI-6. Figures 27 to 40 give the temperature measurements with thermocouples for tests ESSI-4 to ESSI-11. They are in part combined with the pyrometer measurements or shown with comparisons to the electric power input.

The influence of the initial heatup rate on the escalation can be seen in figures 17 and 18. They show the fuel rod simulator and shroud surface temperatures for tests ESSI-4 to ESSI-7. These tests and test ESSI-4/5 are made with the same insulation arrangement as is shown in figure 1 and differ only in the ramp rate of the electric power input. The power inputs are shown as dotted lines in figure 17. The power was raised linearly to ca. 5 KW (7.5 KW for ESSI-4) and then kept constant. Test ESSI-4/5 was a multiple heatup of a single rod and will be discussed later.

In all tests an escalation peak was observed. The temperature at which the escalation began increased from ESSI-7 (below 1200 °C) to ESSI-4 (around 1600 °C). Depending upon the initial temperature rise, caused by the different electric power ramps, different oxide layer thicknesses were formed by the time specific temperatures were reached.

Thus higher temperatures were necessary to get the same reaction rate for slower initial heatup rates. The maximum temperature in all tests stayed below 2100 °C, and the highest temperature was reached in test ESSI-6. The observed temperature escalations were much lower than the early predictions of temperature escalation for the PBF inpile tests /5/. The early predictions for 6 x 6 bundles showed temperature escalations to 3300 and 2600 °C for fast (4 °C/sec) and slow (0.5 °C/sec) heatup rates respectively.

The much lower temperatures observed in the single rod tests suggest that there are inherent processes which limit the temperature escalation. By examining the fuel rod simulators and shrouds shown in Figures 42 to 66 it can be seen that molten zircaloy moved into lower regions of tests ESSI-6, 7 and 8. That means the heatup process was limited by the runoff of zircaloy into the cooler region where the reaction slowed and the energy generation rate was reduced. The amount of zircaloy which moved down into a cooler region during test ESSI-7 was much larger than the amount which relocated in the ESSI-6 test. This may be the reason for the lower peak temperature in ESSI-7 which had the same maximum electric power input but a slower heatup rate.

Another possible mechanism limiting the escalation is oxygen availability. Calculations of the oxygen consumption with the MOP program indicate that in ESSI-7 the maximum oxygen was clearly less than 1 mg/cm²-sec for rod and shroud. Assuming a simultaneous escalating length of 10 cm, the oxygen consumption of rod and shroud was less than 7 g H₂O/min compared to a steam input of 20 g/min. The consumption is even less for the tests with slower initial rates of temperature rise than ESSI-7. Therefore, on an integrated basis there was decidedly more steam available than was consumed.

On the other hand hydrogen is produced at the surface of the zircaloy. And the ratio of hydrogen to steam in the neighbourhood of the zircaloy surface is not known. This effect is known as hydrogen blanketing. The much thinner oxide layers which can be seen in broken parts of the cladding in the upper region of rods E7 and E6 indicate that hydrogen blanketing had some influence in these tests.

Again the influence of the hydrogen blanketing would be stronger with a steeper escalation because a faster reaction rate and energy production is accompanied by a higher hydrogen production rate. Thus hydrogen blanketing appears to be an inherent mechanism to reduce the escalation rate.

The final maximum heatup rate is nearly the same for all tests (around 6 °C/sec). Also, the rate of the temperature decrease is similar for the different tests (around 1.2 °C/sec). These tests had the same geometrical arrangement and insulation. Therefore the cooldown with the decrease of the exothermal energy input is determined by the similar heat losses.

Shroud Temperatures

The temperature escalation of the rod is strongly effected by the temperature behaviour of its surroundings. To simulate the behaviour of neighbouring rods, the fuel rod simulator is surrounded by a zircaloy shroud. The temperatures on this shroud at the same height as measured on the rod (dashed line) and 50 mm lower (dotted line) are given in Fig. 18. The temperatures on the shroud are very similar to that of the rod. This demonstrates that this configuration reasonably simulates the surrounding rods.

The temperatures on the shroud 50 mm lower indicate that the escalation at this elevation begins later. This means that the escalation begins in the upper part of the test section and moves down into the lower region. This movement is caused by the axial temperature gradient. The cold steam (120 °C) entering at the bottom and warming up while moving upward influence the axial temperature distribution so that the highest temperatures occur in the upper section.

Tests with Increasing Initial Heatup Rates

Remarks on the temperature thermocouple measurements grouped for the single tests are given in this section and the two following. For test ESSI-4 the temperatures are given in Figures 17, 18, 27 and 28.

Figure 27 shows the electric power applied to the test rod as well as the pyrometer measurement of the zircaloy shroud temperature and the thermocouple temperatures on the inner and outer surfaces of the insulator at 205 mm above lower end of cladding (140 mm from upper end of shroud). In the region of overlapping temperature measurement on shroud and inner surface of insulation, there is only a small temperature difference before the escalation starts. So the thermocouple measurement of the inner surface insulator temperature gives an indication of the course of shroud temperature. The small bump in the temperature between 20 and 25 min occurs during the start of steam input. The temperature at the outer surface does not change during the heatup, indicating the low conductivity of fiber oxide material.

The decrease of the electric power input at the time of the temperature escalation by the exothermal reaction comes from a decrease in the electric current due to an increase in the tungsten resistance. The temperature at the lower end of the cladding, shown in figure 28, does not increase above about 1200 °C. Here the influence of the "cool" steam, entering at the lower end, can be recognized.

The temperatures measured during ESSI-5 are shown in figures 17, 18, 29 and 30. In this test, the applied voltage ramp is steeper than ESSI-4, resulting in a faster heatup.

The results of the thermocouple measurements are given in fig. 29 to 30. In figure 29 at the 205 mm elevation the pyrometer measurement of the shroud temperature is included. One sees only a small difference between the temperature of shroud and the insulation inner surface. The comparison of temperature curve SI and I shows the steep temperature gradient through the inner 12 mm of insulation. The much slower decrease of the temperature 12 mm into the insulation (cooling curve I) compared to the decrease of the fuel rod temperatures in figure 30 shows the delay of temperature changes through the insulation.

In figure 30 the temperatures on the fuel rod at 70 mm from the lower end and 50 mm from the upper end are compared: Up to 800 °C the temperatures are nearly the same, though the temperature at the top end is 20 mm more to the outside. This is probably caused by the steam entering at the lower end.

Above 1000 °C the temperature at the upper end is distinctly higher than at the lower end. This corresponds to the time when the escalation starts in the maximum temperature region and more heat is transported into the upper region. Because of the resulting higher temperature the contribution from the reaction energy is also higher. The strongest increase in the temperature can be seen after 30 min into the test. At this time the temperature at the lower end measurement shows a strong increase.

In figure 17 the strong escalation in test ESSI-5 happens before 30 min into the test. This shows that the escalation starts at the highest axial temperature and moves to the upper and lower end. Fig. 17 shows for ESSI-5 a small decrease after the first escalation and then a second increase. This second increase in the temperature starts, when the escalation at 70 mm had reached its maximum at about 32 minutes into the test. The occurrence of a peak temperature in the lower region indicates there are lower heat losses at the 205 mm elevation due to convection and axial conduction. The same correlation between the escalation in the lower region and a second increase is found in tests ESSI-6 and ESSI-7. In ESSI-4 no escalation occurs in the lower region and there is no second increase in the escalation peak.

The temperature histories at the various measurement locations of test ESSI-6 are shown in figures 17, 18, 26A, 31, 32 and 33. The combination of the inner shroud surface thermocouple and the outer surface temperature (pyrometer) at 205 mm elevation compared to the temperature 12 mm into the insulation (thermocouple) is given in figure 31. We find again that the first two are similar and that in the third one, the temperature response is delayed.

Fig. 32 gives the temperatures at the upper and lower end of the fuel rod. Up to 900 °C the temperatures are nearly the same. Then the upper temperature increases much faster and the upper thermocouple fails at about 17 min. The temperature at the lower end escalates later but also reaches its maximum value at 17 min. At this time the ESSI-6 temperature shown in figure 17 starts to increase again. Figure 33 compares the temperatures on the upper and lower end of the rod to the temperature 12 mm into the insulation. Again here the much slower relative decrease is seen within the insulation.

The temperatures observed in test ESSI-7 are shown in figures 17, 18 and 34. The initial heatup in this test is quite rapid and the onset of temperature escalation occurs at about 1200 °C. The overall thermal response during this test is similar to ESSI-6 except that the peak temperatures measured on the test rod are somewhat lower. The temperatures on the upper and lower end of the rod together with the temperature 12 mm within the insulation are given in figure 34. Here again one sees the temperature increase later at the lower end and at about the time of the second increase in figure 17. In this test the thermocouples of both ends fail. The temperature 12 mm within the insulation was measured with two different thermocouples and nearly the same time temperature history was obtained in both measurements.

Test rod, shroud wall and insulation temperatures seen in test ESSI-8 are shown in figures 19, 20 and 35. The peak temperature reached by the test rod is 1970 °C, with the first peak occurring after 3.5 minutes. Upon reaching the peak temperature, a drop in temperature occurs and then the temperature of the test rod again increases. The temperatures on the upper and lower end of test rod ESSI-8 are given in figure 35. Again here the temperature increase on the lower end only starts after the first maximum at 205 cm is reached. The second maximum at 205 is reached after a temperature increase occurs at the lower end.

Repeated Heatup Test ESSI-4/5

Test ESSI-4/5 was run through repeated heatups to provide a direct comparison of the temperature escalation which occurs in the presence of the metal water reaction to the heatup which occurs due to electrical heating alone. Figures 17 and 18 show the first heatup observed in test ESSI-4/5. The initial heatup rate of ESSI-4/5 falls between tests ESSI-4 and ESSI-5. The temperature escalation in ESSI-4/5 starts at a test rod temperature of about 1650 °C and the temperature escalation reaches a peak temperature of 1970 °C. The initial heatup rate of test ESSI-4/5 is slow enough so that a thick oxide layer is produced prior to reaching the melting point of the zircaloy and the geometry of the test rod and shroud is preserved. This is necessary for reproducing the electrical power, heating rate and heat losses in the second heatup of ESSI-4/5.

A comparison of the two heatups in test ESSI-4/5 is shown in figure 20A. This figure shows the electrical heating, the test rod temperature and the temperature of the flow shroud for each of the two ESSI-4/5 heatups. The time scale shown on this figure is for the first heatup with the second heatup superimposed over the first. The second heatup was run at the same voltage ramp rate and steam flow as the first and, as can be seen in figure 20A, resulted in virtually the same initial heating curve. Between the two heatups, the electric heating of the test rod was reduced until the temperature had dropped to about 1200 °C, which is the lower operating limit of the two color pyrometer.

During the second heatup, there was only electrical heating as the zircaloy cladding and shroud are nearly completely oxidized in the temperature escalation of the first heatup. In the second heatup, the rod surface temperature measured by the pyrometer is initially about 60 °C above the rod temperature at the same power in the first heatup. This may be due to starting the second heatup from test rod temperature of 1200 °C.

The temperature escalation of the test rod begins at about 1600 °C and when compared to the temperatures reached in the second heatup, reaches a peak which is 270 °C higher than the temperature reached at the same power by electrical heating alone. The temperature escalation of the shroud starts at 1460 °C at the 140 mm elevation and the peak temperature in this case is 340 °C higher than the temperature measured in the second test ramp. At the 190 mm elevation the escalation starts a little lower from 1360 °C and the peak temperature reached in the first heatup is 370 °C higher than the temperature reached at a similar point during the second heatup. This behaviour is due to the time temperature history of the particular location and is a consequence of the metal water reaction. When the escalation starts from a lower temperature, there is less initial oxide on the surface of the zircaloy. In this case, the oxidation rate is higher and there is also more unoxidized zircaloy available for the metal water reaction.

Tests with 6 mm and 12 mm Insulation

Tests ESSI-4 through ESSI-8 were run using 101.6 mm of ceramic fiber insulation. This insulation was intended to minimize the radial heat loss from the shroud by radiation heat transfer. Tests ESSI-9, ESSI-10 and ESSI-11 were performed to investigate the influence of the insulation on the temperature escalation.

Test ESSI-9 was run with the same power history and the same steam flow as ESSI-6. The insulation used in this test was a ZrO_2 ceramic fiber cylinder with a wall thickness of 12.7 mm. The test arrangement is shown schematically in figure 3 and a photograph of the test assembly in the insulator is shown in figure 59. Although the configuration was different, a gap was left between the shroud and insulation which allowed a convective heat loss as occurred in the earlier tests.

The electric power and test rod temperatures for both tests ESSI-6 and ESSI-9 are shown in figure 25. As can be seen, the electric power of the two tests is quite similar up to a time of 17.5 minutes into the transient. After 17.5 minutes into the transient the electric power in test ESSI-9 increases relative to ESSI-6.

In both tests, the escalation has a double peak. The escalation in ESSI-9 started later and reached a lower maximum value. This behaviour was presumably caused by the larger heat losses, due to the reduced insulation thickness.

The last two tests of this series, ESSI-10 and ESSI-11, were run with the shroud insulated by only 6 mm of ZrO_2 ceramic fiber insulation. However, in contrast to the earlier tests, the insulation was wrapped directly on the zircaloy flow shroud leaving no gap between the flow shroud and the insulation. A cross sectional view of the test arrangement is shown schematically in figure 4. Figure 62 shows pictures of this test arrangement before and after the test.

Test ESSI-10 was run under the same conditions of inlet steam flow and voltage ramp rate as test ESSI-6. Figure 23 gives a comparison of both the test rod temperature and the test rod electric power for the two tests. The power ramp rate is the same for the two tests but the thermal response is quite different. In ESSI-10 the escalation is much faster and the maximum temperature is reached much earlier. The temperature maximum is about 70 °C less, but one has to take into account that the maximum is reached at only about half the electric power input. In ESSI-10 there is only a single peak.

Figure 24 shows a comparison of both the shroud and test rod temperatures for tests ESSI-6 and ESSI-10. During the temperature escalation in test ESSI-10, the shroud temperature is much closer to the test rod temperature than in test ESSI-6. This apparently comes from the convection heat losses from the flow shroud to the steam in ESSI-6. The low heat capacity and low thermal conductivity of the ZrO₂ fiber ceramic insulation permit a steep thermal gradient to develop in the insulator in ESSI-10 and the elimination of the convective heat loss results in a faster escalation of the shroud temperature.

The last test run in this series is ESSI-11. This test is a repetition of test ESSI-5 but again with the insulation wrapped directly on the flow shroud. The power histories and test rod temperatures for ESSI-5 and ESSI-11 are shown in figure 21. As in the case of ESSI-10, the temperature escalation in test ESSI-11 starts earlier and, at the outset, is significantly steeper than the escalation in ESSI-5. The peak temperature reached in ESSI-11 is about the same as the peak temperature reached in ESSI-5 while the power in ESSI-11 is only 1.3 kW compared to 2.2 kW for test ESSI-5.

Figure 22 shows the test rod temperatures for these two tests, along with the shroud temperatures at two locations. At the beginning of the temperature escalation, the temperature of the shroud is quite close to the test rod temperature, minimizing the radiation heat losses and enhancing the escalation of the test rod. Also ESSI-11, a single peak temperature is observed as in ESSI-10.

Post Test Examination

A post test visual examination was made after each test. Figures 42-45 show the test rod and shroud of ESSI-4. In this test, substantial oxidation occurs during the heatup and major dissolution of the UO_2 is avoided. The geometry of the shroud and test rod is preserved. The deformation of the cladding in the middle region (Fig. 43) seems to be connected with different shrinking of the pellets and oxidized cladding during cool down. Figure 45 shows part of the shroud after dismantling the test. One clearly recognizes the double oxidation from inside and outside of the shroud. This indicates natural convection in the gap between shroud and insulation.

The post test appearance of test ESSI-4/5 is shown in figure 46. In this test, the test rod cladding is seen to be highly oxidized and the test rod and shroud geometry was preserved with the oxide shells almost completely retained. Thus for this test sequence, the repeated heatups that were performed were made with the same geometry.

The post test photographs of ESSI-5 are given in figures 47 and 48. In ESSI-5, the shroud is once again fairly intact, preserved by a thick oxide layer. In the test rod, one can see the formation of liquified fuel material. The details of the test rod are shown in figure 48. In the central region, the test rod shows the formation of a molten zone just beneath the outer surface. Only a thin oxide layer has formed which just retains the molten zircaloy. The oxide layer does not have much mechanical strength and dimpling of the outer surface occurs. This is seen in the center region where the temperature first escalated and the highest temperature was reached. Lower down on the rod the temperature increase is slower, and a thicker oxide layer has formed. The missing cladding broke away after cool down. This is shown by the smooth surface of the refrozen melt which filled the gap between pellet and oxide shell.

The post test photographs of ESSI-6 through ESSI-8 are shown in figures 49 to 59. In these three tests, the heatup rates are faster and there is not sufficient time to form a thick enough oxide layer prior to reaching the melting point of the zircaloy to contain the melt.

As the heatup rate increases, the oxide layer formed before the melting temperature of the zircaloy is reached becomes thinner and thinner. Consequently more of the UO_2 is dissolved by liquid zircaloy in the faster heatups. The same tendency is seen for the shroud. As the heatup rate increases, the oxide layer becomes thinner and more molten material can be seen, refrozen in the lower end of the shroud.

Figure 49 to 51 give pictures from test ESA-6. The post test appearance from 4 different sides of the full length rod and shroud are shown in figure 49. Figure 50 concentrates on the damaged region in the upper part. The details from 3 different elevations are give in figure 51. The left picture shows that only the surface region of the UO_2 pellet is attacked in this test. The zircaloy cladding was only partly oxidized prior to reaching the melting temperature of the zircaloy and the unoxidized zircaloy melted. The melt penetrated into the gaps between the pellets but only a thin surface region of the pellet was dissolved by the liquid zircaloy. The middle picture in figure 51 shows the refrozen melt in the middle axial region. The right picture gives an enlarged view from a lower section of the rod, where the axial layer was thick enough to contain the melt. As in test ESSI-5, the oxidized part of the cladding again broke away.

Figure 52 to 56 gives the post test appearance of test ESSI-7. In this test the fast heatup allowed only minor oxidation before the melting temperature of the zircaloy was reached. This results in nearly complete dissolution of the UO_2 in the hottest region of the fuel rod. Consequently, a significant relocation of molten material can be seen. The same relocation of molten zircaloy can also be seen on the shroud.

Figures 57 to 59 demonstrates the post test appearance of test ESSI-8. This was the test with the fastest heatup and consequently the most dissolution. Figure 58 shows that the UO_2 nearly over the whole length has disappeared. Also on the shroud only a paper like oxide layer was left at the end of the test. Most of the material melted and flowed away.

The post test condition of the ESSI-9 fuel rod simulator and shroud is shown in figure 61. As is evident in the photographs, melting of the zircaloy has occurred with dissolution of the UO_2 and relocation. The amount of material that melted and ran into the lower region is somewhat less than the amount that relocated in test ESSI-6. The distortion of the shroud in this test is also not as severe as in the earlier test. The reason probably is that the initial heating of the test assembly in ESSI-9 is slower than the heating of test ESSI-6, due to the thinner insulation.

Figures 62 to 64 show the post test appearance of the ESSI-10 insulation test rod and flow shroud. The insulation and shroud have retained their initial geometry, except that some melting of the shroud surface has occurred.

ESSI-10 had the same power history as ESSI-6 but the escalation occurred earlier and faster due to the absence of a gap between shroud and insulation. This resulted in a thinner, less stable oxide layer. This is seen in figure 63 which shows a large axial zone of exposed and eroded fuel pellets in the test rod. At the lower end of this zone, one can also see the UO_2 -zircaloy mixture refrozen in the gap between the test rod and the oxidized cladding.

The post test condition of the ESSI-11 fuel rod simulator and shroud is shown in figures 65 and 66. ESSI-11 was heated up with the same electric power increase as ESSI-5. As in the case of ESSI-10 there was no gap between the insulation and the shroud. This resulted in an earlier and faster temperature increase in ESSI-11 compared to ESSI-5 (fig. 21). Consequently a thinner oxide layer developed and the melt, formed inside the oxide layer, penetrated the oxide shell on one side. Also more dissolution of the UO_2 can be seen. If one compares in figure 65 the outer left side picture of the fuel rod simulator (showing melt running down) with the outer right side picture (showing refrozen melt in the gap between pellet and the now missing oxide layer - broken away after cool down -) one can realize, that melt is retained between the pellets and oxidized cladding on one side of the rod, while there is no cladding left on the opposite side of the same rod.

In general, the post test visual examinations show that the damage to the test rods and the flow shrouds becomes more severe as the initial heatup rate is increased and as the radial heat losses are decreased.

With slow initial heatups, a thick oxide layer forms, which delays the onset of escalation to higher temperatures. The thick oxide layer also retains molten material that may form and acts to preserve the initial geometry of the test assembly. As the initial heatup rate is increased and with reduced radial heat losses, the initial oxide layer becomes thinner and the onset of escalation occurs at lower temperatures. Under these conditions, the oxygen content of the molten zircaloy is reduced resulting in a more extensive reaction with the UO₂ pellets. The molten zircaloy is also able to dissolve the thin oxide film which is formed. This is seen in the post test visual examination of the fast initial heatup tests. In these tests melting and relocation of the zircaloy shroud and cladding is observed and substantial dissolution of the UO₂ pellets is also seen.

Conclusions

- In all tests a temperature escalation due to the zircaloy steam reaction was observed.
- The maximum measured surface temperature was limited to about 2200 °C.
- The temperature at which the escalation begins increases with decreasing initial heatup rate.
- For fast initial heatups, run off of molten zircaloy is a limiting process for the escalation. There are indications that hydrogen blanketing may also have a limiting influence on the escalation.
- For slow heatups the formation of a protective oxide layer is a mechanism which reduces the reaction rate.
- The comparison of tests with the same electric power input and different insulation thicknesses and arrangements show that the gap between shroud and insulation has a stronger influence on the heat losses than the insulation thickness. An earlier and faster escalation occurs with no gap between shroud and insulation. This effect is due to heat losses of the shroud to steam moving through the gap by natural convection.

- In these tests, with 120 °C steam entering at the lower end, the escalation started in the upper region and moved towards the lower end.
- The damage to the fuel rods increases with the heatup rate. For slow heatup rates nearly no interaction between the oxidized cladding and the UO₂ was observed. For fast heatup rates the entire annular pellet was dissolved by the molten zircaloy.

Acknowledgements

The authors would like to thank Mr. A. Grünhaghen for the calculations with the MOP-Program and Mr. S. Malang for the delivery of the MOP-Program. We thank Mr. Abliez for the data processing and graph preparation, Mr. Brand for taking photographs and Mrs. Ivanitsch for her careful typing of the manuscript.

Literature

- /1/ A. Fiege
Severe Fuel Damage Investigations of KfK/PNS;
KfK 3431B, Jan. 1983

- /2/ S. Hagen, H. Malauschek, K.P. Wallenfels, S.O. Peck
Temperature Escalation in PWR Fuel Rod Simulators due to the
Zircaloy/Steam Reaction: Tests ESS1 1-3, Test Results Report;
KfK 3507, 1983

- /3/ S. Hagen, H. Malauschek, K.P. Wallenfels, S.O. Peck
Temperature Escalation in PWR Fuel Rod Simulators due to the
Zircaloy/Steam Reaction: Bundle Test ESB1 1, Test Results Report;
KfK 3508, 1983

- /4/ S. Hagen, H. Malauschek, K.P. Wallenfels, B.J. Buescher
Temperature Escalation in PWR Fuel Rod Simulators due to the
Zircaloy/Steam Reaction: Bundle Test ESB1 2A, Test Results Report;
KfK 3509, 1984

- /5/ S. Hagen, S.O. Peck
Out-of-pile Bundle Temperature Escalation under Severe Fuel Damage
Conditions;
KfK 3568, 1983

- /6/ S. Hagen, S.O. Peck
Temperature Escalation of Zircaloy-Clad Fuel Rods and Bundles under
Severe Fuel Damage Conditions;
KfK 3656, 1983

- /7/ B.J. Buescher
"PBF Severe Fuel Damage Test Predictions"
PBF Program Review Group Meeting, Washington, DC, October 1981.

List of Figures

Fig. 01: Sideview of the experimental arrangement and positions of the thermocouples for tests ESSI 4-8.

Fig. 02: Topview of the experimental arrangement and positions of the thermocouples for tests ESSI 4-8.

Fig. 03: Experimental arrangement and positions of the thermocouples for test ESSI 9.

Fig. 04: Experimental arrangement and positions of the thermocouples for tests ESSI 10-11.

Fig. 05: Voltage V , current I , electric power E and resistance R for test ESSI-4.

Fig. 06: Voltage V , current I , electric power E and resistance R for test ESSI-4/5.

Fig. 07: Voltage V , current I , electric power E and resistance R for test ESSI-5.

Fig. 08: Voltage V , current I , electric power E and resistance R for test ESSI-6.

Fig. 09: Voltage V , current I , electric power E and resistance R for test ESSI-7.

Fig. 10: Voltage V , current I , electric power E and resistance R for test ESSI-8.

Fig. 11: Voltage V , current I , electric power E and resistance R for test ESSI-9.

Fig. 12: Voltage V , current I , electric power E and resistance R for test ESSI-10.

- Fig. 13: Voltage V , current I , electric power E and resistance R for test ESSI-11.
- Fig. 14: Comparison of voltage V and current I for tests ESSI 9-10.
- Fig. 15: Comparison of voltage V and current I for tests ESSI 6 + 10.
- Fig. 16: Comparison of voltage V and current I for tests ESSI 5 + 11.
- Fig. 17: Temperatures (—) on rods and electric powers (...) for tests ESSI 4.4/5.5.6.7.
- Fig. 18: Temperatures on rod (—) at 140 mm and on shroud at 140 mm (---) and 190 mm (...) from upper end of shroud for tests ESSI 4.4/5.5.6.7.
- Fig. 19: Temperature (T) on the rod and electric power (E) for test ESSI-8.
- Fig. 20: Temperature on rod (R) at 140 mm and on shroud at 140 mm (S140) and 190 mm (S190) from upper end of shroud for test ESSI-8.
- Fig. 21: Temperatures on rod (—) and electric power (...) for ESSI-11 (6.4 mm insulation no gap) and ESSI-5 (101.6 mm insulation gap).
- Fig. 22: Temperatures on rod (—) at 140 mm and on shroud at 140 mm (---) and 190 mm (...) from upper end of shroud for tests ESSI 5 and 11
- Fig. 23: Temperatures on rod (—) and electric powers (...) for ESSI-10 (6.4 mm insulation no gap) and ESSI-6 (101.6 mm insulation gap).
- Fig. 24: Temperatures on rod (—) at 140 mm and on shroud at 140 mm (---) and 190 mm (...) from upper end of shroud for tests ESSI 6 and 10
- Fig. 25: Temperatures (T) and electric powers (E) for ESSI-9 (12.8 mm insulation) and ESSI-6 (101.6 mm insulation).

- Fig. 26: Temperature on the rod (R) in 140 mm and on the shroud in 140 mm (S4) and 190 mm (S9) from the upper end of the shroud for ESSI-6.
- Fig. 27: Temperatures on the shroud (S), 12 mm within the insulation (I) and on the outer surface (O) of the insulation 205 mm above the lower end of the cladding and electric power (E), ESSI-4.
- Fig. 28: Temperatures on the rod 70 mm above the lower end of the cladding in comparison to electric power (E), ESSI-4.
- Fig. 29: Temperatures on the shroud (S) and on the insulation inner surface (SI), outer surface (SO) and interior (I) (12 mm from the inner surface) at the 205 mm elevation for test ESSI-5.
- Fig. 30: Temperatures on the rod 70 mm above the lower (LO) and 50 mm below the upper (UP) end of the cladding, ESSI-5.
- Fig. 31: Temperatures on the shroud (S) and on the inner surface (SI) and 12 mm within the insulation (I) 205 mm above the lower end of the cladding, ESSI-6.
- Fig. 32: Temperatures on the rod 70 mm above the lower (LO) and 50 mm below the upper (UP) end of the cladding, ESSI-6.
- Fig. 33: Comparison of the rod temperatures at the 70 mm (L) and 297 mm (H) elevations with the temperature in the insulation (I) at 205 mm for ESSI-6.
- Fig. 34: Temperatures on the rod 70 mm above the lower (LO) and 50 mm below the upper (UP) end of the cladding. And 12 mm within (I) and on the outer surface (SO) of the insulation at 205 mm elevation, ESSI-7.
- Fig. 35: Temperatures on the rod 70 mm above the lower (LO) and 50 mm below the upper (UP) end of the cladding. And on the inner surface (SI), 12 mm within (I), and on the outer surface (SO) of the insulation, ESSI-8.

- Fig. 36: Temperatures on the rod 30 mm above the lower (LO) end of the cladding, ESSI-9.
- Fig. 37: Temperatures on the rod 30 mm above the lower (LO) and 30 mm below the upper (UP) end of the cladding, ESSI-10.
- Fig. 38: Temperatures on the rod 30 mm above the lower (LO) and 30 mm below the upper (UP) end of the cladding ESSI-11.
- Fig. 39: Temperatures on the shroud (S) and 2.4 mm (I2) and 4.8 (I4) within the insulation 205 mm above the lower end of the cladding, ESSI-11.
- Fig. 40: Temperature on the shroud (ST) measured with a thermocouple compared to temperatures on the shroud (S) and rod (R) measured with two color pyrometers 205 mm above the lower end of the cladding ESSI-11.
- Fig. 41: Experiment arrangement showing the insulation in place around the shroud and fuel rod simulator.
- Fig. 42: Posttest appearance of the ESSI-4 fuel rod simulator and shroud.
- Fig. 43: Details of the ESSI-4 posttest appearance near the middle of the rod.
- Fig. 44: Details of the ESSI-4 posttest appearance near the top of the rod.
- Fig. 45: Details of the ESSI-4 shroud showing two sided oxidation.
- Fig. 46: Posttest appearance of the ESSI-4/5 fuel rod simulator and shroud
- Fig. 47: Posttest appearance of the ESSI-5 fuel rod simulator and shroud.
- Fig. 48: Details of the ESSI-5 posttest appearance.

Fig. 49: Posttest appearance of the ESSI-6 fuel rod simulator and shroud.

Fig. 50: Details of the ESSI-6 fuel rod simulator and shroud.

Fig. 51: Enlargement of the ESSI-6 fuel rod simulator.

Fig. 52: Posttest appearance of the ESSI-7 fuel rod simulator and shroud.

Fig. 53: Details fo the ESSI-7 fuel rod simulator and shroud.

Fig. 54: Posttest appearance of the ESSI-7 fuel rod simulator after removal of the upper part of the shroud.

Fig. 55: Details of the ESSI-7 fuel rod simulator.

Fig. 56: Enlargement of the ESSI-7 fuel rod simulator and shroud.

Fig. 57: Posttest appearance of the ESSI-8 shroud.

Fig. 58: Posttest appearance of the ESSI-8 fuel rod simulator after dismantling.

Fig. 59: Details fo the ESSI-8 fuel rod simulator and shroud.

Fig. 60: 12 mm fiber ceramic insulation in ESSI-9.

Fig. 61: Posttest appearance of the ESSI-9 fuel rod simulator and shroud.

Fig. 62: ESSI-10 fiber ceramic insulation before and after the test.

Fig. 63: Posttest appearance of the ESSI-10 fuel rod simulator and shroud.

Fig. 64: Details of the ESSI-10 fuel rod simulator and shroud.

Fig. 65: Posttest appearance of the ESSI-11 fuel rod simulator and shroud.

Fig. 66: Details of the ESSI-11 shroud.

Table 1. TEST ASSEMBLY DESIGN CHARACTERISTICS

Parameter	Value
Fuel Rod Simulator	
Length	37.0mm
Tungsten Heater O.D.	6.0mm
Fuel Material	Annular UO_2 pellets
Pellet I.D.	6.1mm
Pellet O.D.	9.2mm
Cladding Material	Zircaloy-4
Cladding I.D.	9.29mm
Cladding O.D.	10.75mm
Shroud	
Material	Zircaloy-4
Shroud I.D.	26.5mm
Wall Thickness	1.0mm
Insulator	
ZrO_2 Thickness (Tests 4-8)	25.4mm
Al_2O_3/SiO_2 Thickness (Tests 4-8)	76.2mm
ZrO_2 Thickness (Test 9)	12.7mm
ZrO_2 Thickness (Tests 10-11)	6.35mm

Table 2. TEST THERMOCOUPLES

TEST	LOCATION ON ROD SIMULATORS		INSULATOR TCs AT 140mm ELEVATION				OTHER
	FROM UPPER END (mm)	FROM LOWER END (mm)	DISTANCE FROM INNER WALL (mm)				
ESSI-4	50	70	12.7	101.6			
ESSI-4/5	22	60	0.0	12.7	25.4		Shroud TCs at Rod TCs elevation
ESSI-5	50	70	0.0	12.7	101.6		
ESSI-6	50	70	0.0	12.7			
ESSI-7	50	70	0.0	10.0	12.7	101.6	
ESSI-8	32	32	0.0	10.0	101.6		
ESSI-9	30	30					
ESSI-10	30	30					
ESSI-11	30	30	2.4	4.8			

Table 3. Test Conditions for Tests ESSI-4 to -11

Test	Initial Heatup Rate (°C/s)	Steam Flow (g/min)	Insulation Thickness (mm)	Flow Shroud/ Insulation Gap	Peak Temperature (°C)
ESSI-4	0.3	21	100	yes	2050
ESSI-4/5	0.5	20	100	yes	1970
ESSI-5	0.8	20	100	yes	1900
ESSI-6	1.1	20	100	yes	2100
ESSI-7	2.3	22	100	yes	1925
ESSI-8	3.6	25	100	yes	1970
ESSI-9	E-6	25	12.5	yes	1950
ESSI-10	E-6	25	6.2	no	2025
ESSI-11	E-5	25	6.2	no	1900

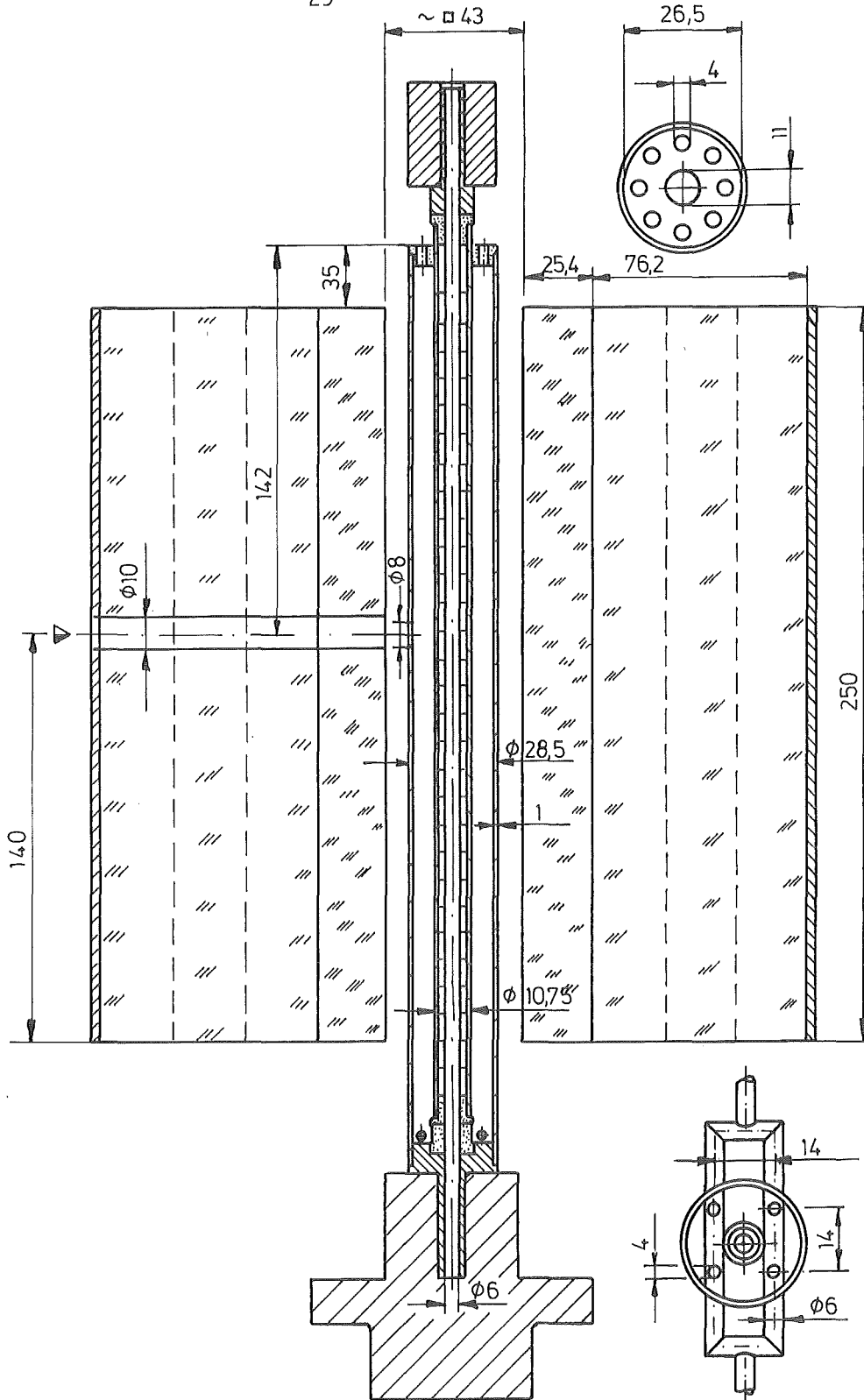


FIG.01: SIDEVIEW OF THE EXPERIMENTAL ARRANGEMENT AND POSITIONS OF THE THERMOCOUPLES FOR TESTS ESSI 4-8

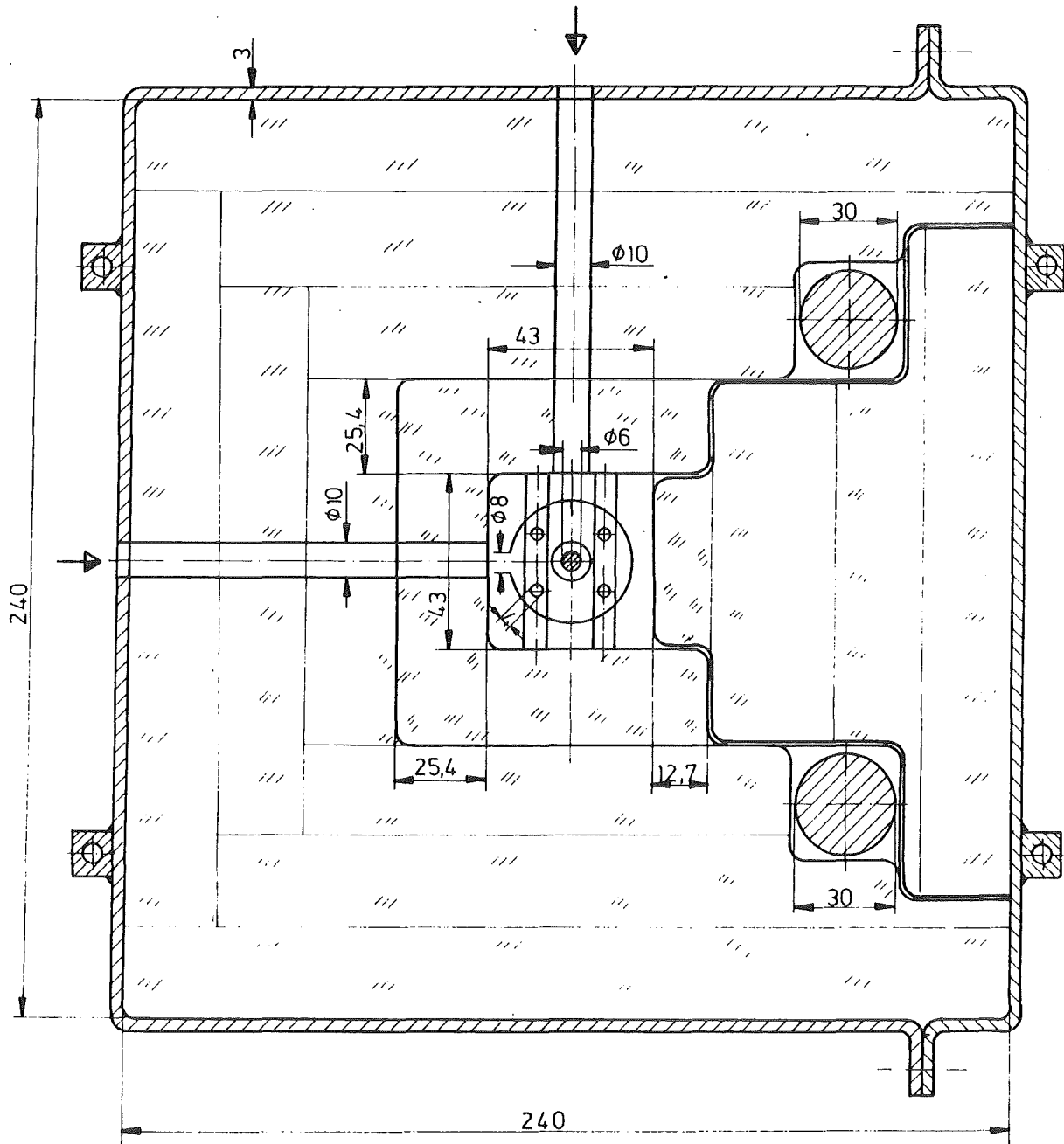


FIG.02: TOPVIEW OF THE EXPERIMENTAL ARRANGEMENT AND POSITIONS OF THE THERMOCOUPLES FOR TESTS ESSI 4-8.

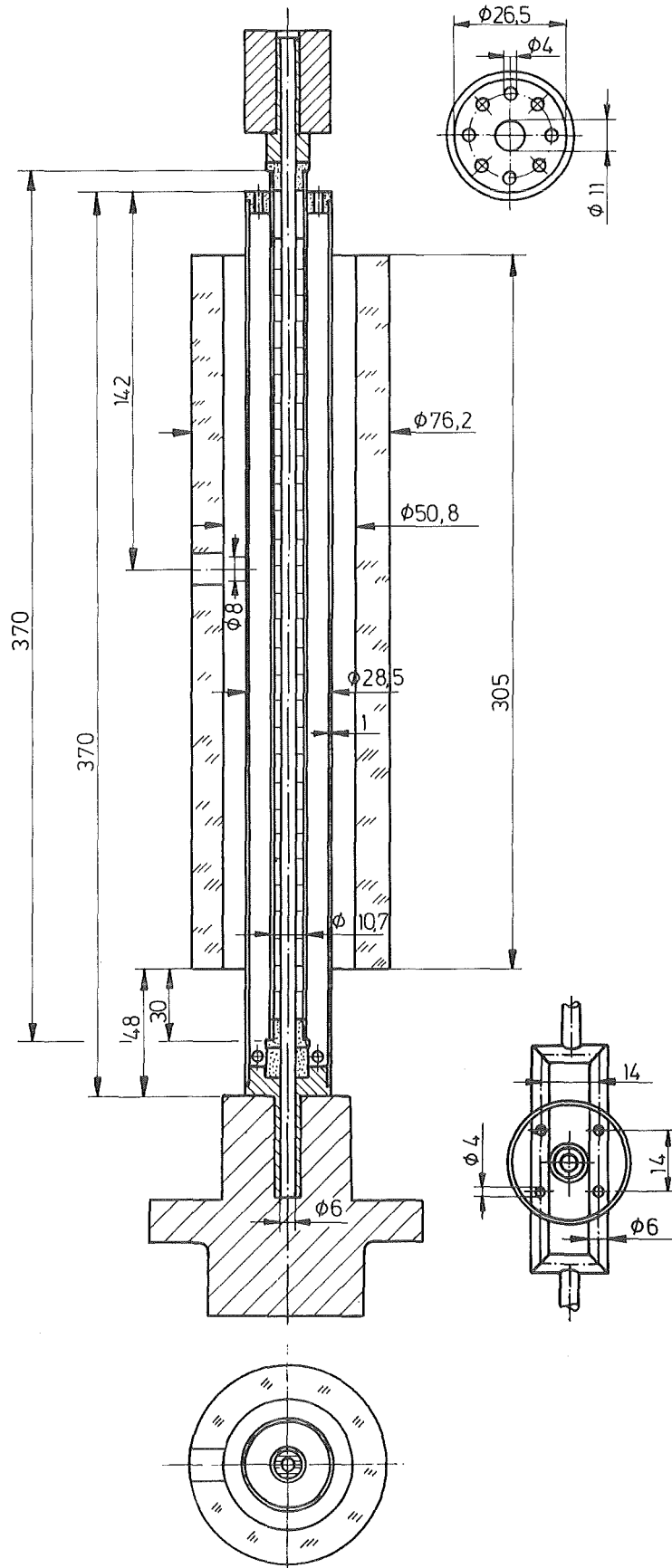


FIG.03: EXPERIMENTAL ARRANGEMENT AND POSITIONS OF THE THERMOCOUPLES FOR TEST ESS1 9

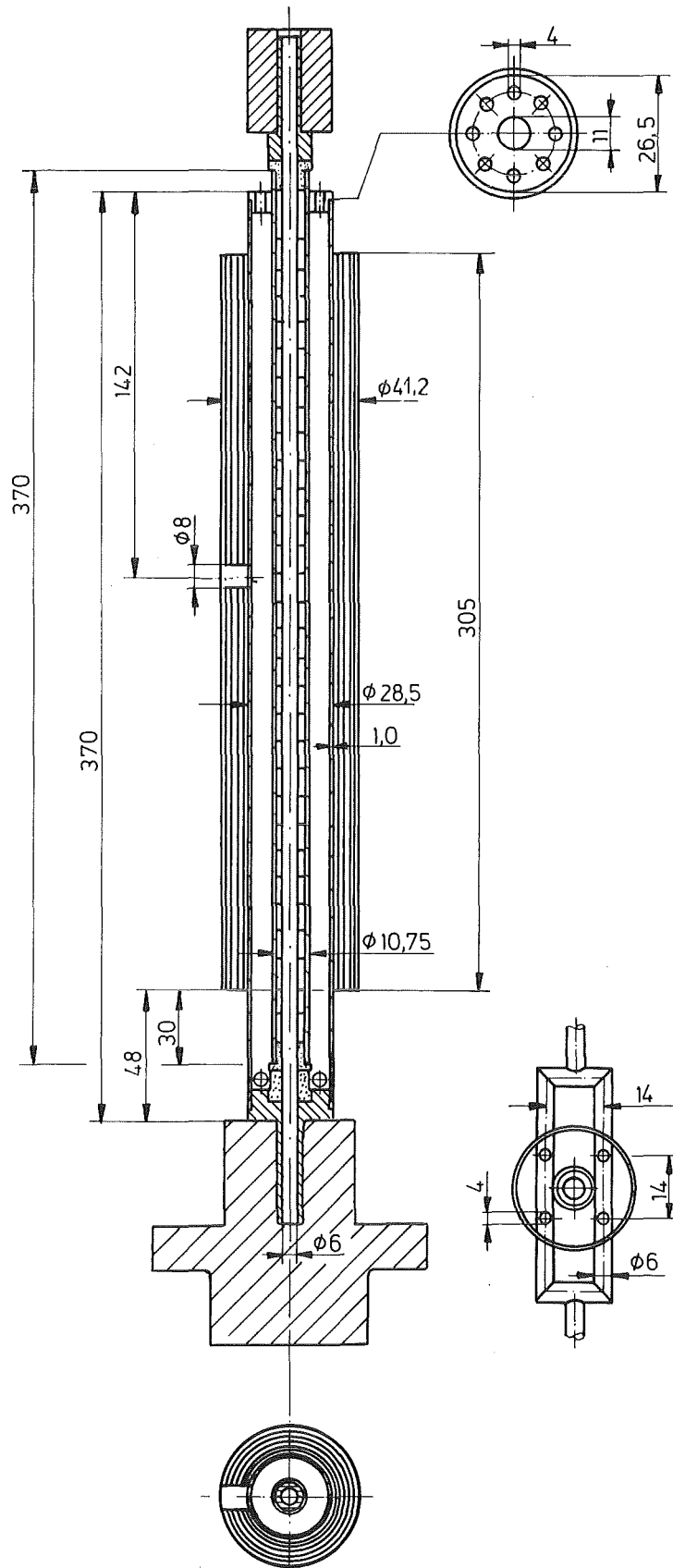


FIG.04: EXPERIMENTAL ARRANGEMENT AND POSITIONS OF THE THERMOCOUPLES FOR TESTS ESSI 10+11

FIG. 5 : VOLTAGE V, CURRENT I, ELECTRIC POWER E AND RESISTANCE R FOR TEST ESS1-4

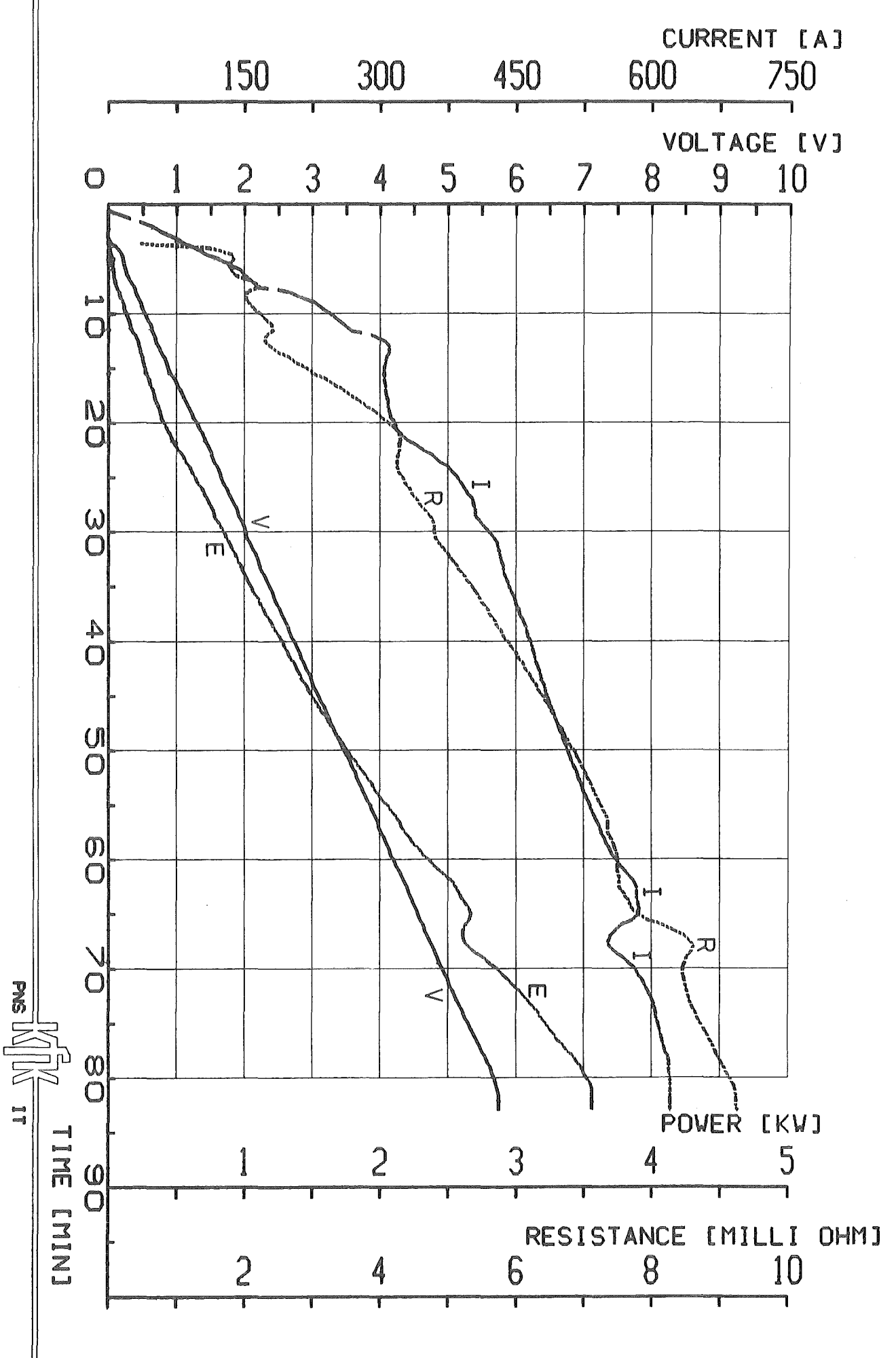



FIG. 06: VOLTAGE V, CURRENT I, ELECTRIC POWER E AND RESISTANCE R FOR TEST ESS1-4/5

PNS

 IT
 TIME [MIN]

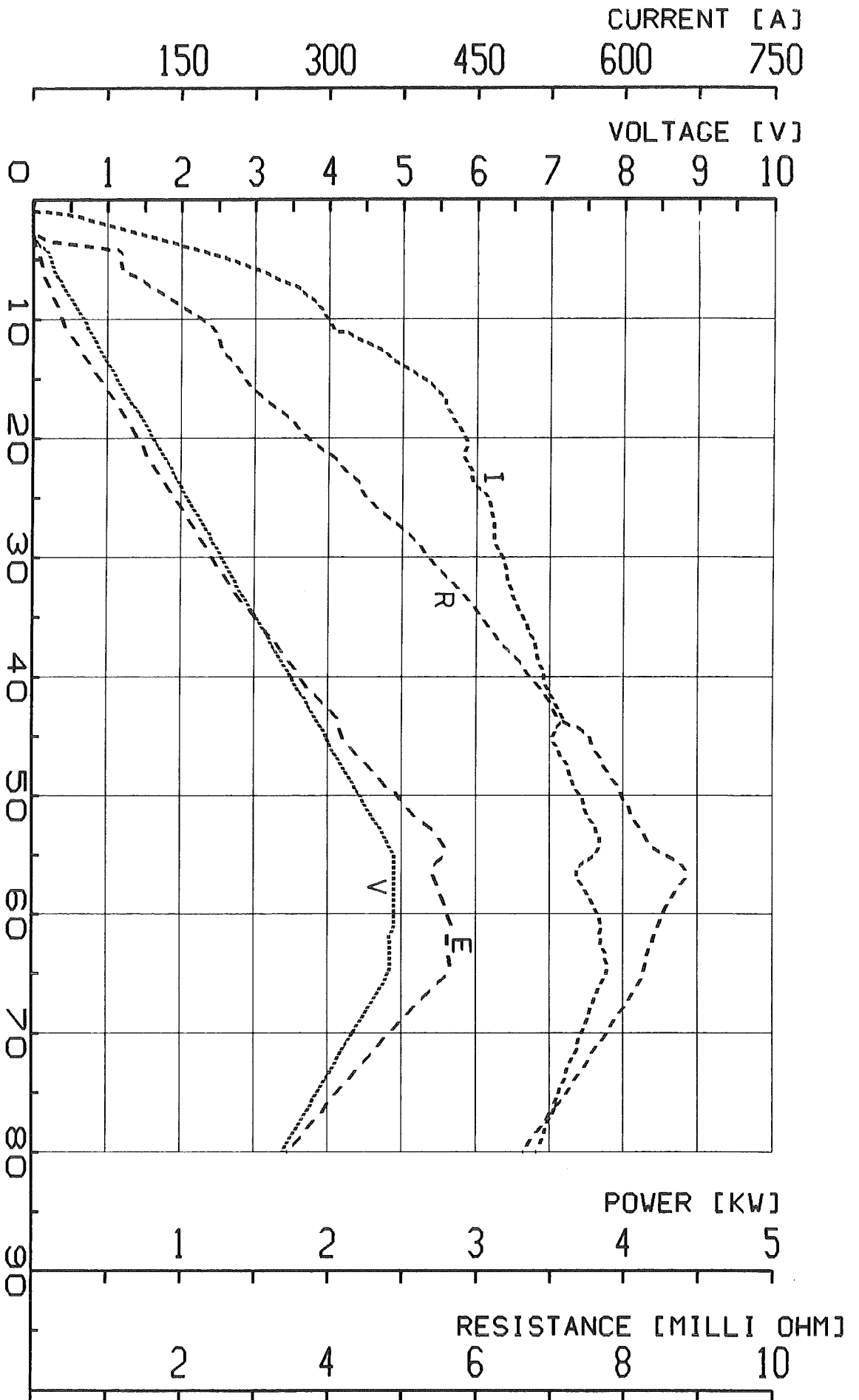
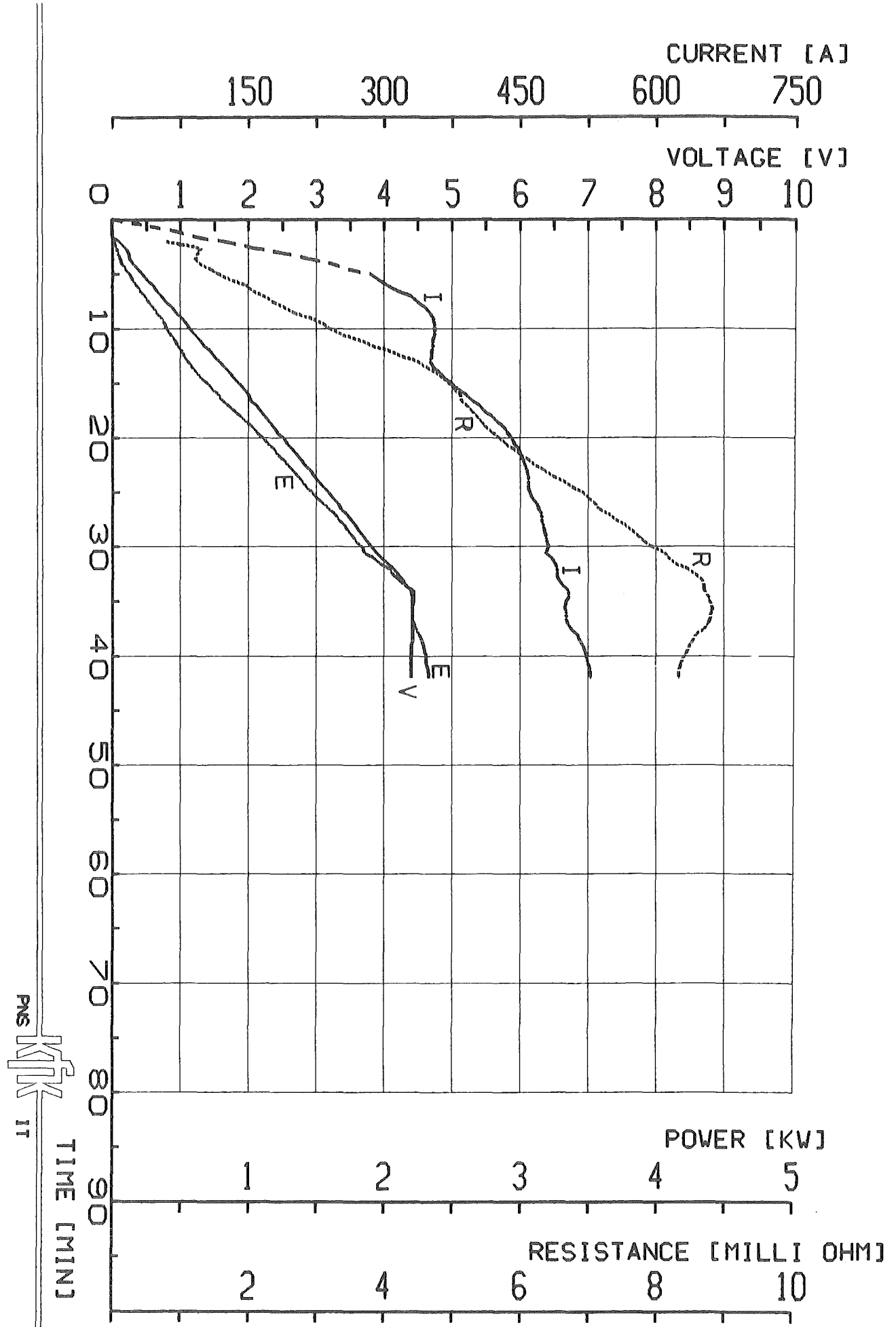
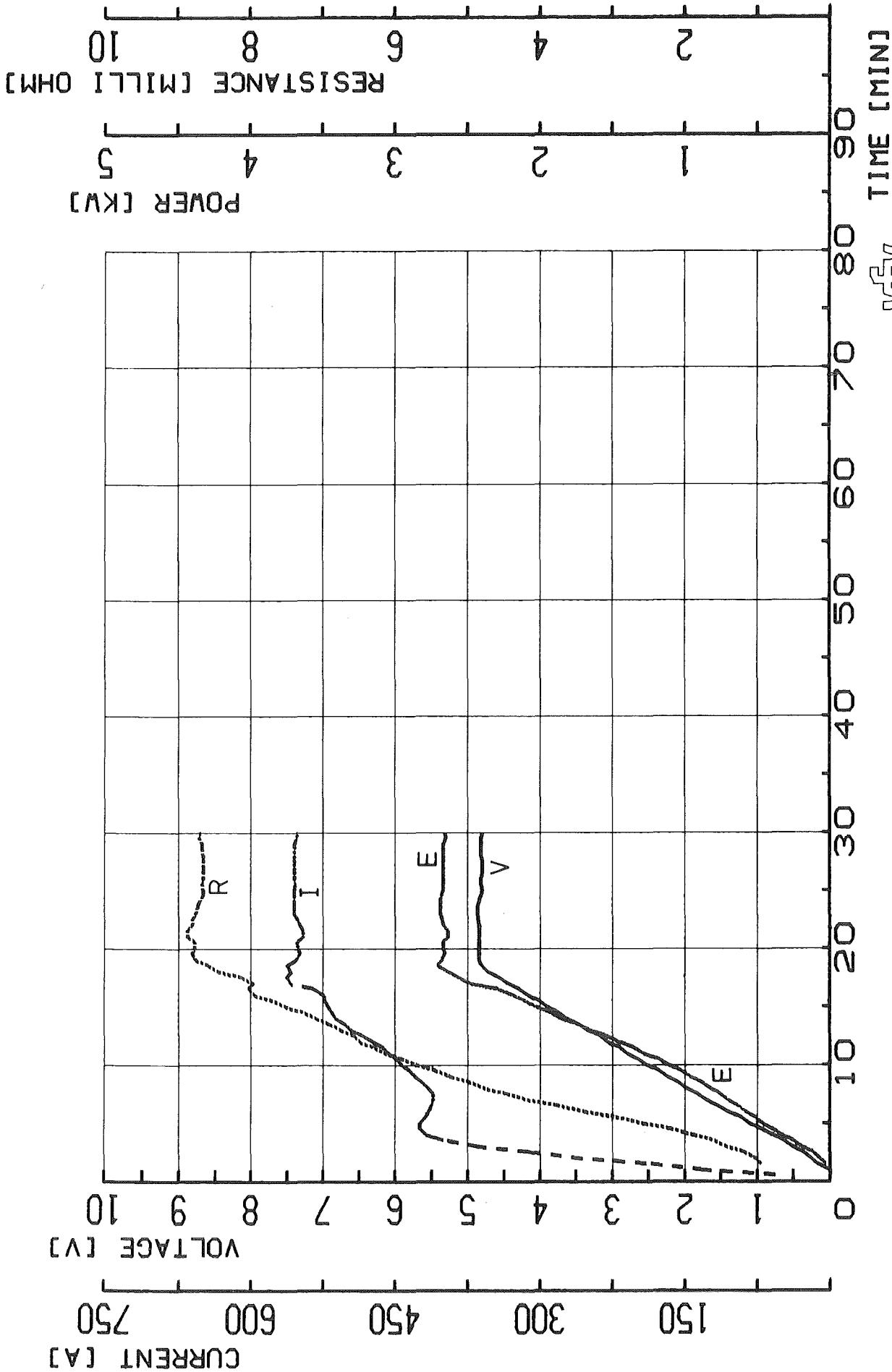


FIG 7 : VOLTAGE V, CURRENT I, ELECTRIC POWER E AND RESISTANCE R FOR TEST ESS1-5



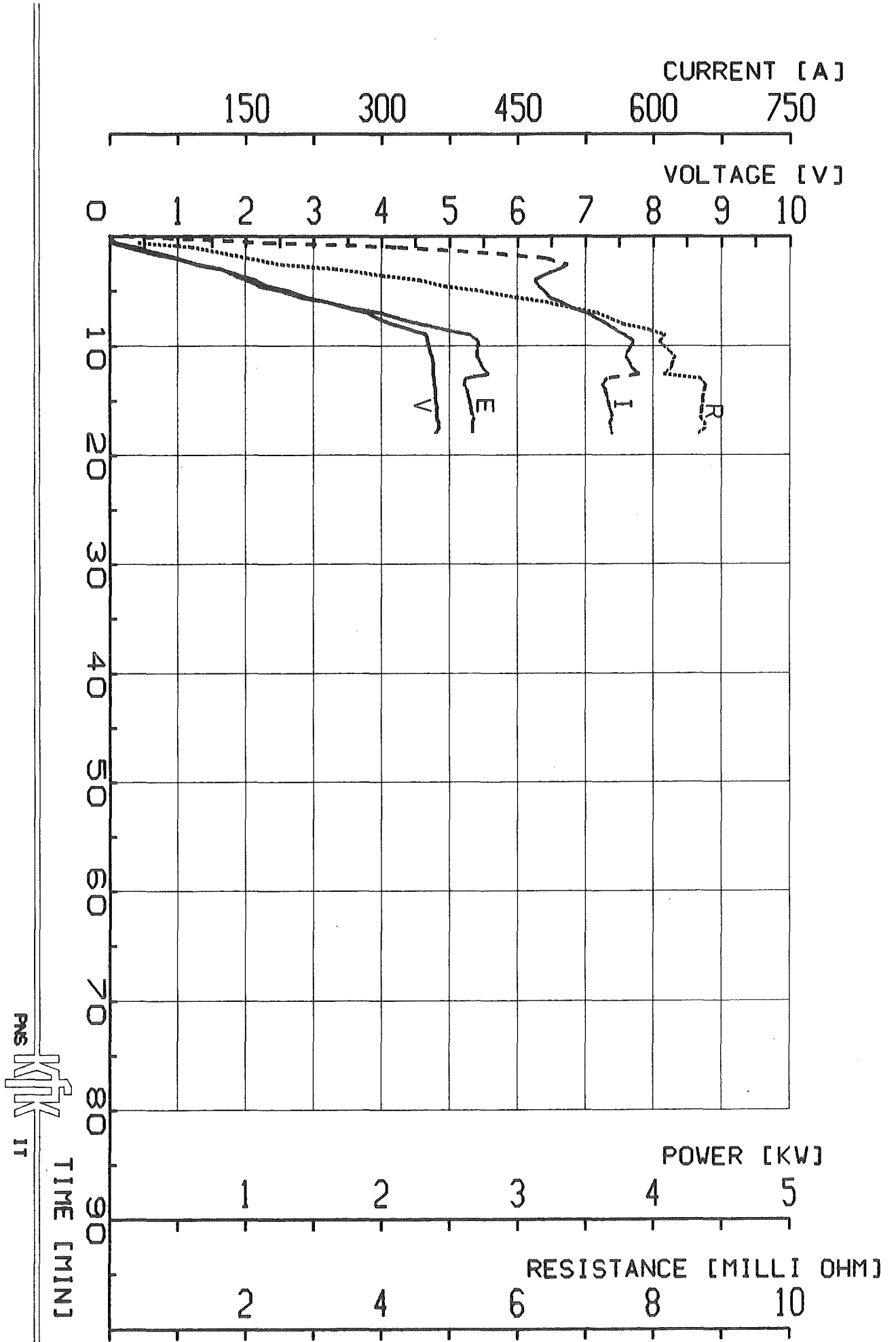
PNS KfK IT



PNS KJK IT

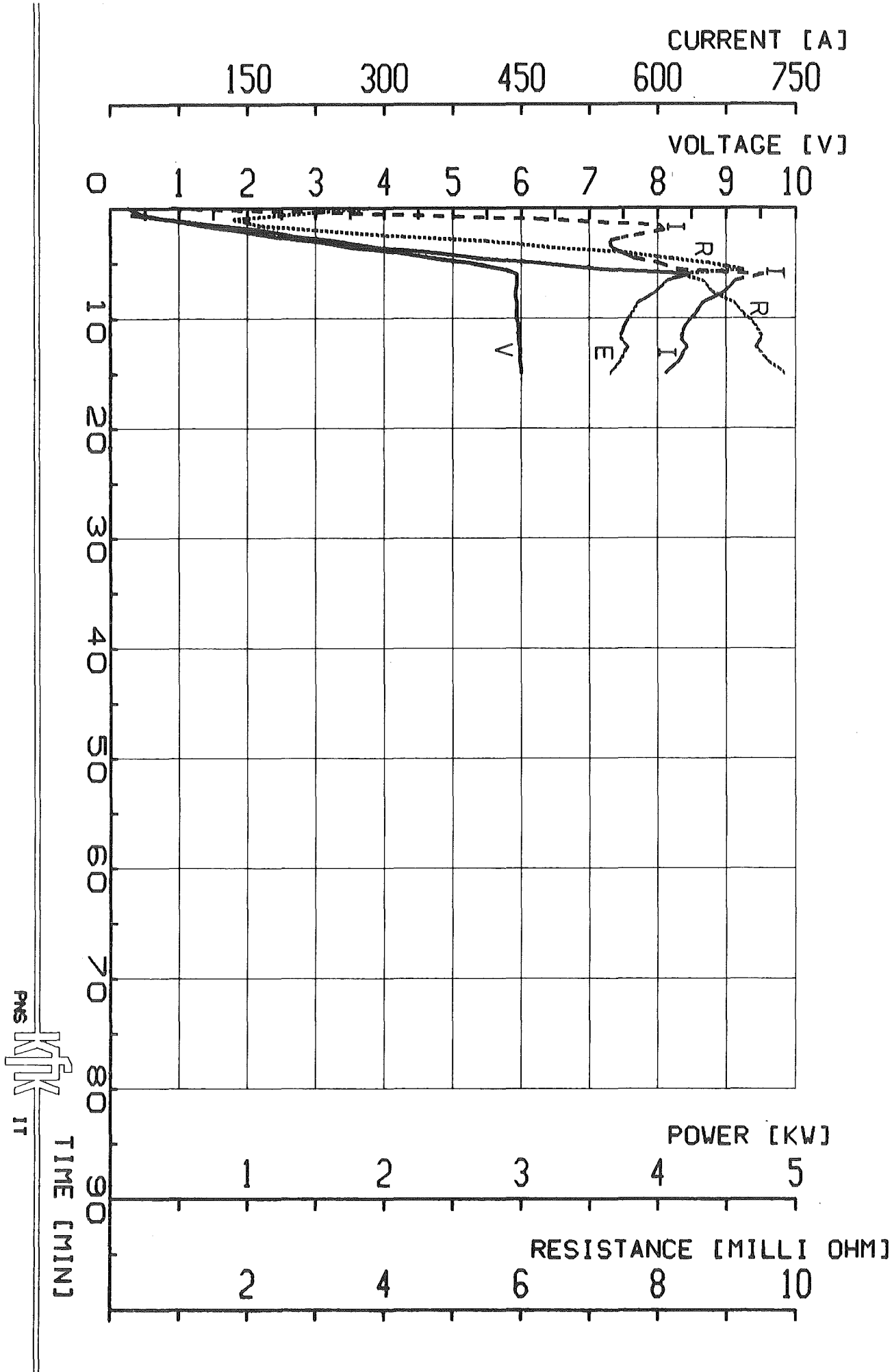
FIG. 8 : VOLTAGE V, CURRENT I, ELECTRIC POWER E AND RESISTANCE R FOR TEST ESS1-6

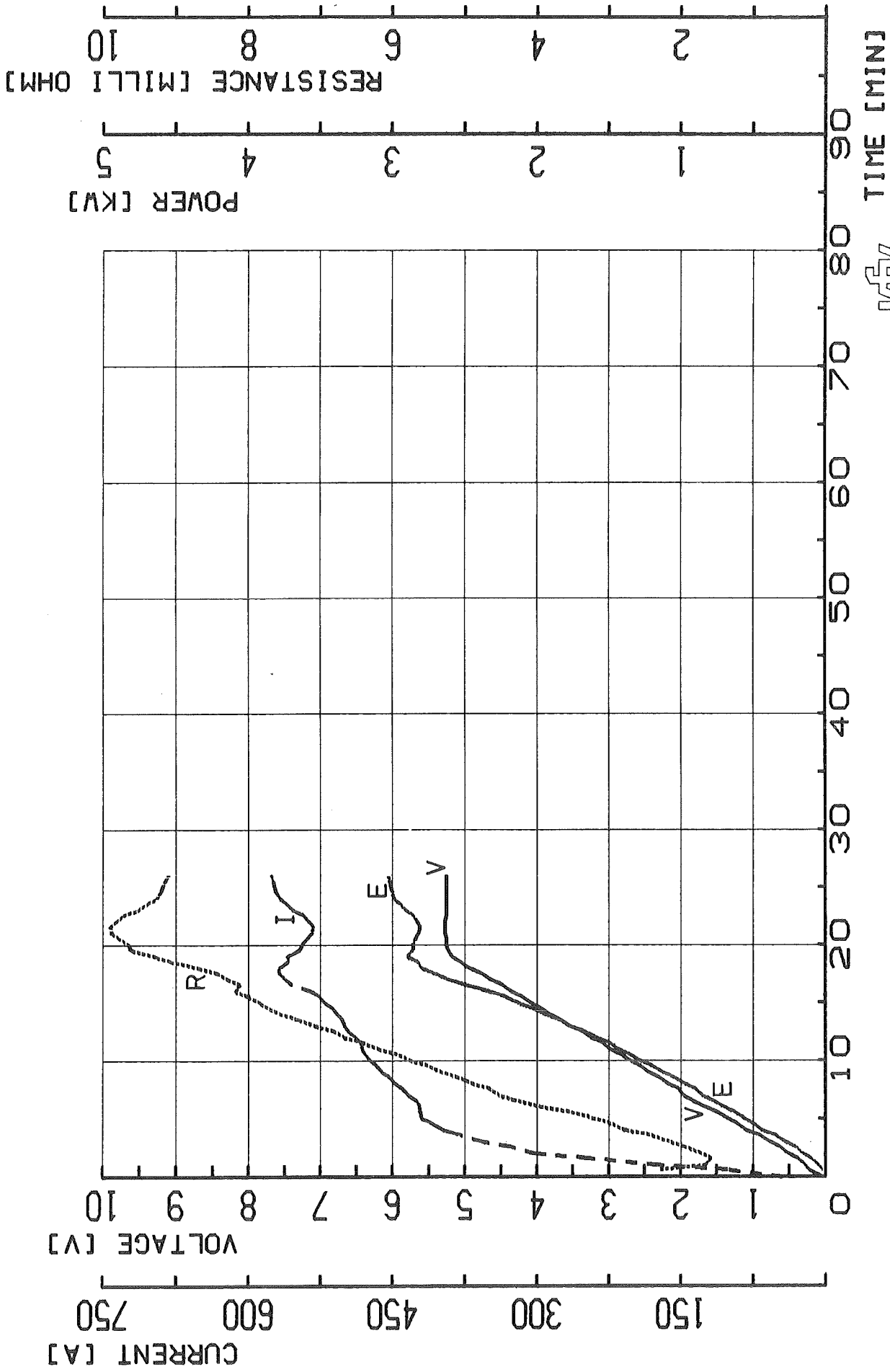
FIG. 9 : VOLTAGE V, CURRENT I, ELECTRIC POWER E AND RESISTANCE R FOR TEST ESS1-7



PNS
KIK
IT

FIG. 10 : VOLTAGE V, CURRENT I, ELECTRIC POWER E AND RESISTANCE R FOR TEST ESS1-8



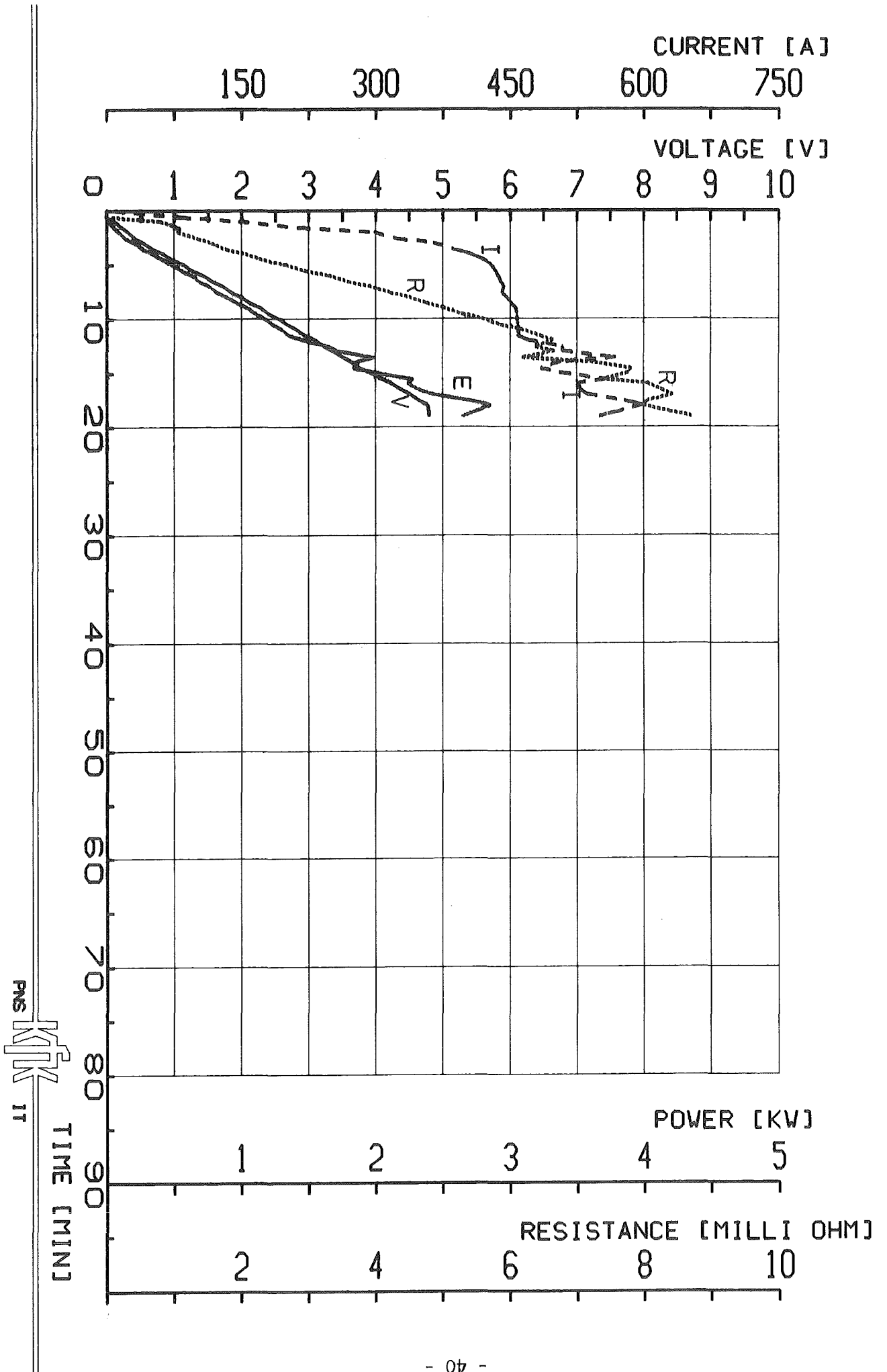


TIME [MIN]

KJK
PMS 17

FIG-11 : VOLTAGE V, CURRENT I, ELECTRIC POWER E AND RESISTANCE R FOR TEST ESS1-9

FIG. 12 : VOLTAGE V, CURRENT I, ELECTRIC POWER E AND RESISTANCE R FOR TEST ESS1-10



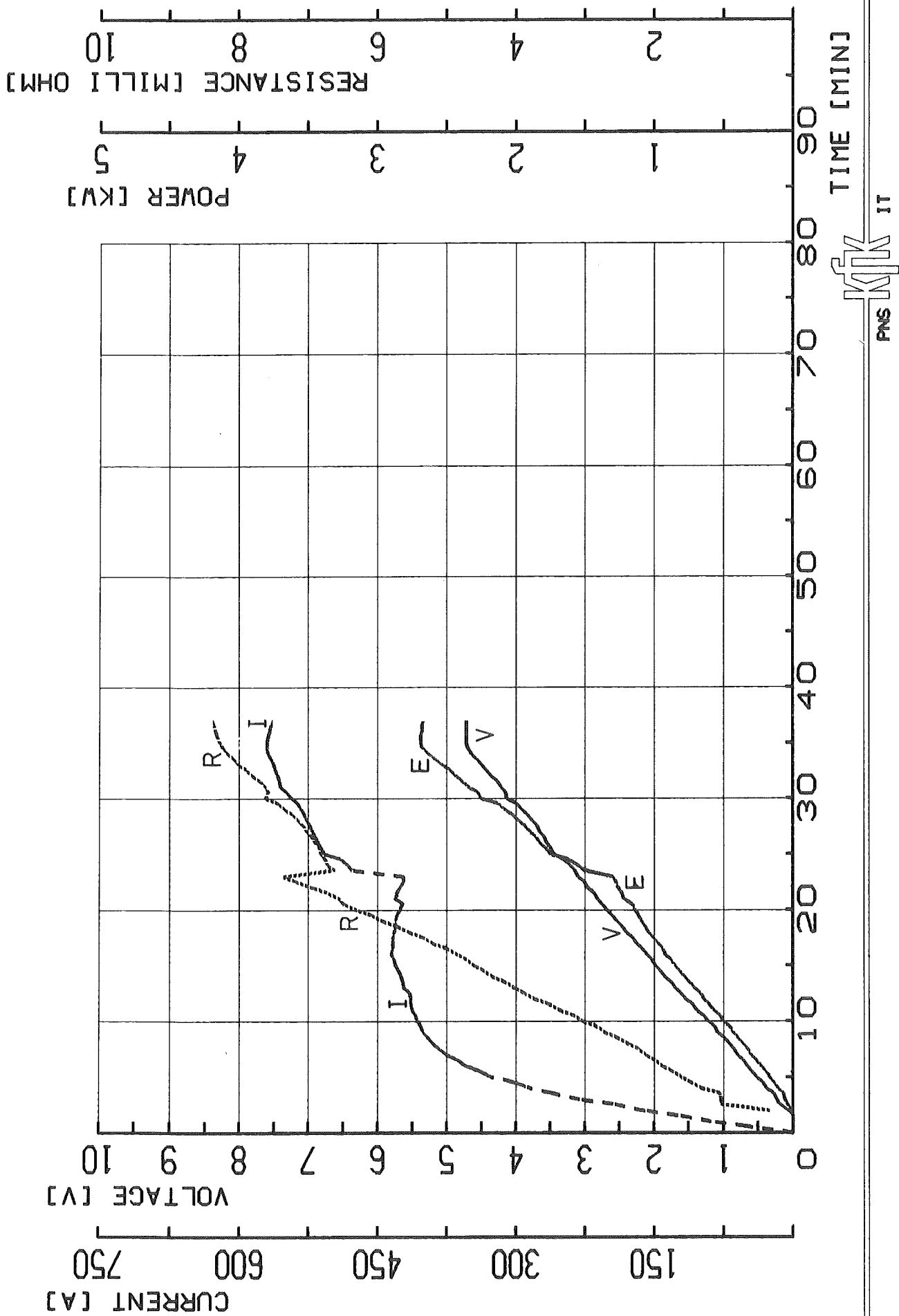
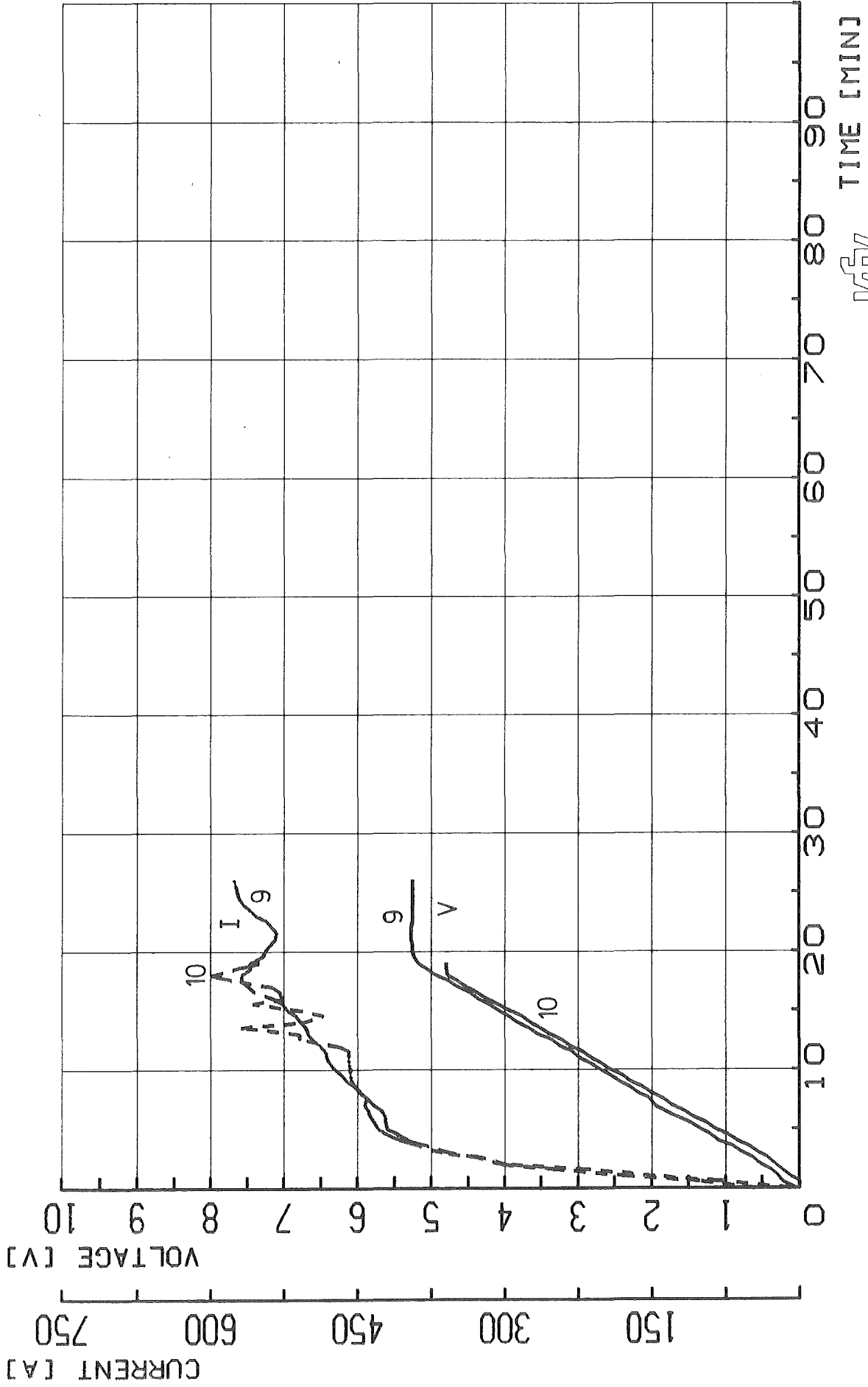
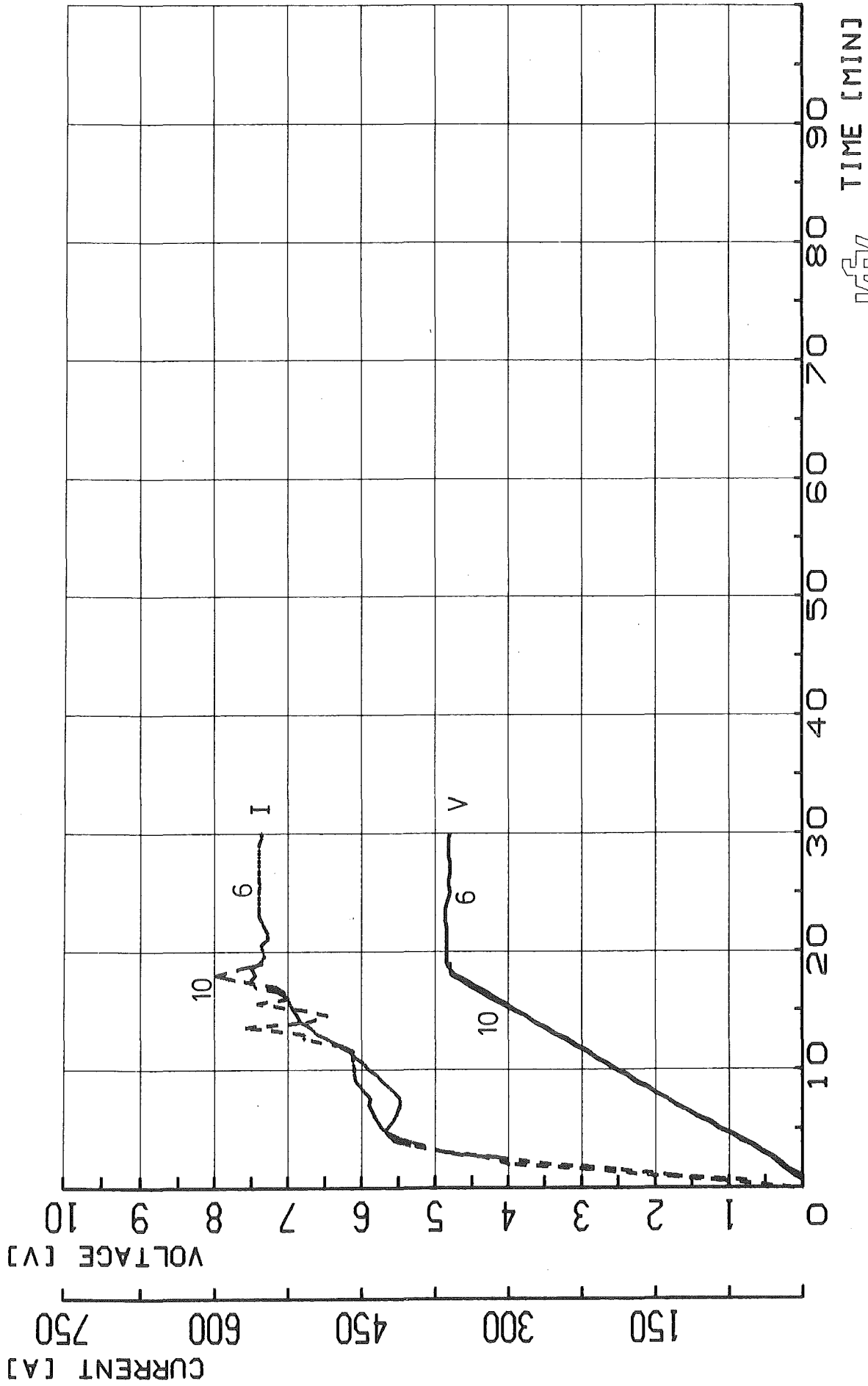


FIG-13: VOLTAGE V, CURRENT I, ELECTRIC POWER E AND RESISTANCE R FOR TEST ESS1-11



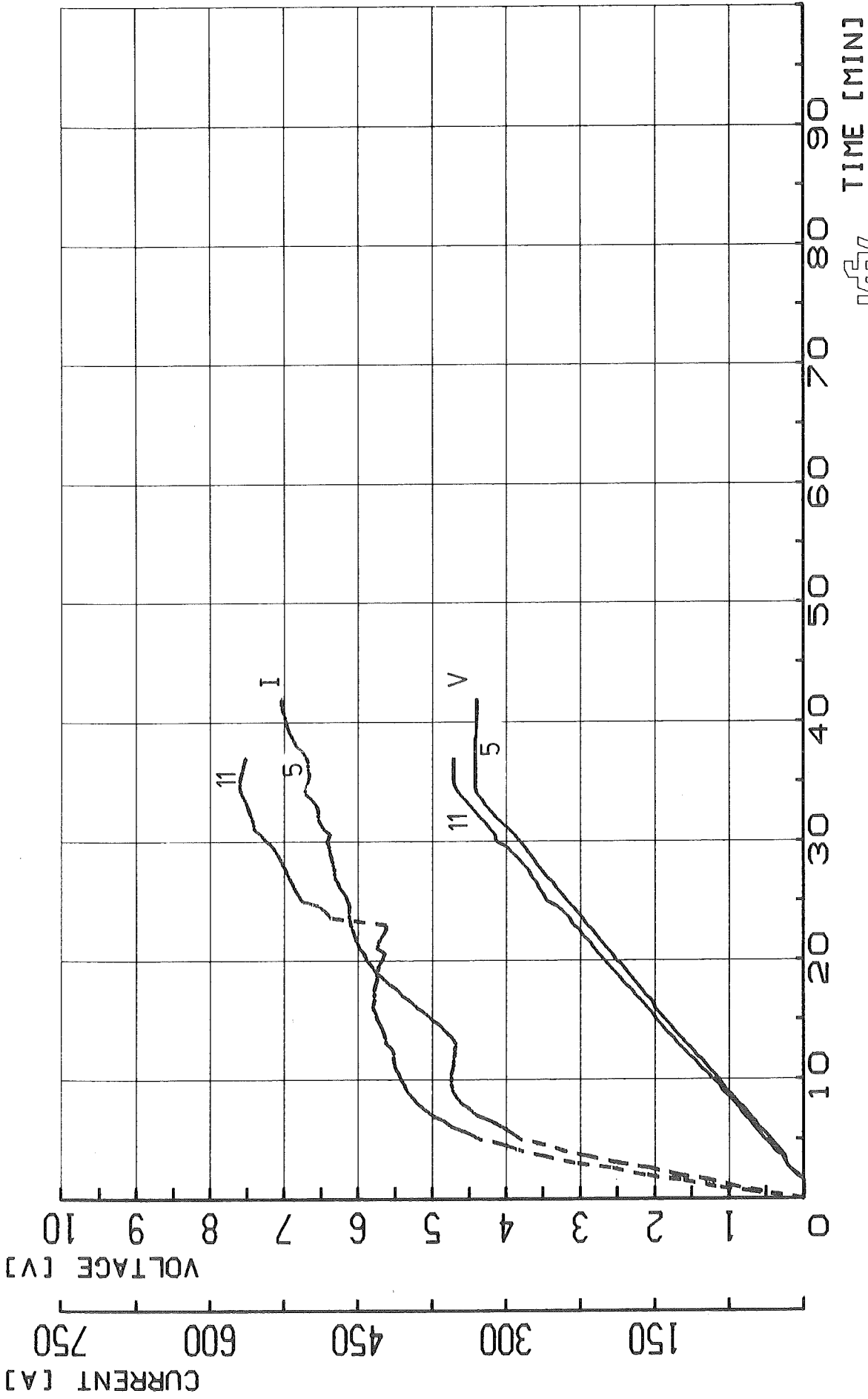
PNS KKK IT

FIG. 14 · COMPARISON OF VOLTAGE V AND CURRENT I FOR TESTS ESS1-9+10



PNS MKK IT

FIG 15 : COMPARISON OF VOLTAGE V AND CURRENT I FOR TESTS ESS1-6+10



PNS KJK IT

FIG. 16 : COMPARISON OF VOLTAGE V AND CURRENT I FOR TESTS 5+11

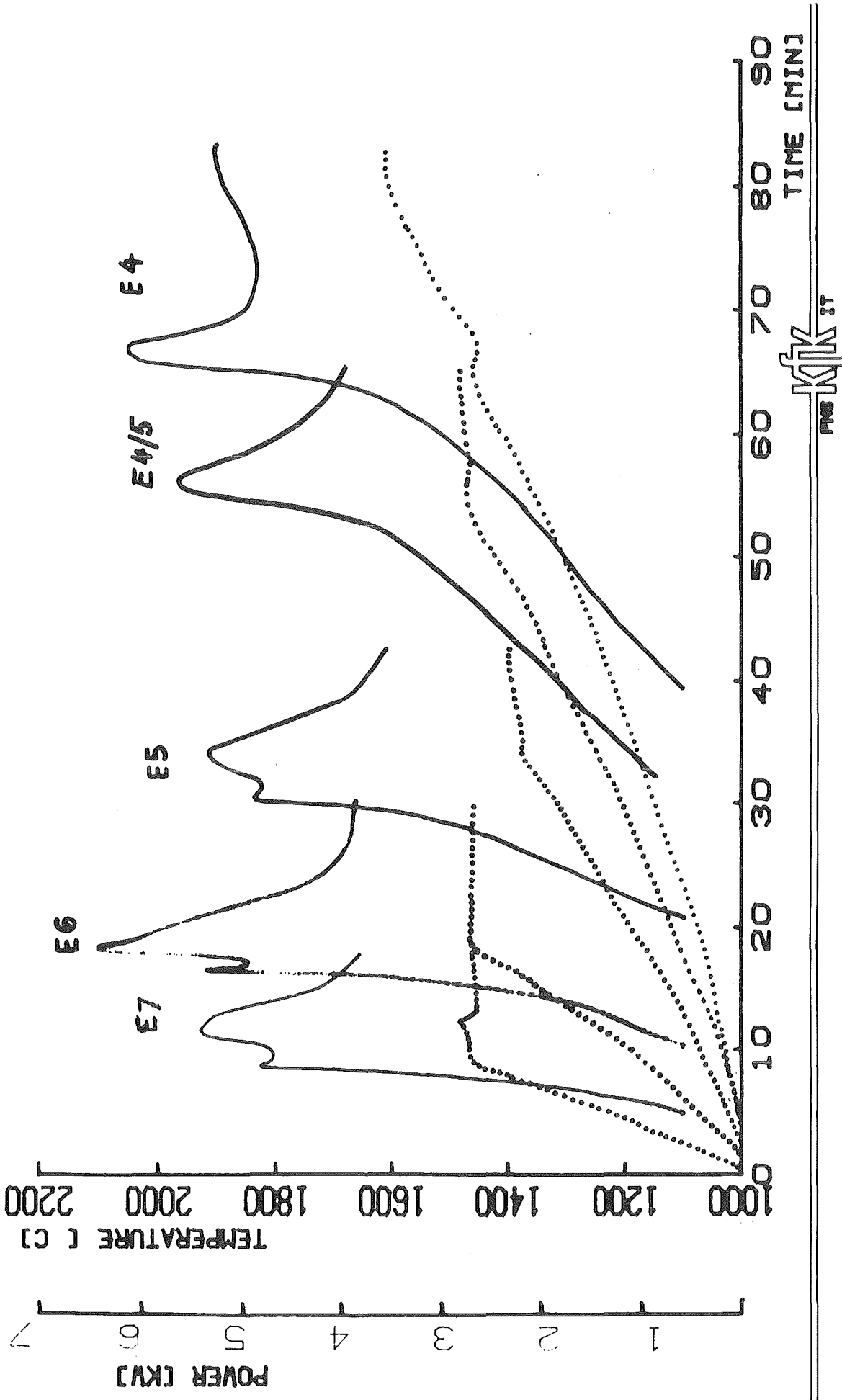


FIG.17: TEMPERATURES (——) ON RODS AND ELECTRIC POWERS (.....) FOR TESTS ESS1 4.4/5.5.6.7.

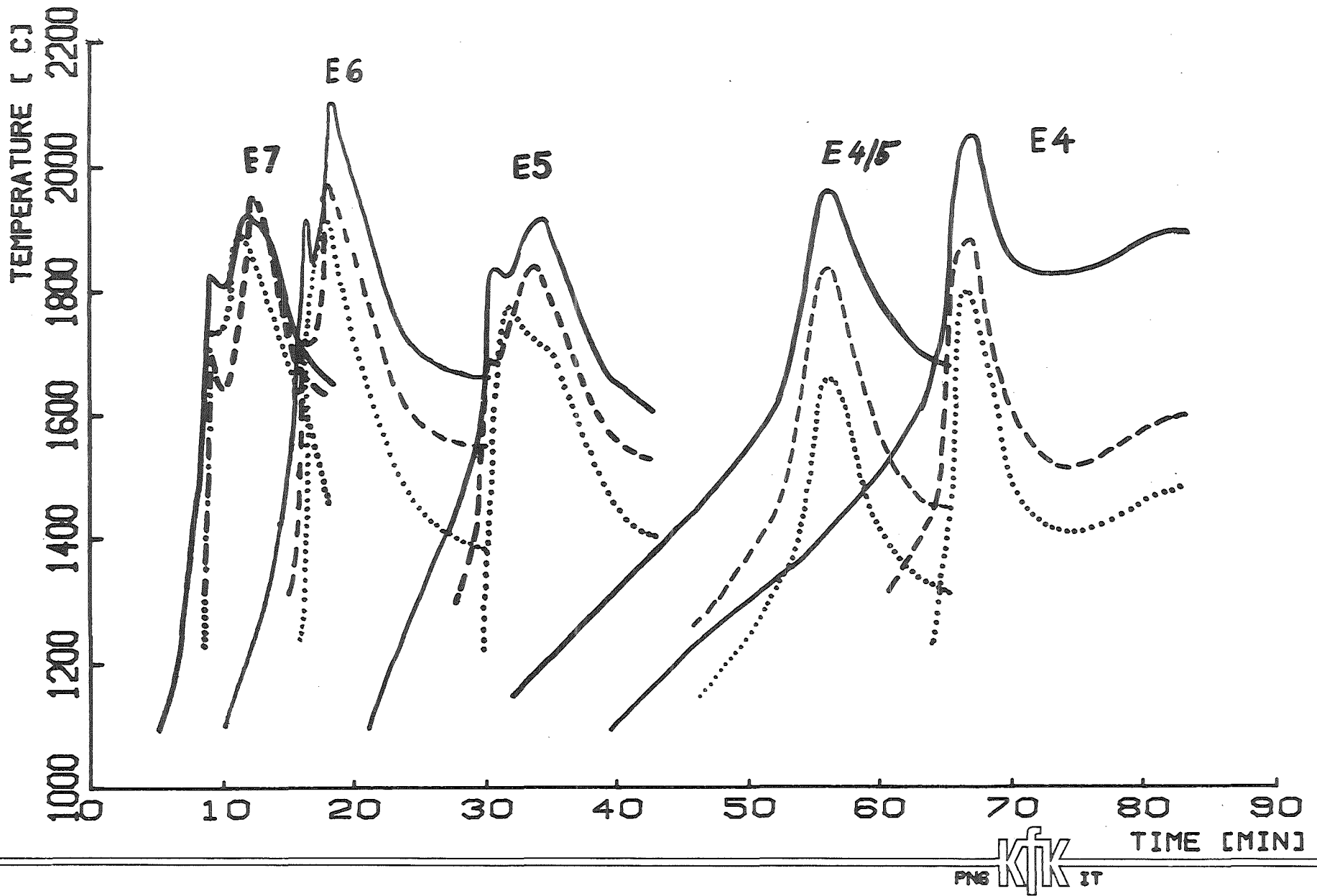


FIG. 18: TEMPERATURES ON ROD (—) AT 140 MM AND ON SHROUD AT 140 MM (---) AND 190 MM (.....) FROM UPPER END OF SHROUD FOR TESTS ESS1 4.4/5.5.6.7.

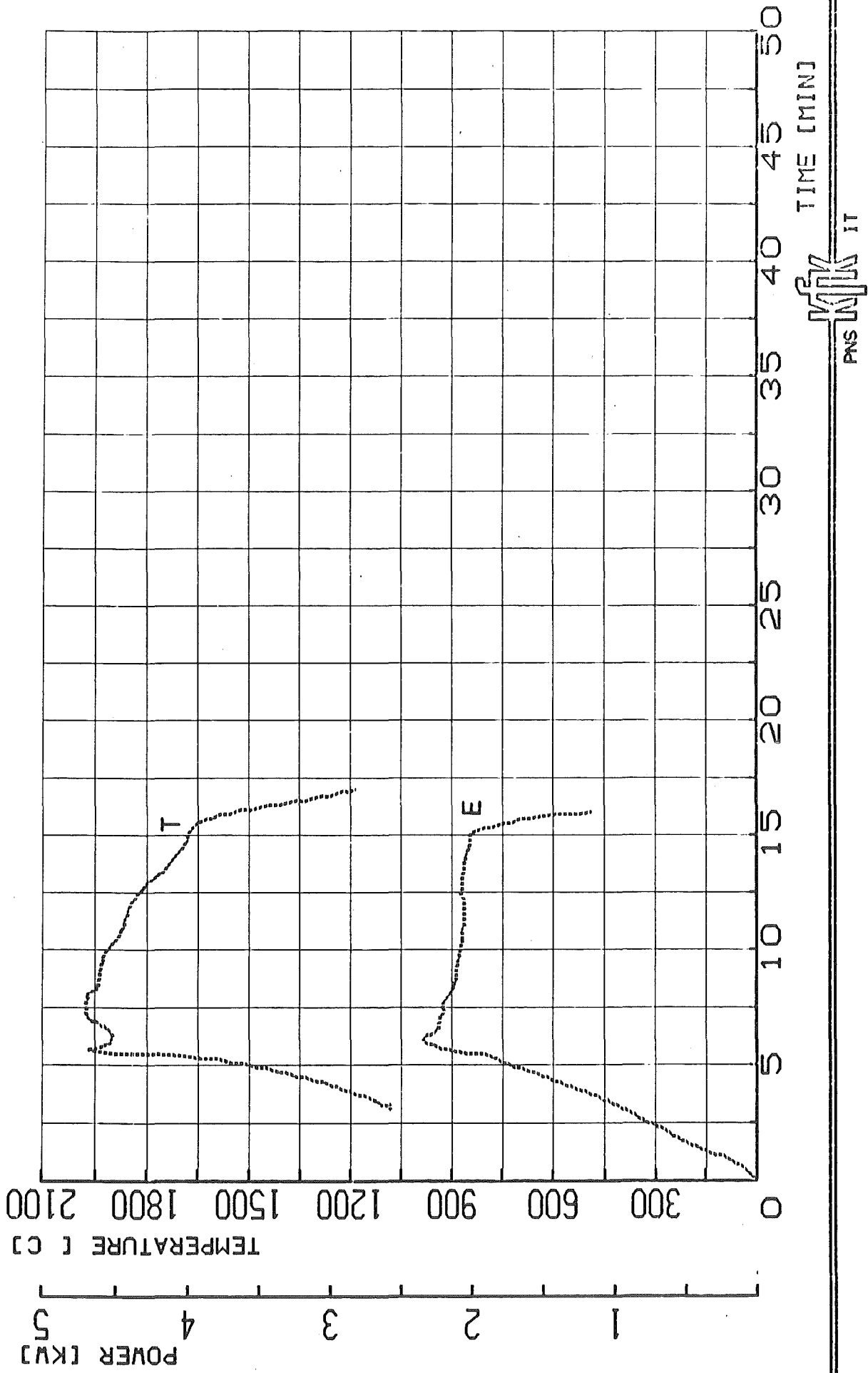
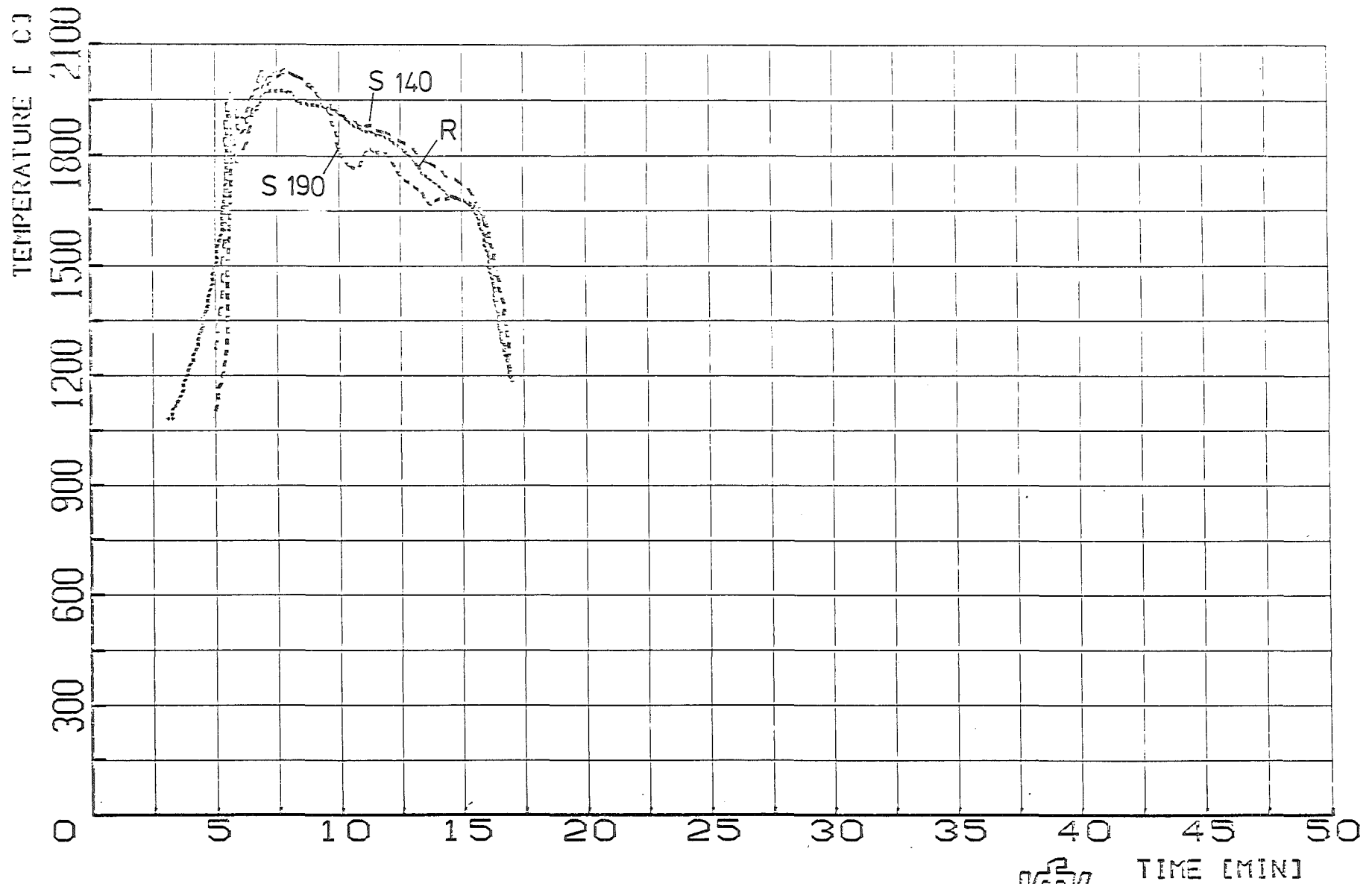


FIG-19: TEMPERATURE (T) ON THE ROD AND ELECTRIC POWER (E) FOR TEST ESS1-8.



PNS  IT

FIG. 20: TEMPERATURE ON ROD (R) AT 140 MM AND ON SHROUD AT 140 MM (S140) AND 190 MM (S190) FROM UPPER END OF SHROUD FOR TEST ESSI 8

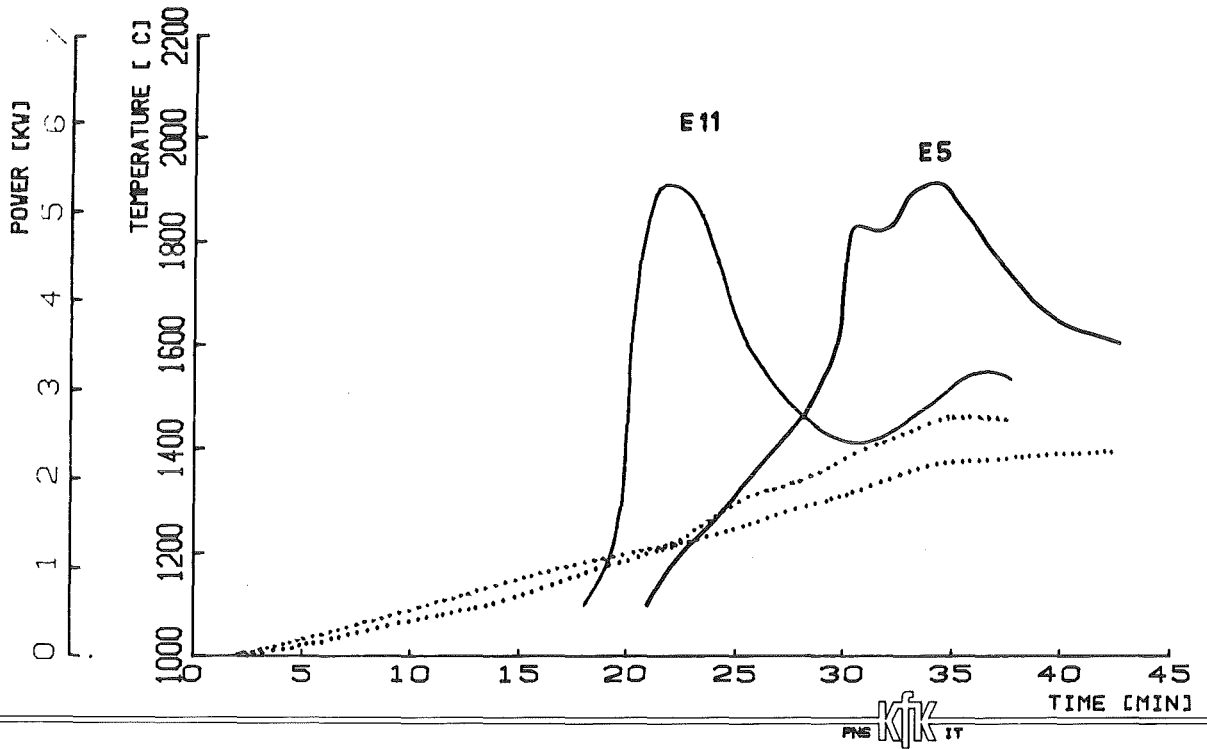


FIG.21: TEMPERATURES ON ROD (—) AND ELECTRIC POWERS (.....) FOR ESS1-11 (6.4 MM INSULATION.NO GAP) AND ESS1-5 (101.6 MM INSULATION.GAP)

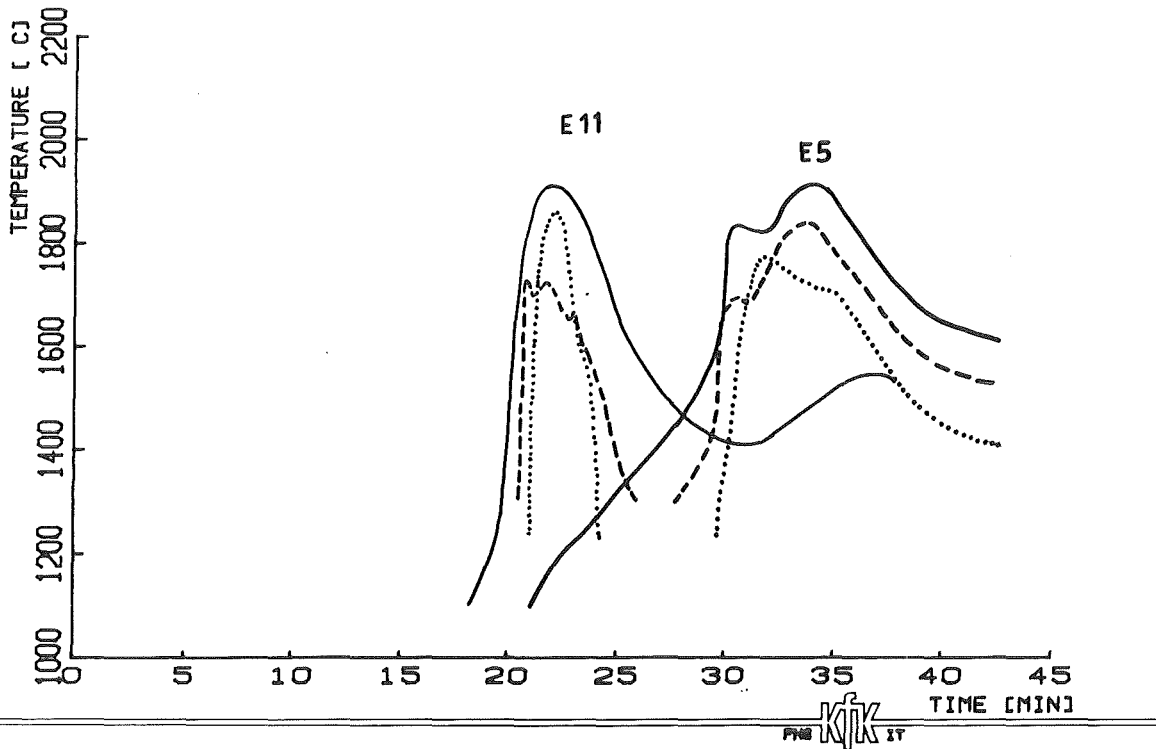


FIG.22: TEMPERATURES ON ROD (—) AT 140 MM AND ON SHROUD AT 140 MM (----) AND 190 MM (.....) FROM UPPER END OF SHROUD FOR TESTS ESS1 5 AND 11

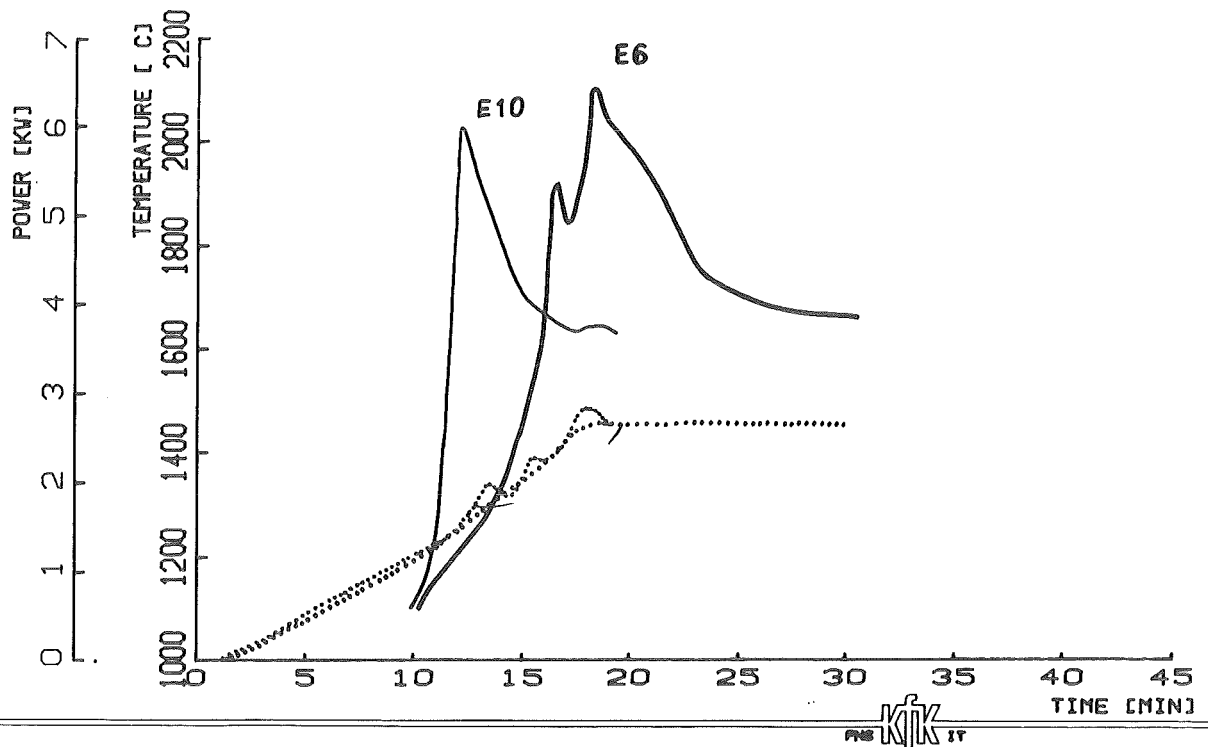


FIG.23: TEMPERATURES ON ROD (—) AND ELECTRIC POWERS (.....) FOR ESSI-10 (6.4 MM INSULATION.NO GAP) AND ESSI-6 (101.6 MM INSULATION.CAP)

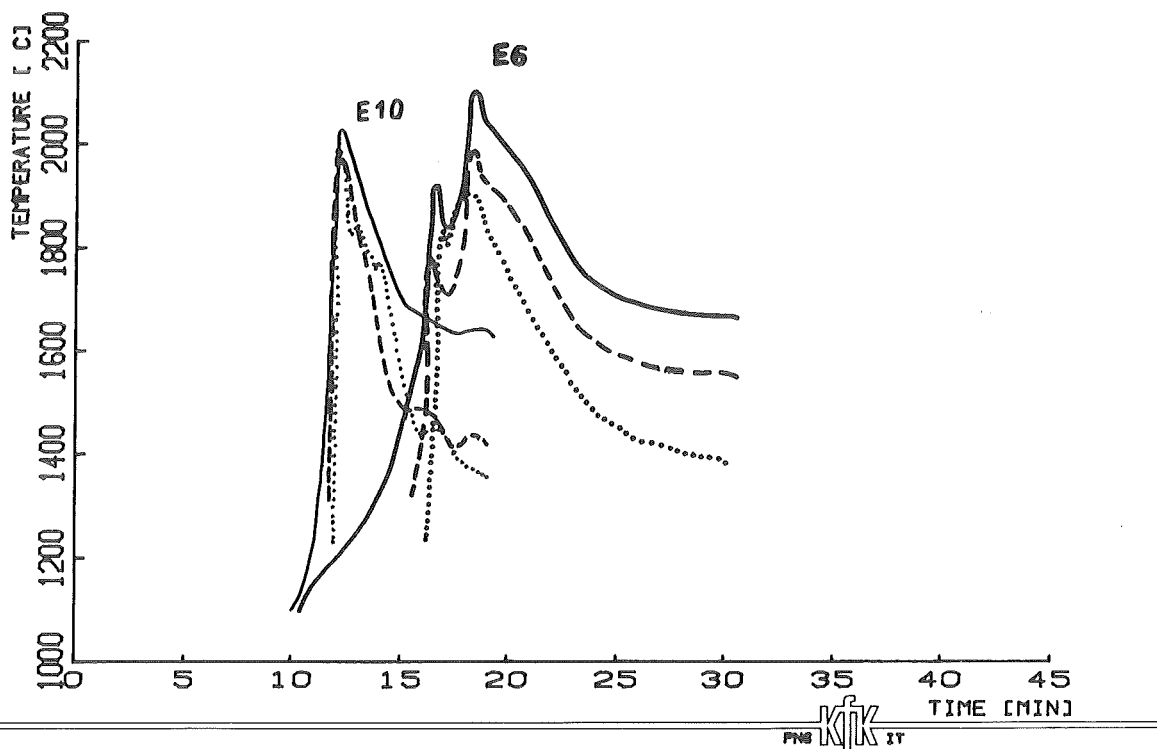


FIG.24: TEMPERATURES ON ROD (—) AT 140 MM AND ON SHROUD AT 140 MM (---) AND 190 MM (.....) FROM UPPER END OF SHROUD FOR TESTS ESSI 6 AND 10

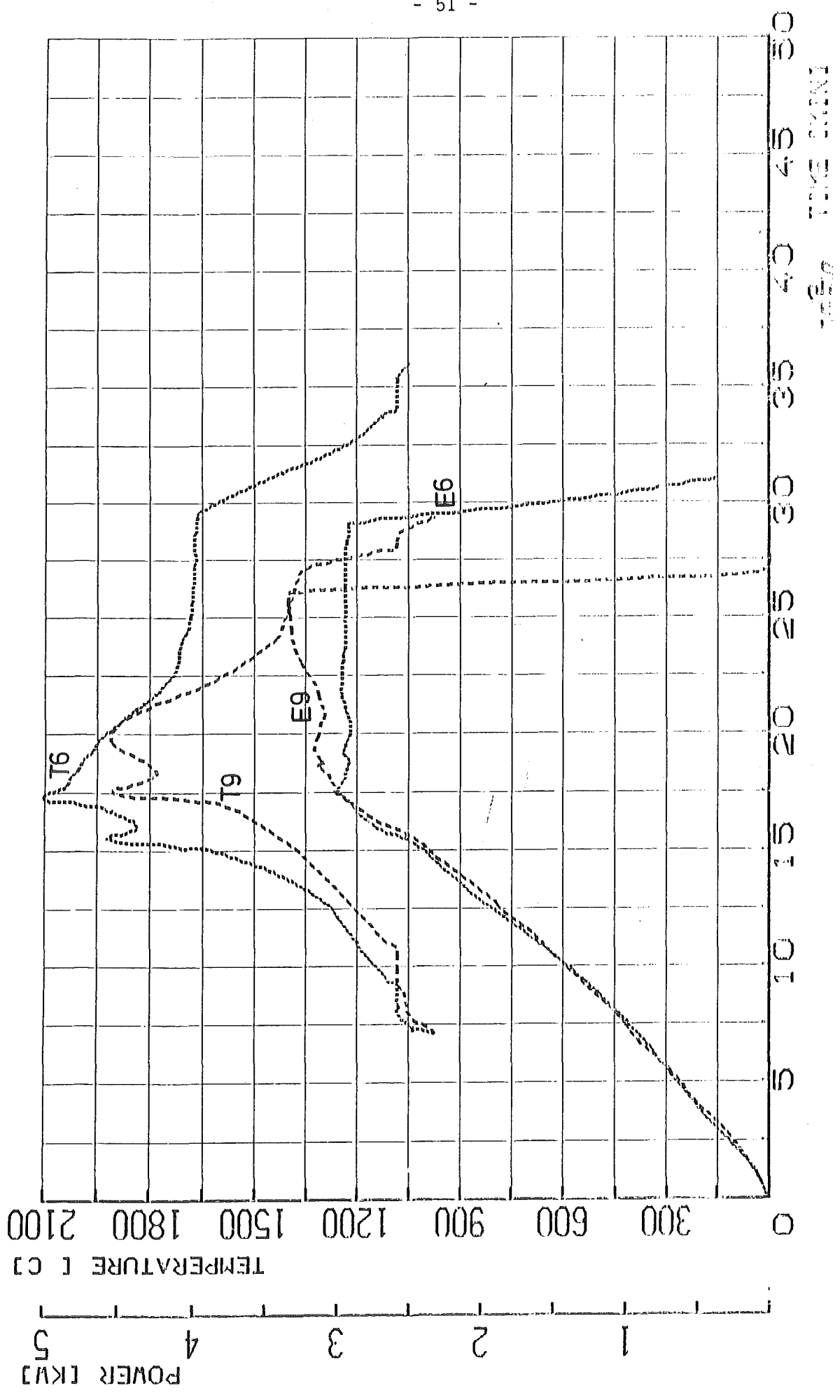
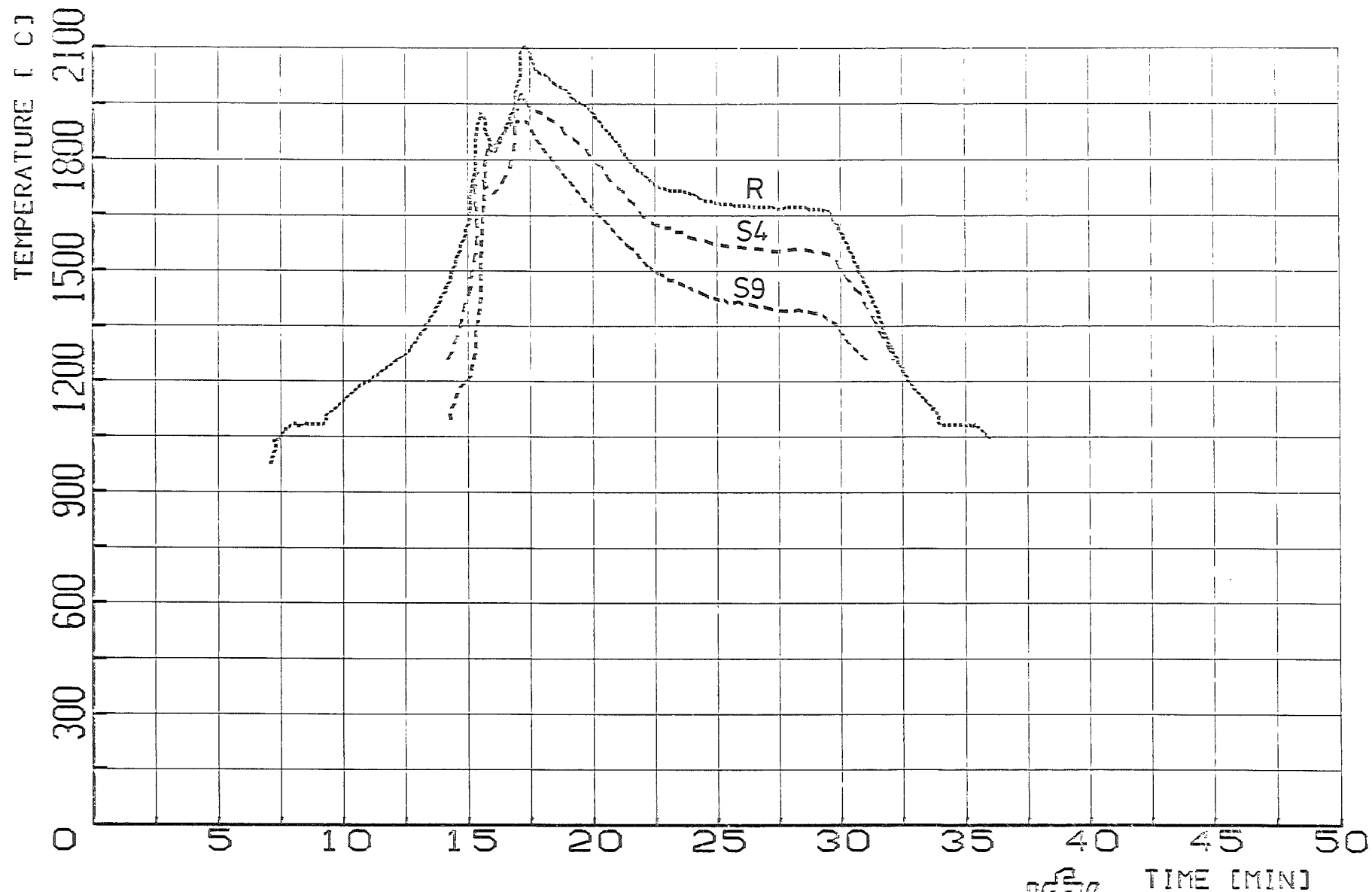


FIG. 25: TEMPERATURES (T) AND ELECTRIC POWERS (E) FOR ESSI-9 (12.8 MM INSULATION) AND ESSI-6 (101.6 MM INSULATION)



PKS  IT

FIG. 26 TEMPERATURE ON THE ROD (R) IN 140 MM AND ON THE SHROUD IN 140 MM (S4) AND 190 MM (S9) FROM THE UPPER END OF THE SHROUD FOR ESSI-6

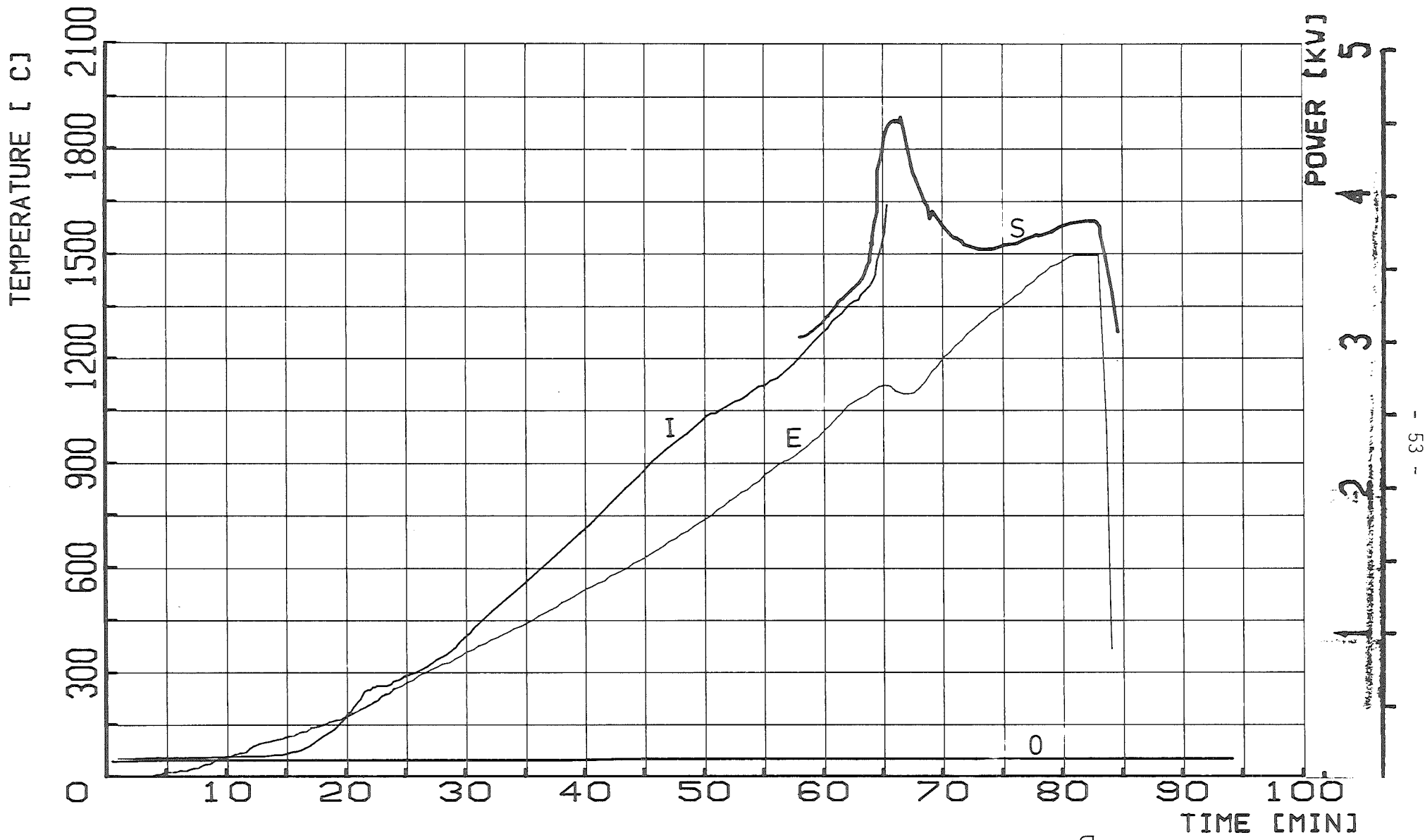


FIG.27: TEMPERATURES ON THE SHROUD (S), 12 MM WITHIN THE INSULATION (I) AND ON THE OUTER SURFACE (O) OF THE INSULATION 205 MM ABOVE THE LOWER END OF THE CLADDING AND ELECTRIC POWER (E). ESSI-4

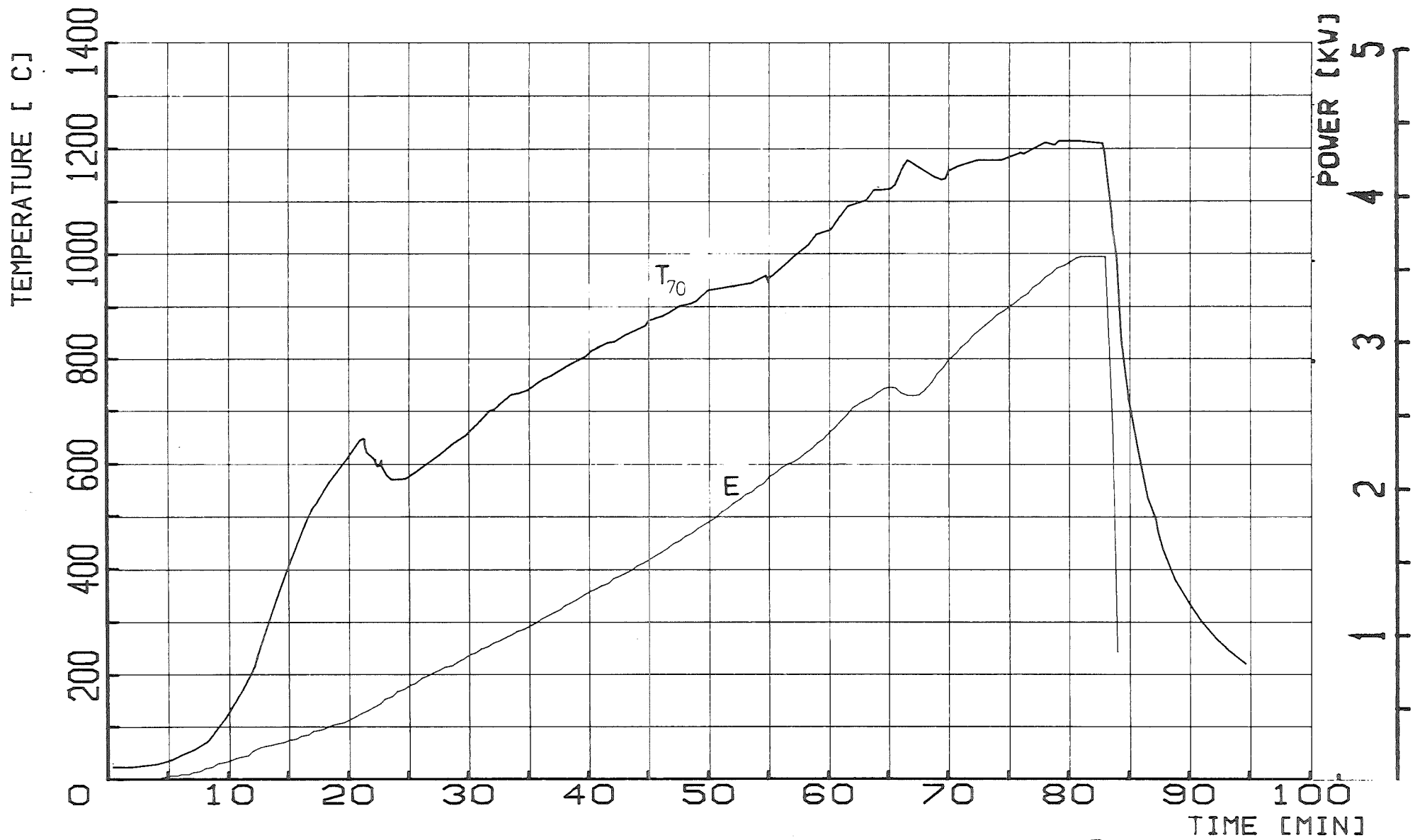


FIG.28 : TEMPERATURES ON THE ROD 70 MM ABOVE THE LOWER END OF THE CLADDING IN COMPARISON TO ELECTRIC POWER (E). ESSI-4

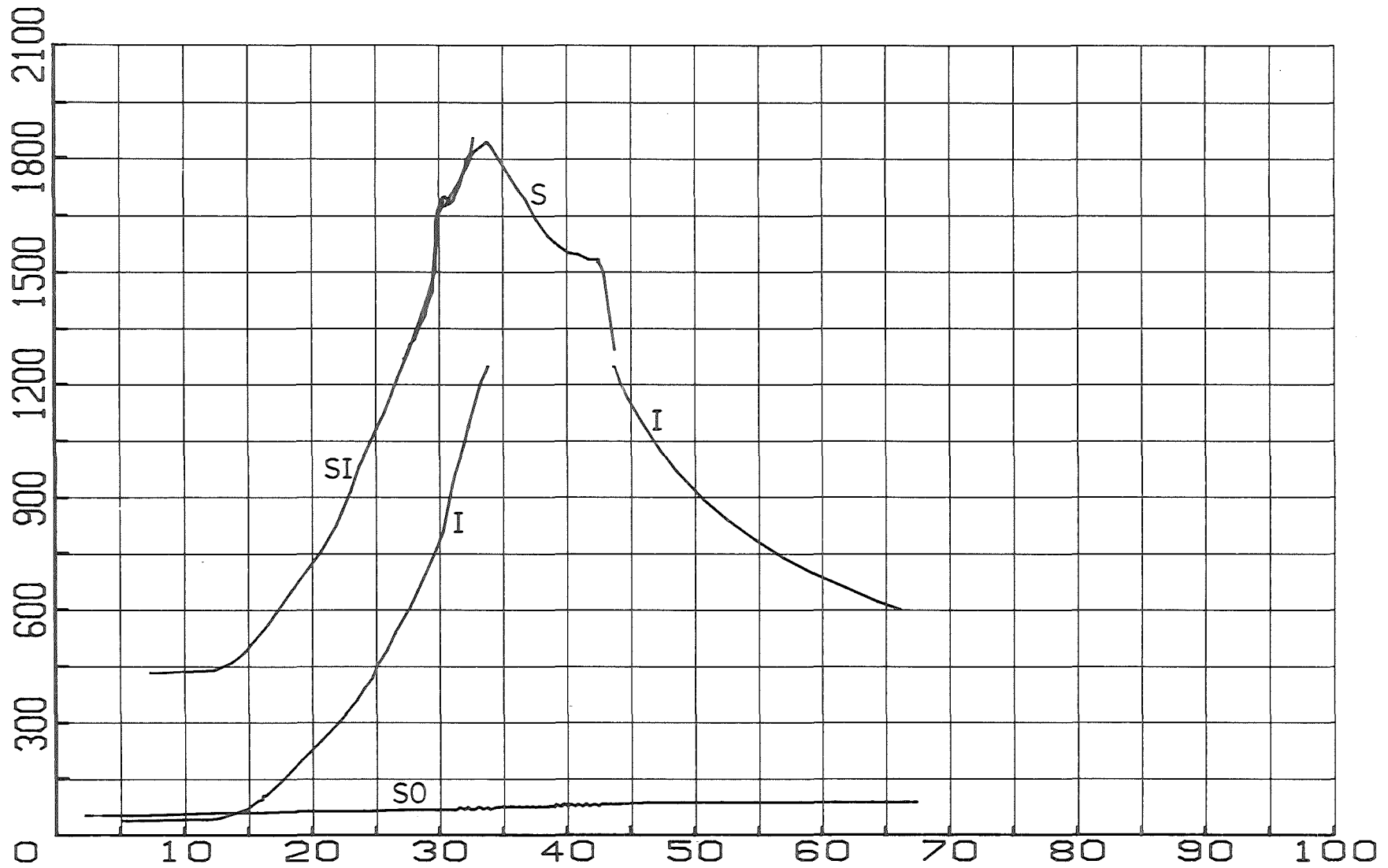


FIG.29: TEMPERATURES ON THE SHROUD (S) AND ON THE INSULATION INNER SURFACE (SI), OUTER SURFACE (SO) AND INTERIOR (I) (12 MM FROM THE INNER SURFACE) AT THE 205 MM ELEVATION FOR TEST ESS1-5

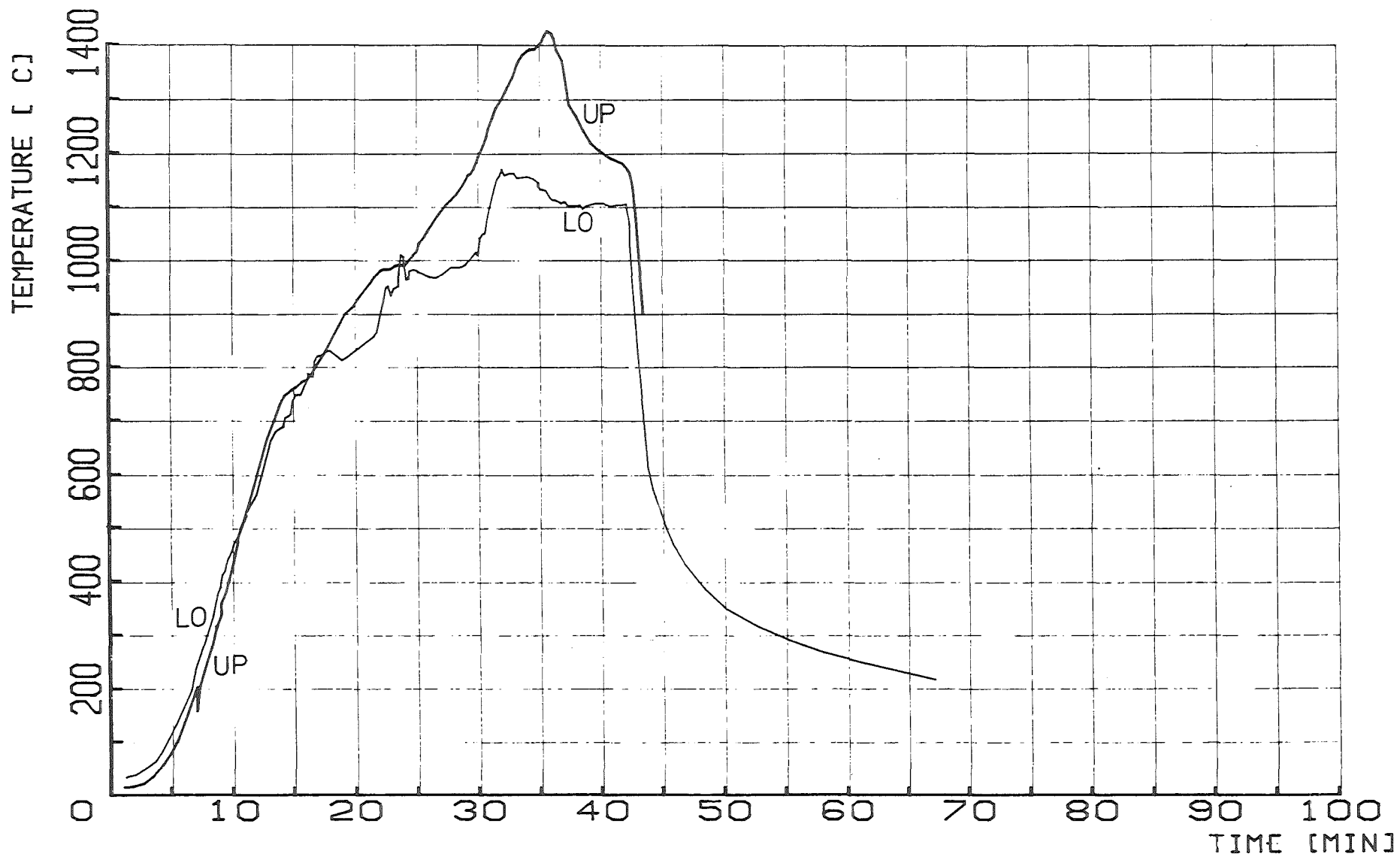


FIG.30 : TEMPERATURES ON THE ROD 70 MM ABOVE THE LOWER (LO) AND 50 MM BELOW THE UPPER (UP) END OF THE CLADDING. ESSI-5

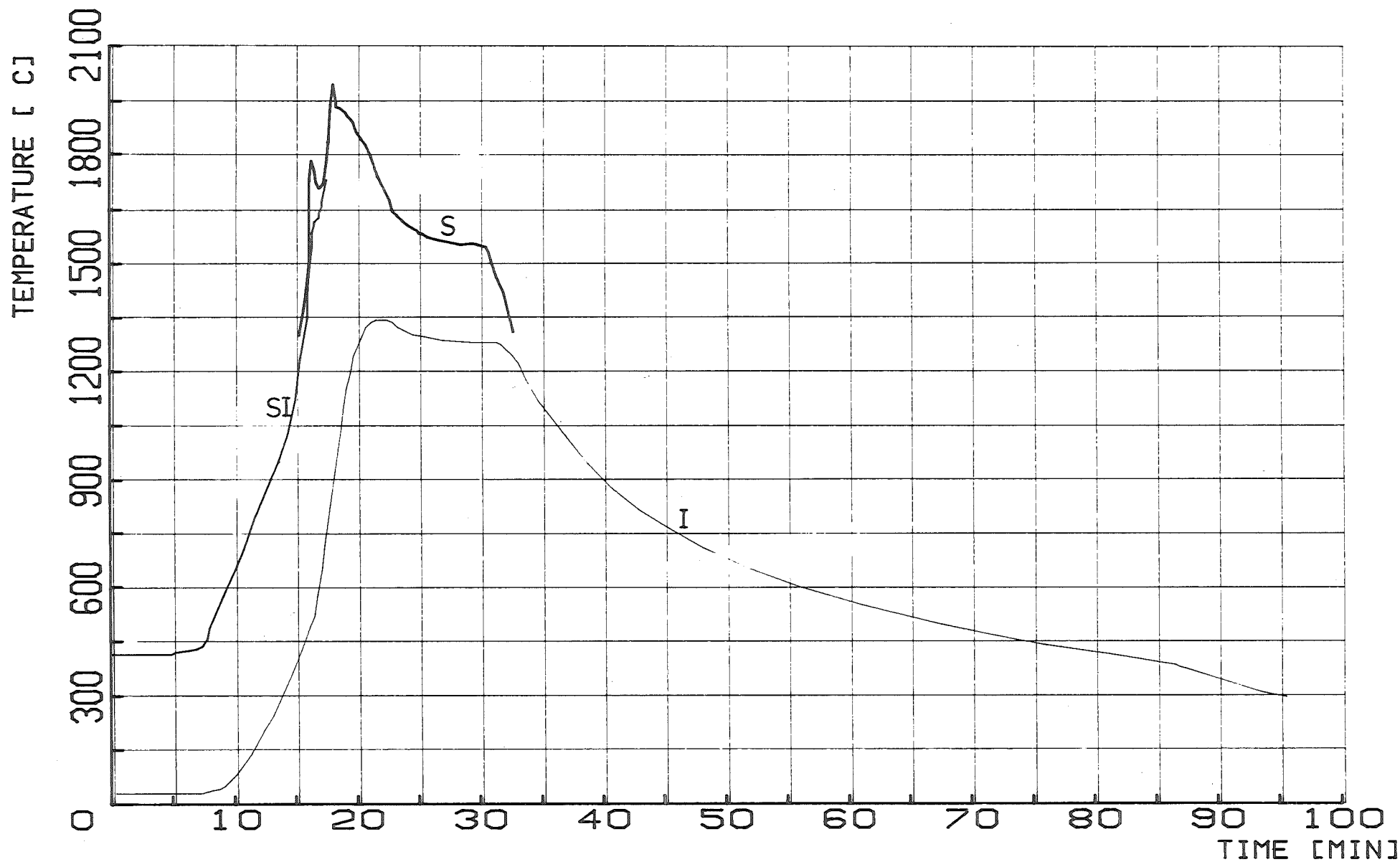


FIG. 31: TEMPERATURES ON THE SHROUD (S), AND ON THE INNER SURFACE (SI) AND 12 MM WITHIN THE INSULATION (I) 205 MM ABOVE THE LOWER END OF THE CLADDING. ESSI-6

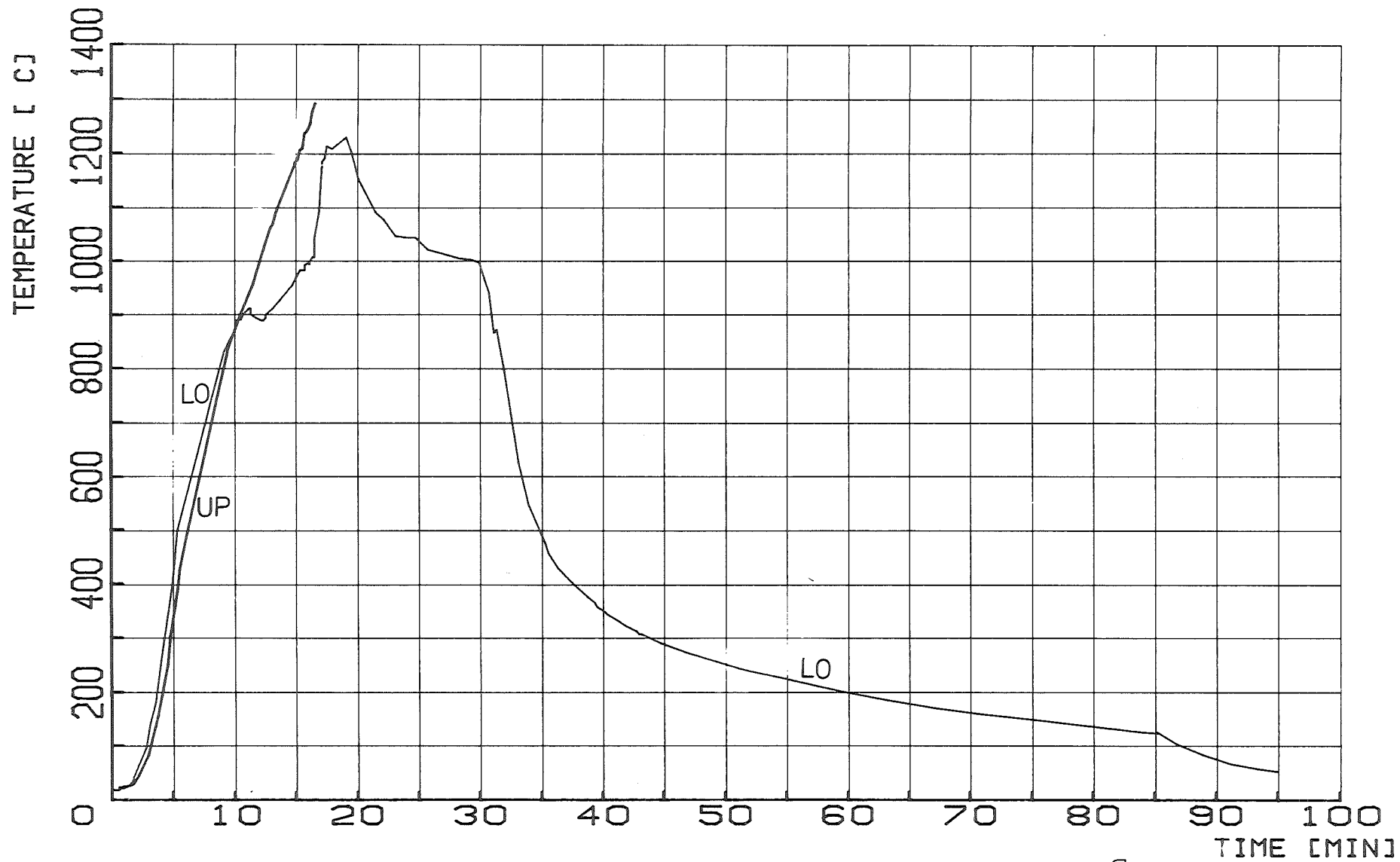


FIG. 32 : TEMPERATURES ON THE ROD 70 MM ABOVE THE LOWER (LO) AND 50 MM BELOW THE UPPER (UP) END OF THE CLADDING. ESSI-6

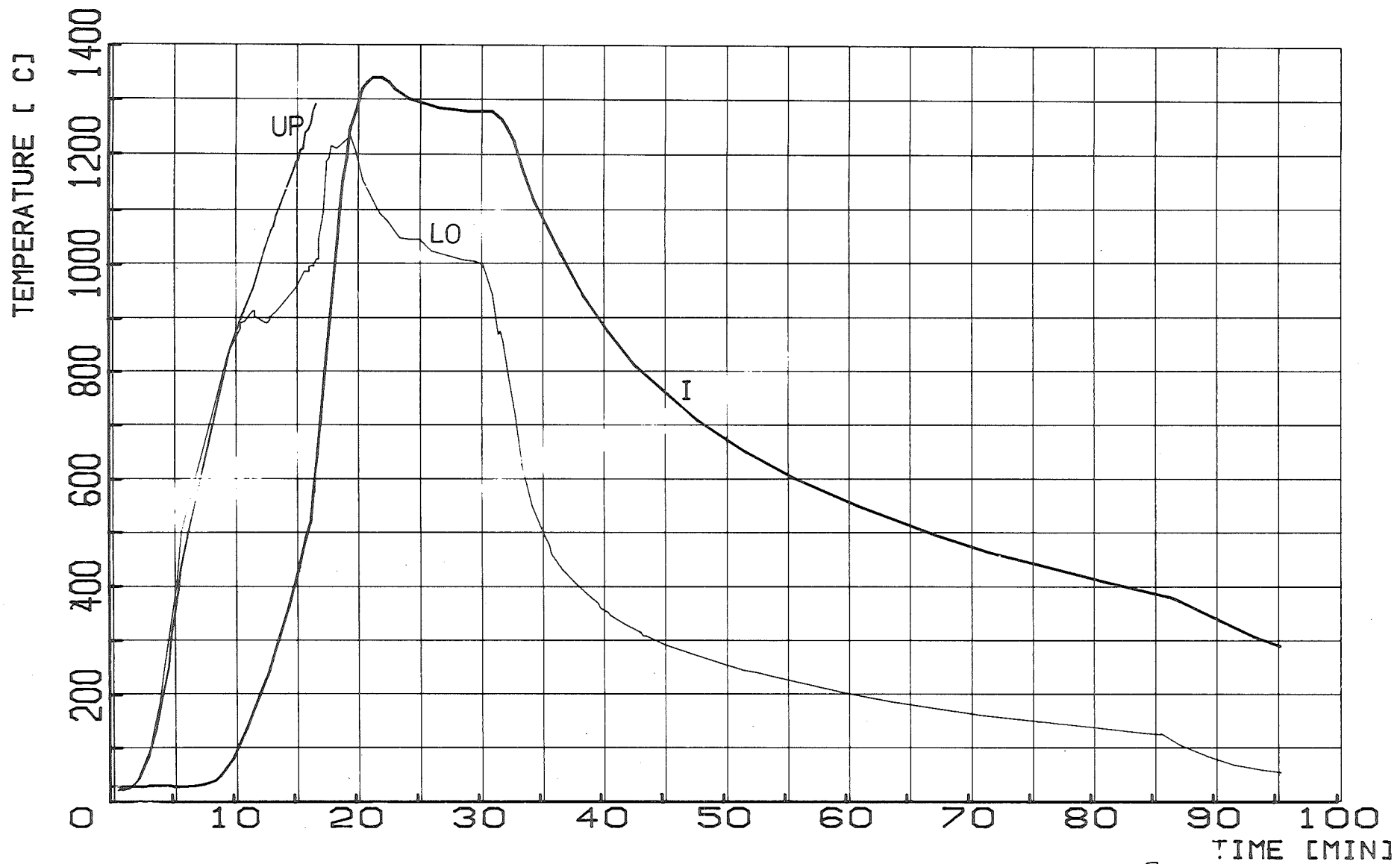


FIG.33: COMPARISON OF THE ROD TEMPERATURES AT THE 70 MM (L) AND 297 MM (H) ELEVATIONS WITH THE TEMPERATURE IN THE INSULATION (I) AT 205 MM FOR ESSI-6

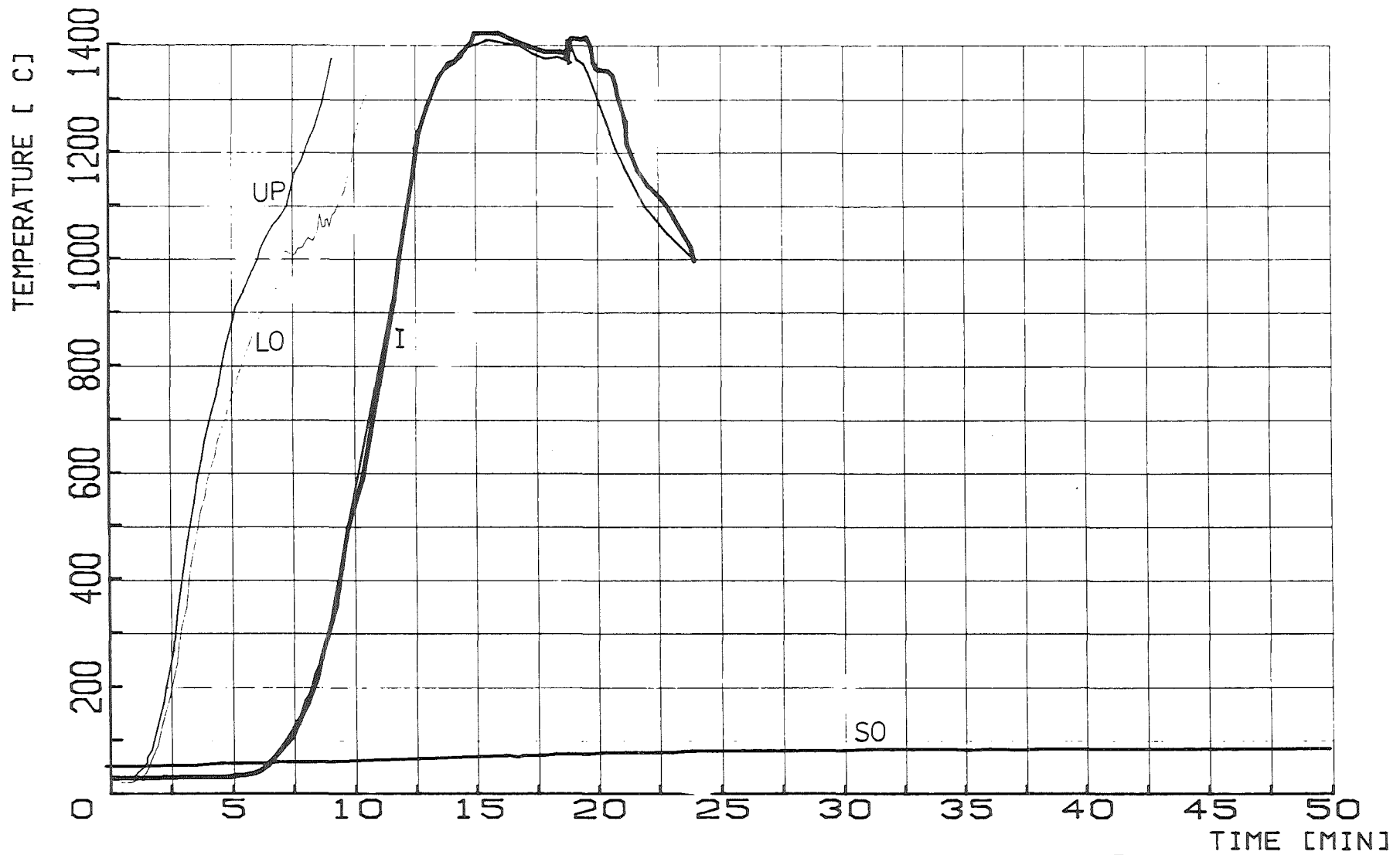


FIG. 34: TEMPERATURES ON THE ROD 70 MM ABOVE THE LOWER (LO) AND 50 MM BELOW THE UPPER (UP) END OF THE CLADDING, AND 12 MM WITHIN (I) AND ON THE OUTER SURFACE (SO) OF THE INSULATION AT 205 MM ELEVATION. ESSI-7

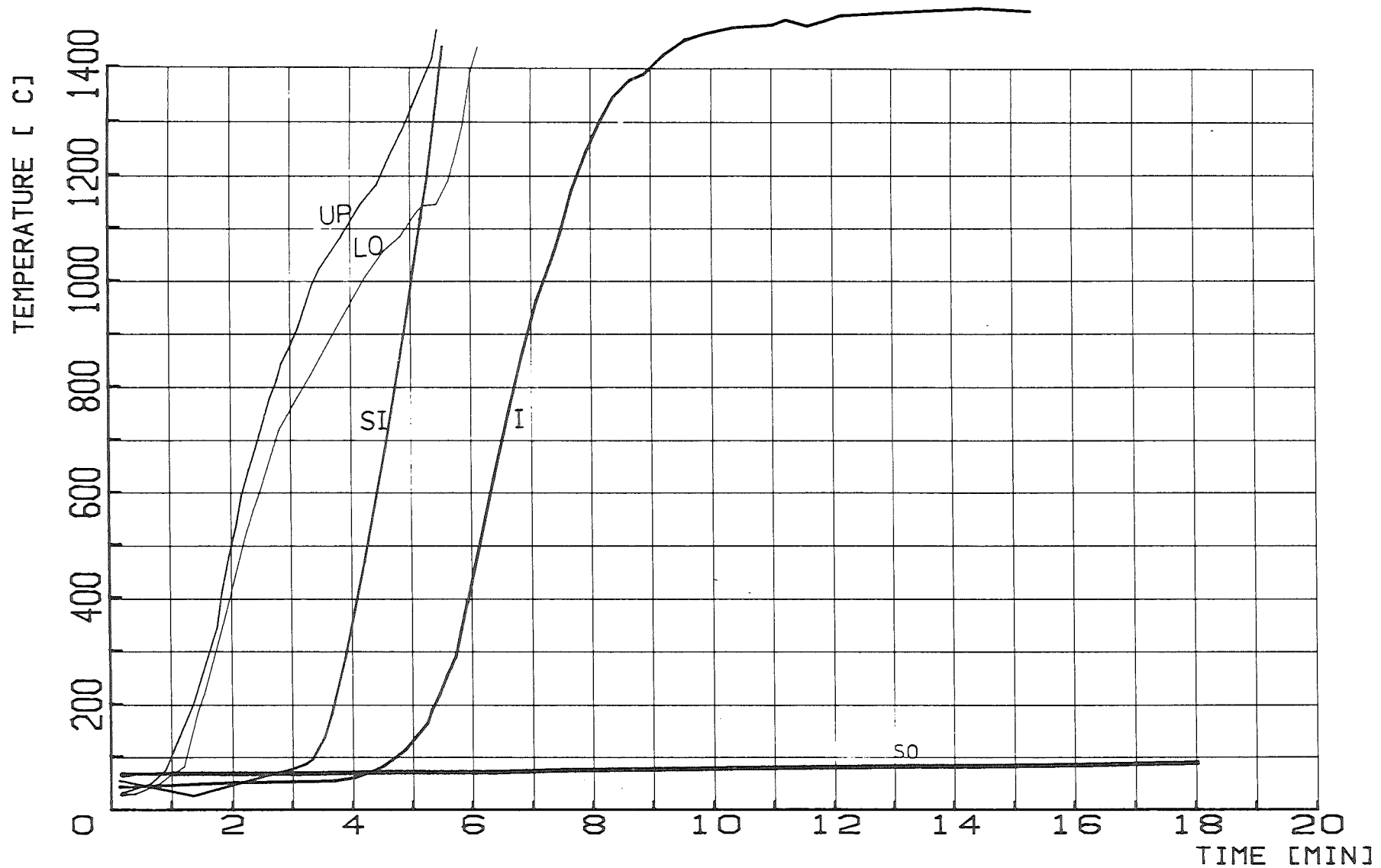
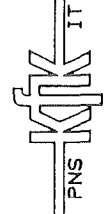
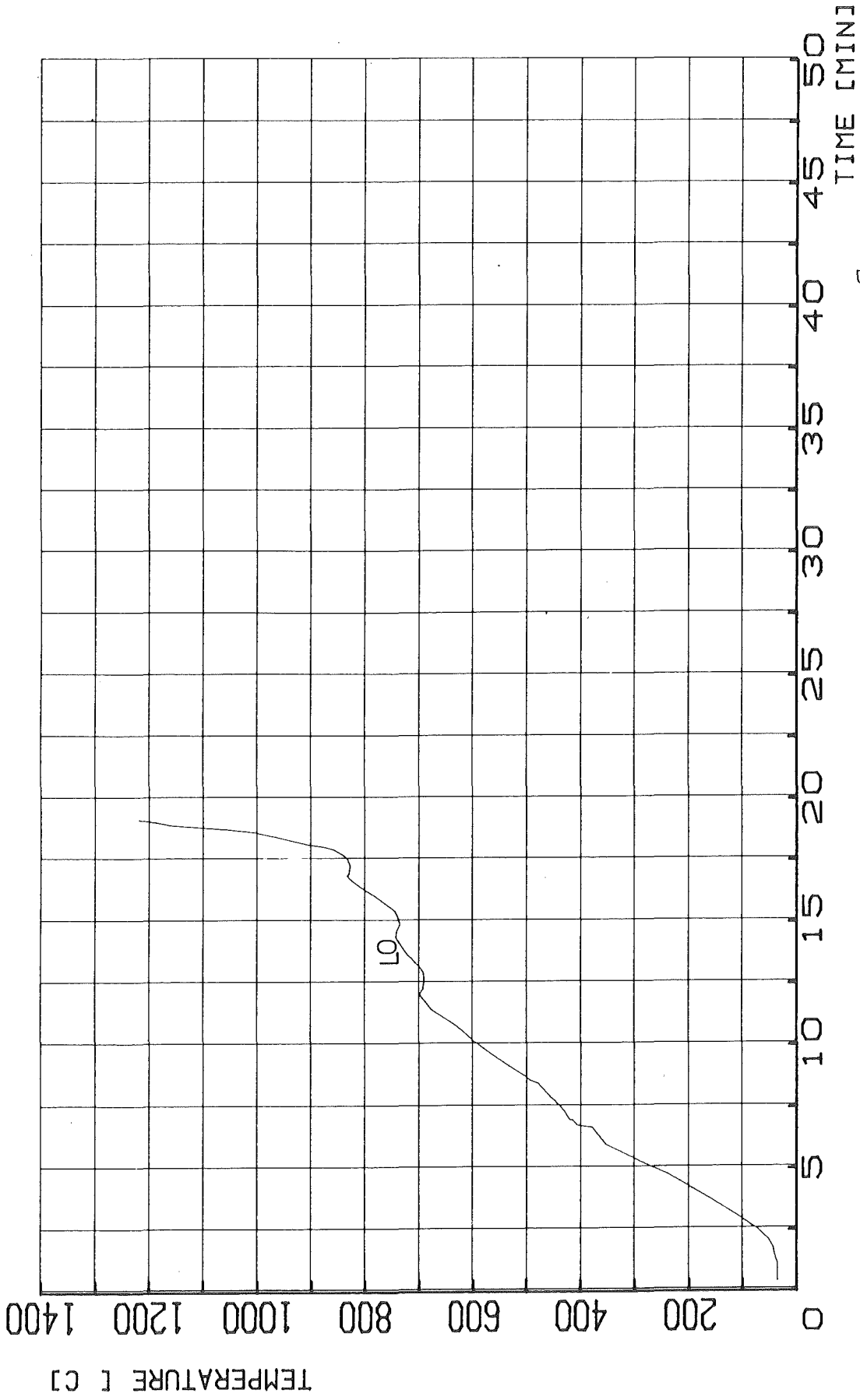


FIG. 35: TEMPERATURES ON THE ROD 70 MM ABOVE THE LOWER (LO) AND 50 MM BELOW THE UPPER (UP) END OF THE CLADDING, AND ON THE INNER SURFACE (SI), 12 MM WITHIN (I), AND ON THE OUTER SURFACE (SO) OF THE INSULATION. ESSI-8



HAGEN ET AL. KFK-REPORT 3557

FIG. 36: TEMPERATURES ON THE ROD 30 MM ABOVE THE LOWER (LO) END OF THE CLADDING. ESSI-9

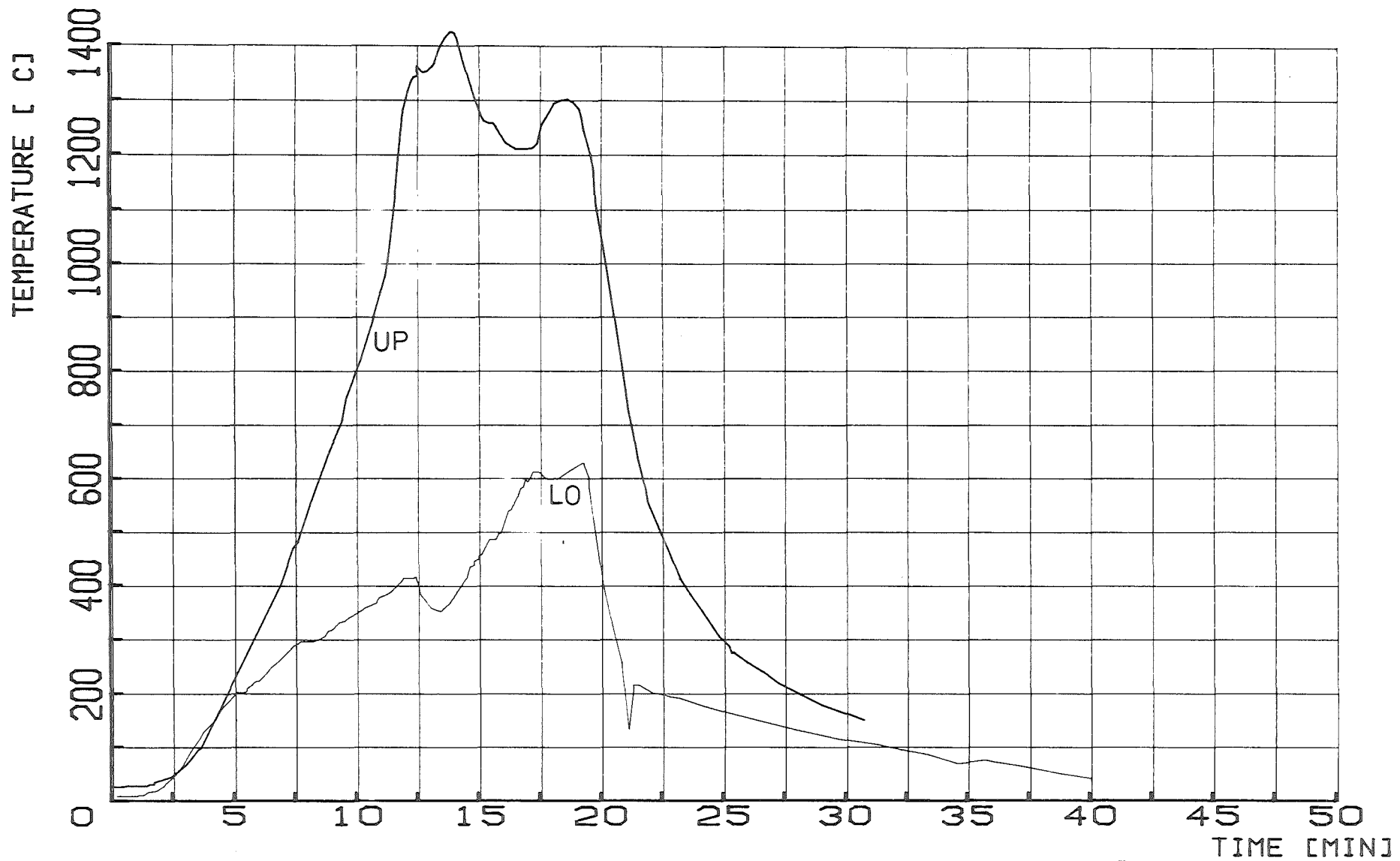


FIG.37 : TEMPERATURES ON THE ROD 30 MM ABOVE THE LOWER (LO) AND 30 MM BELOW THE UPPER (UP) END OF THE CLADDING. ESSI-10

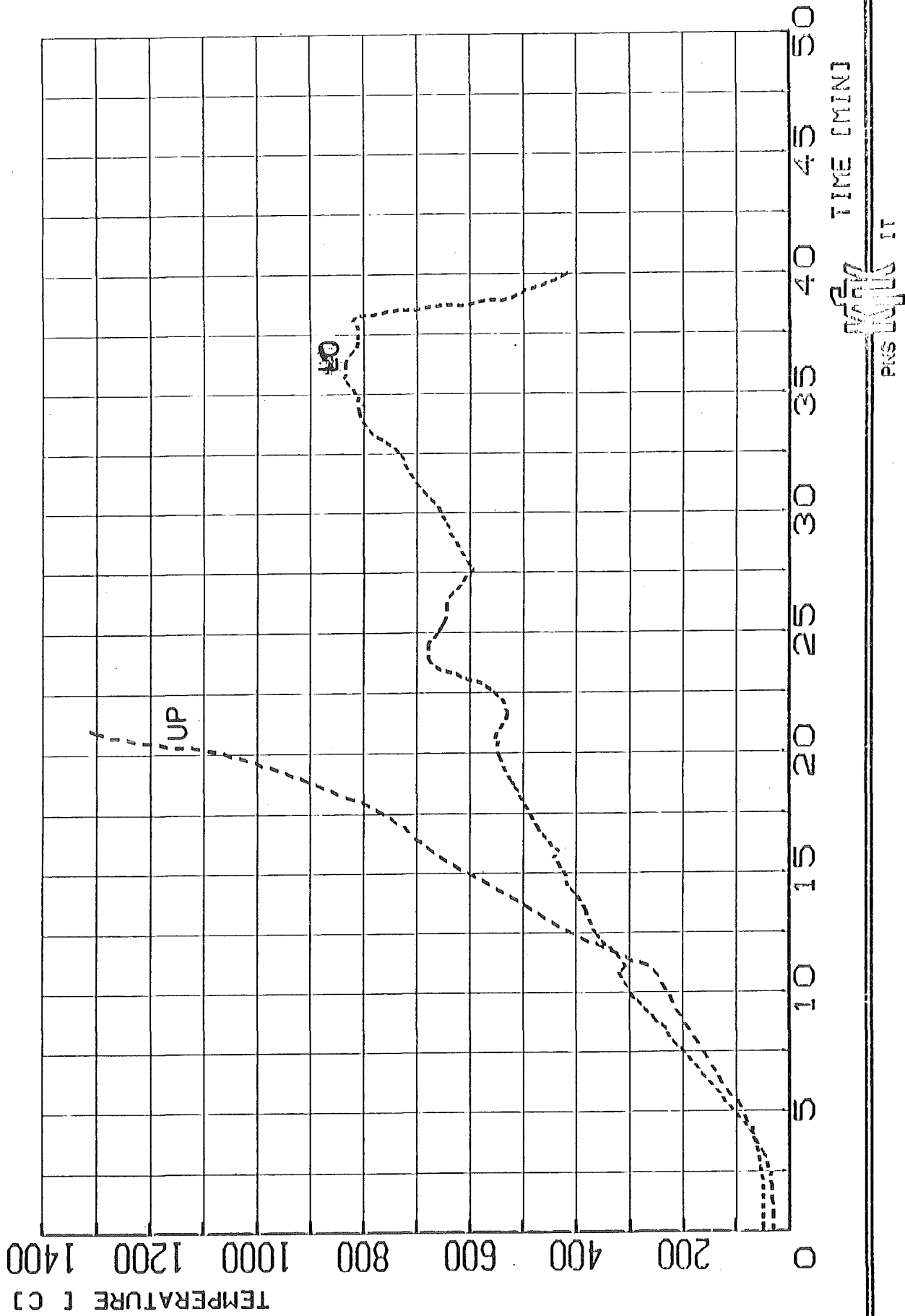


FIG. 38: TEMPERATURES ON THE ROD 30 MM ABOVE THE LOWER (LO) AND 30 MM BELOW THE UPPER (UP) END OF THE CLADDING. ESSI-11

PKS 10/11 IT

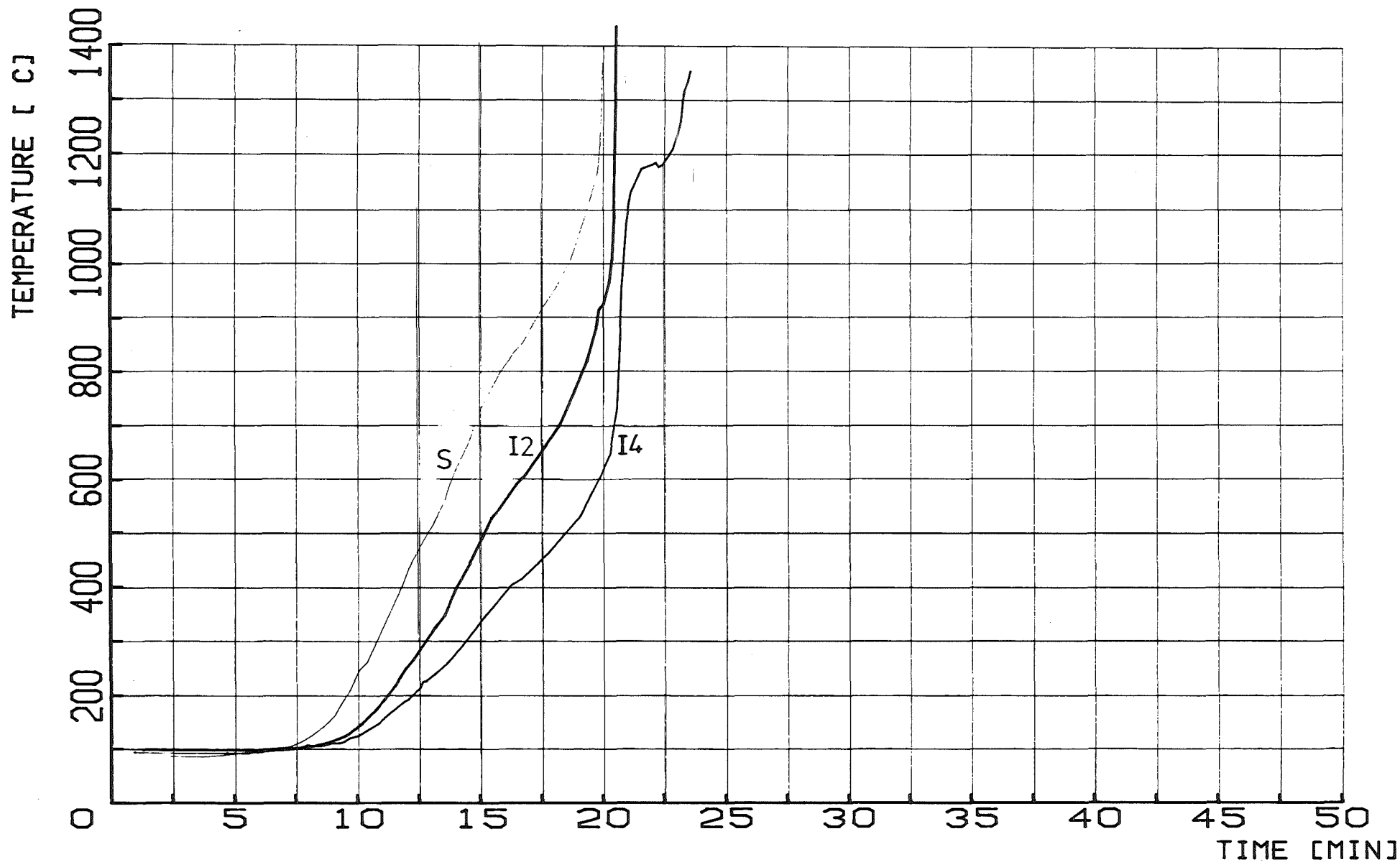


FIG.39: TEMPERATURES ON THE SHROUD (S) AND 2.4 MM (I2) AND 4.8 MM (I4) WITHIN THE INSULATION 205 MM ABOVE THE LOWER END OF THE CLADDING. ESSI-11

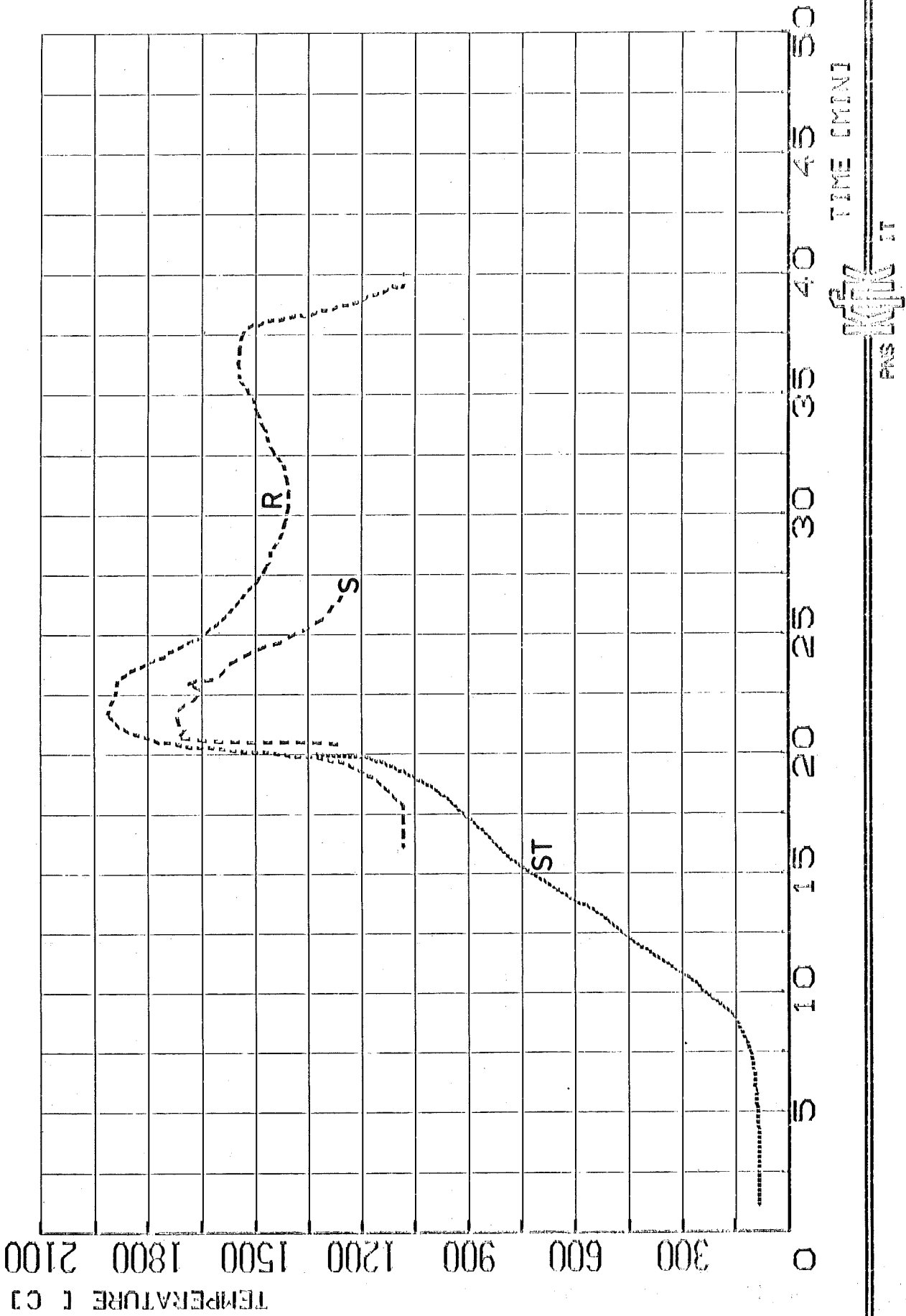
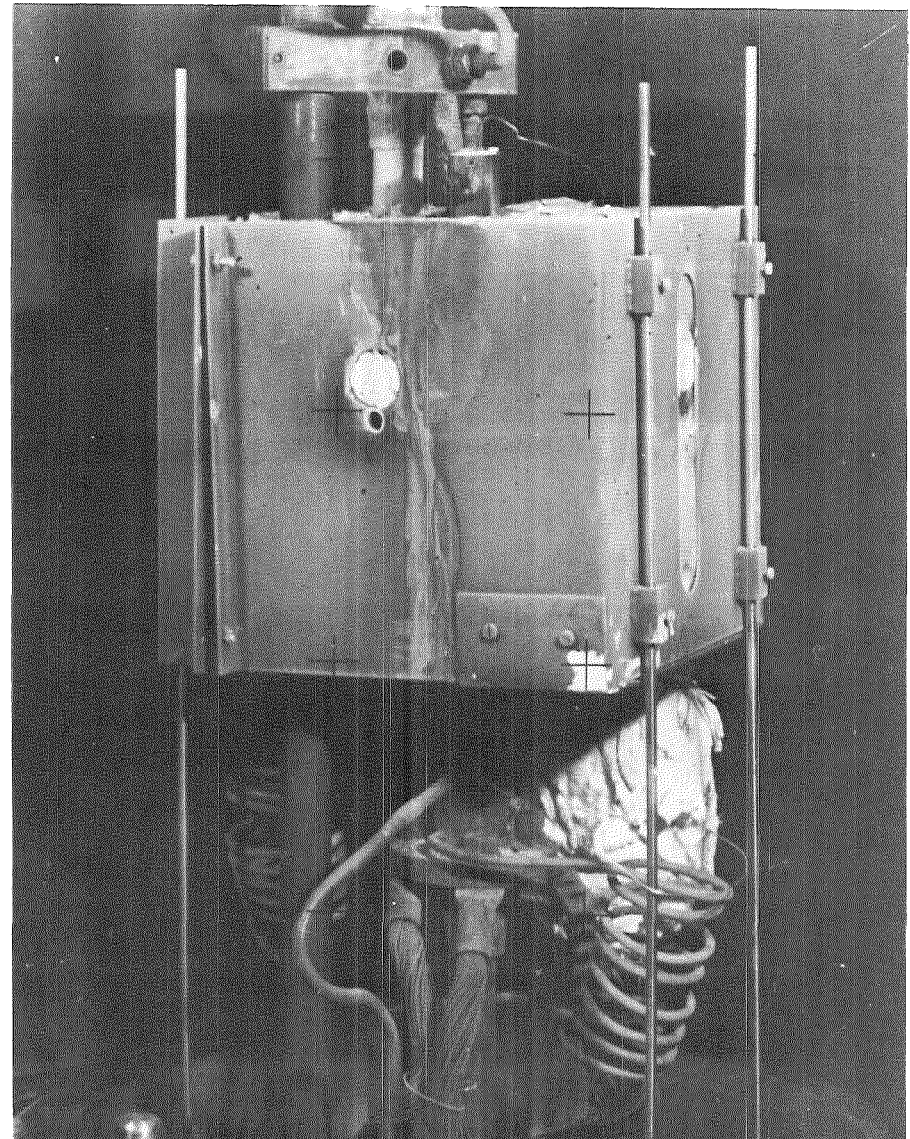
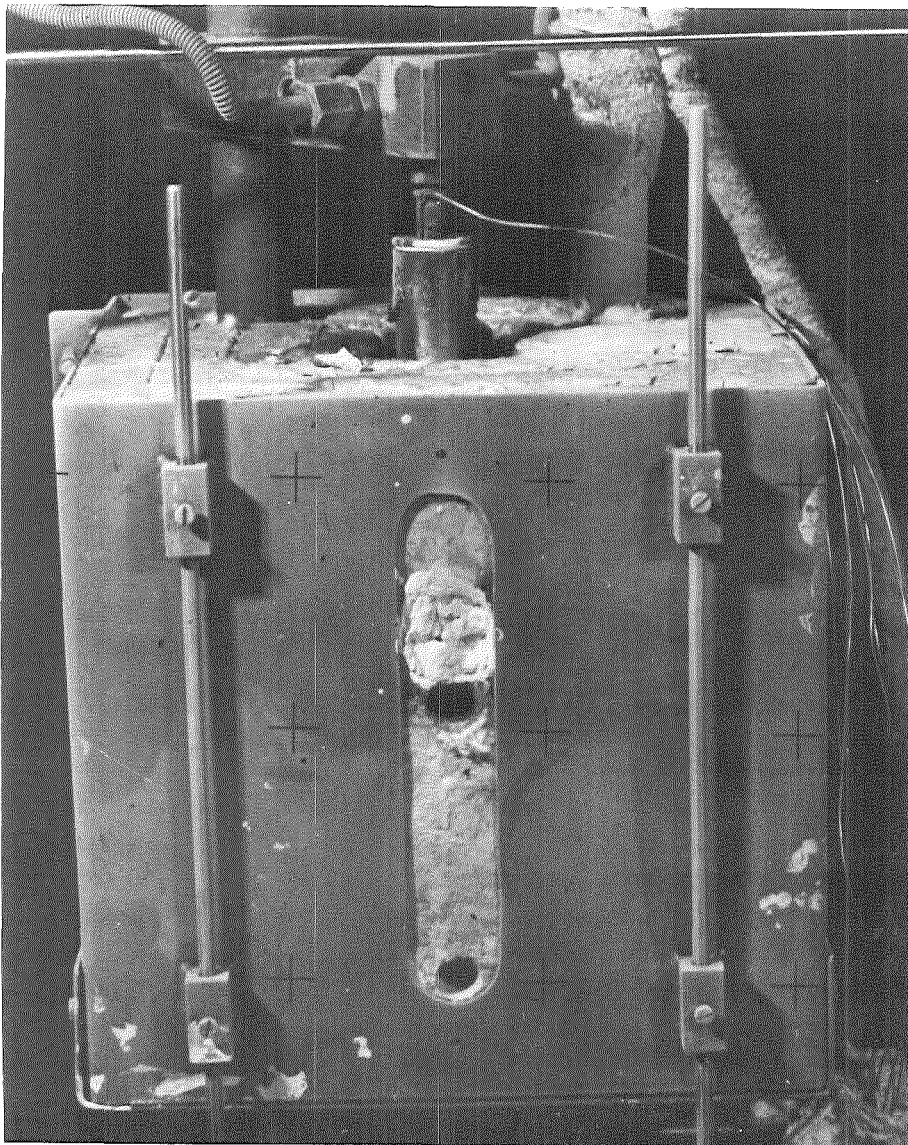


FIG. 40: TEMPERATURE ON THE SHROUD (ST) MEASURED WITH A THERMOCOUPLE COMPARED TO TEMPERATURES ON THE SHROUD (S) AND ROD (R) MEASURED WITH TWO COLOR PYROMETERS 205 MM ABOVE THE LOWER END OF THE CLADDING. ESS1-11

PAS WJK IT



HAGEN ET AL. KFK-REPORT 3557

PNS **KfK** IT

FIG.41 : EXPERIMENT ARRANGEMENT SHOWING THE INSULATION IN PLACE
AROUND THE SHROUD AND FUEL ROD SIMULATOR

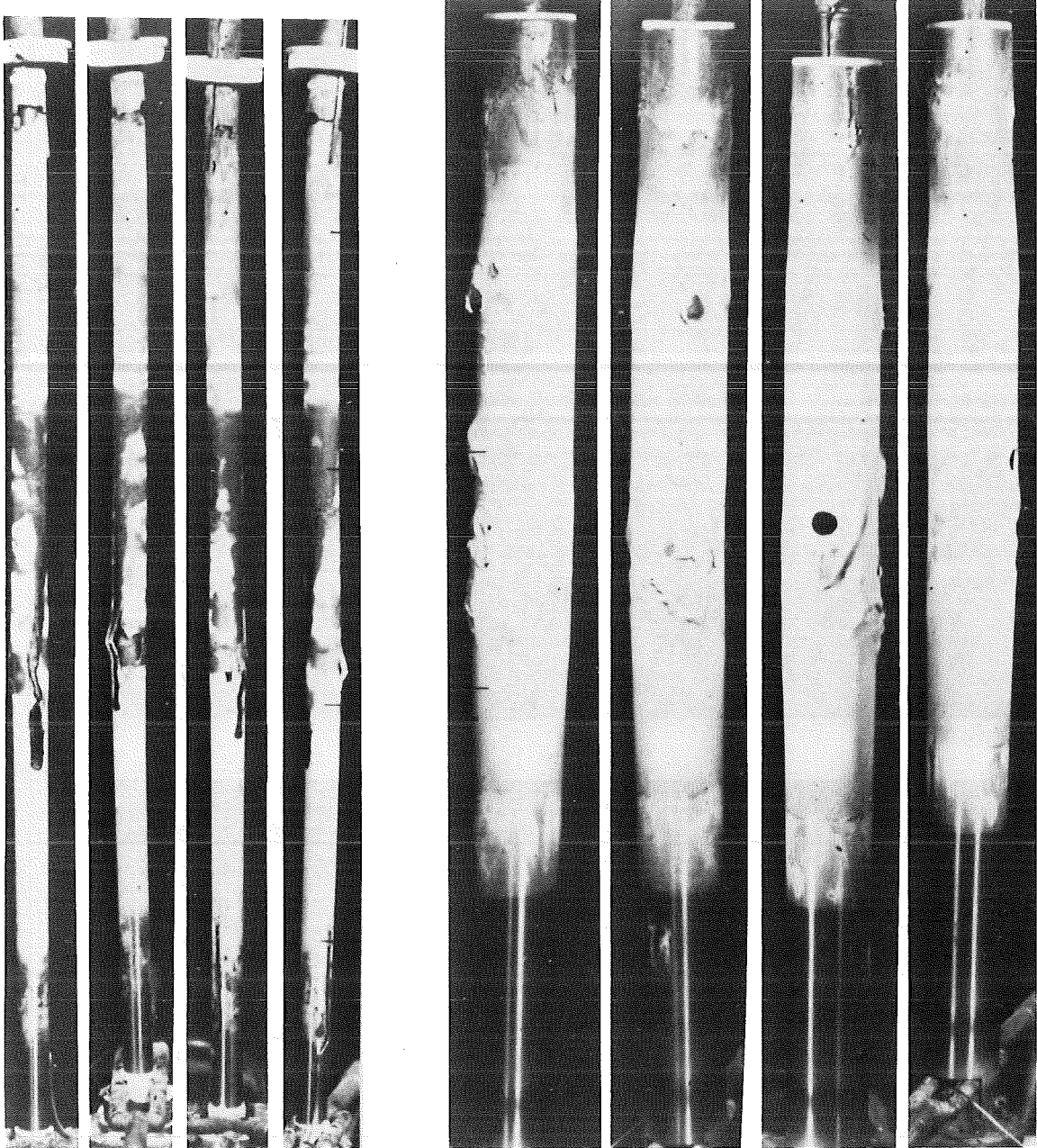


FIG.42 : POSTTEST APPEARANCE OF THE ESSI-4 FUEL ROD SIMULATOR AND SHROUD

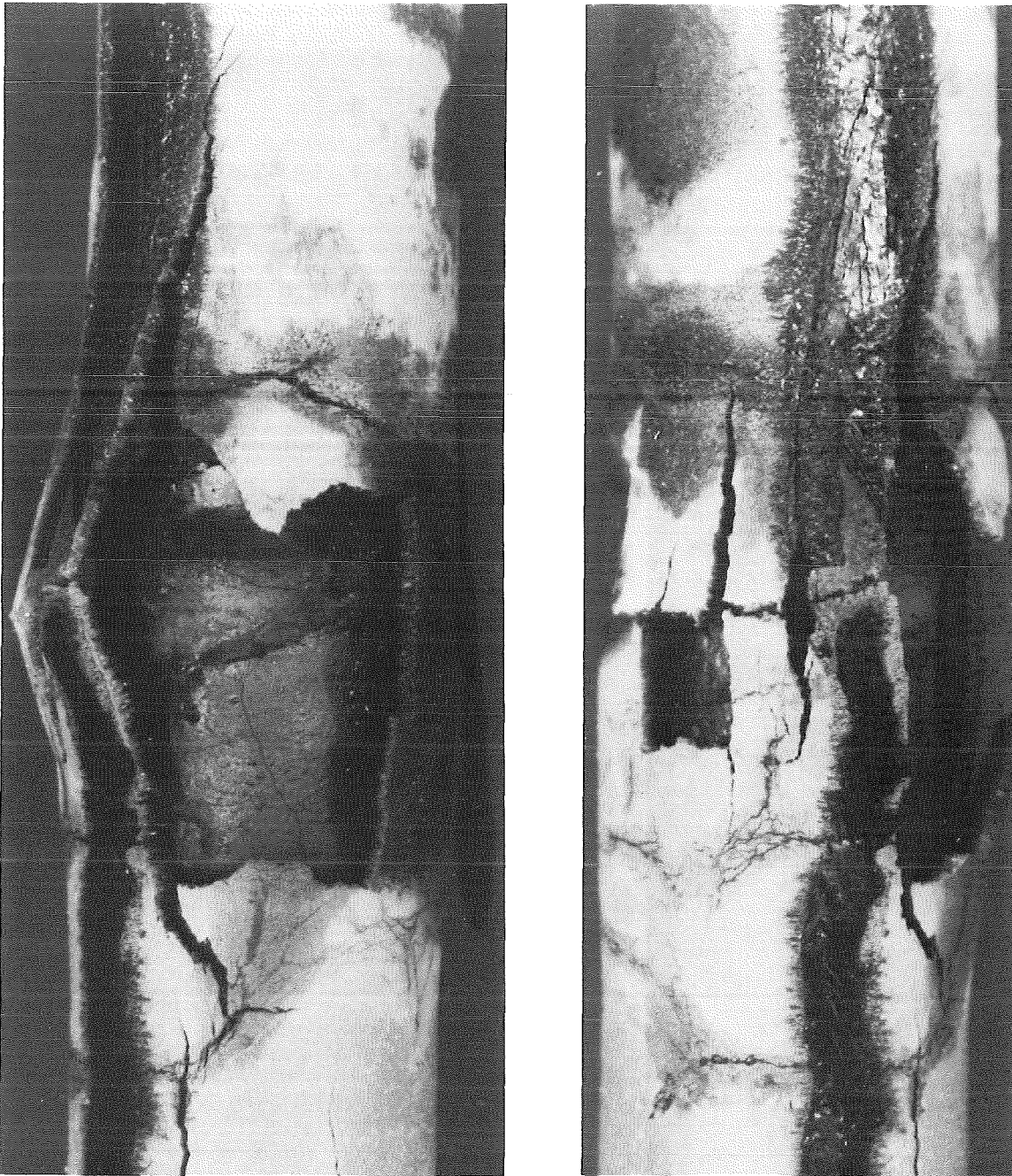


FIG.43 : DETAILS OF THE ESSI-4 POSTTEST APPEARANCE
NEAR THE MIDDLE OF THE ROD

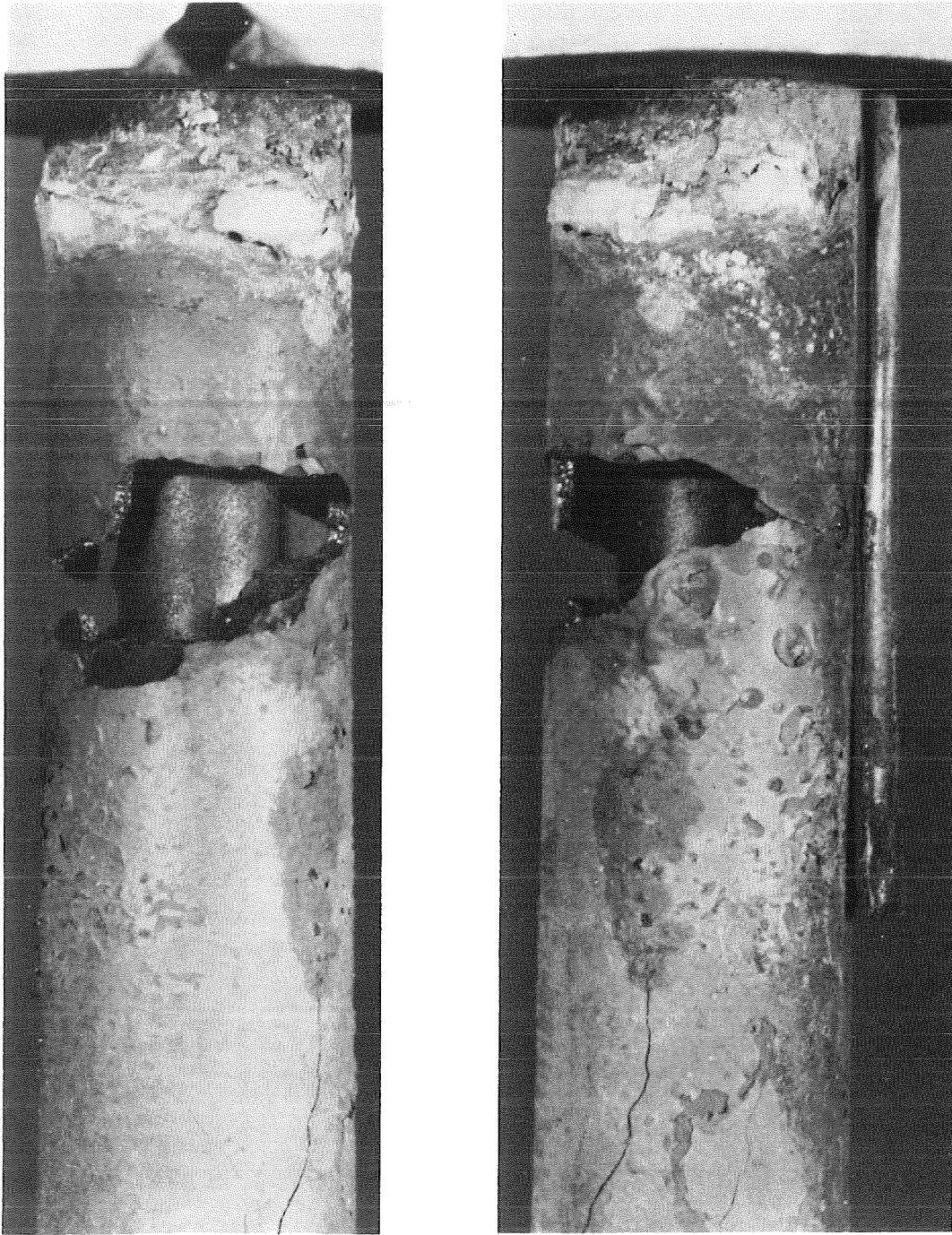


FIG.44 : DETAILS OF THE ESSI-4 POSTTEST APPEARANCE
NEAR THE TOP OF THE ROD



FIG.45: DETAILS OF THE ESSI-4 SHROUD SHOWING TWO SIDED OXIDATION

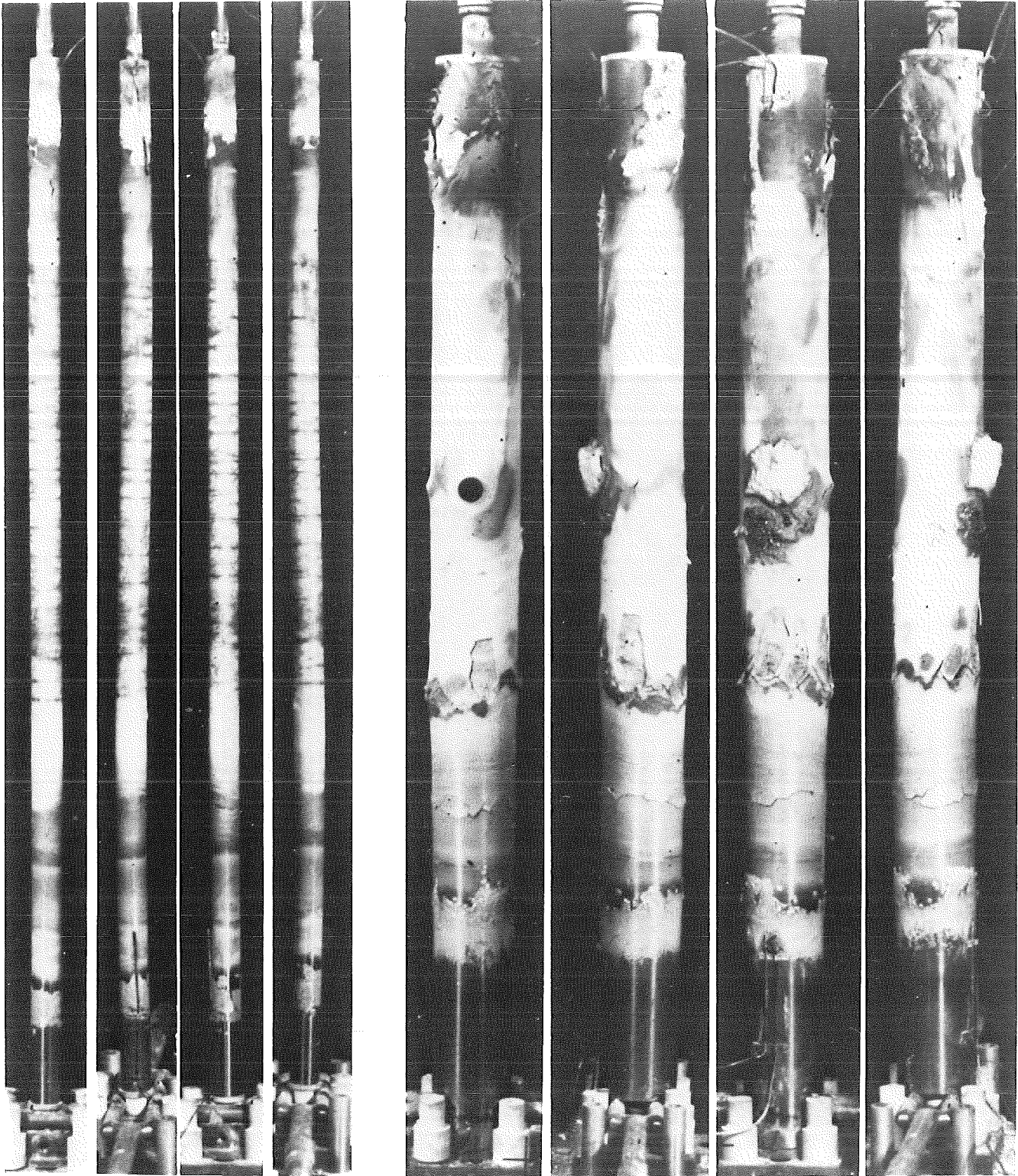


FIG.46 : POSTTEST APPEARANCE OF THE ESSI-4/5 FUEL ROD SIMULATOR AND SHROUD

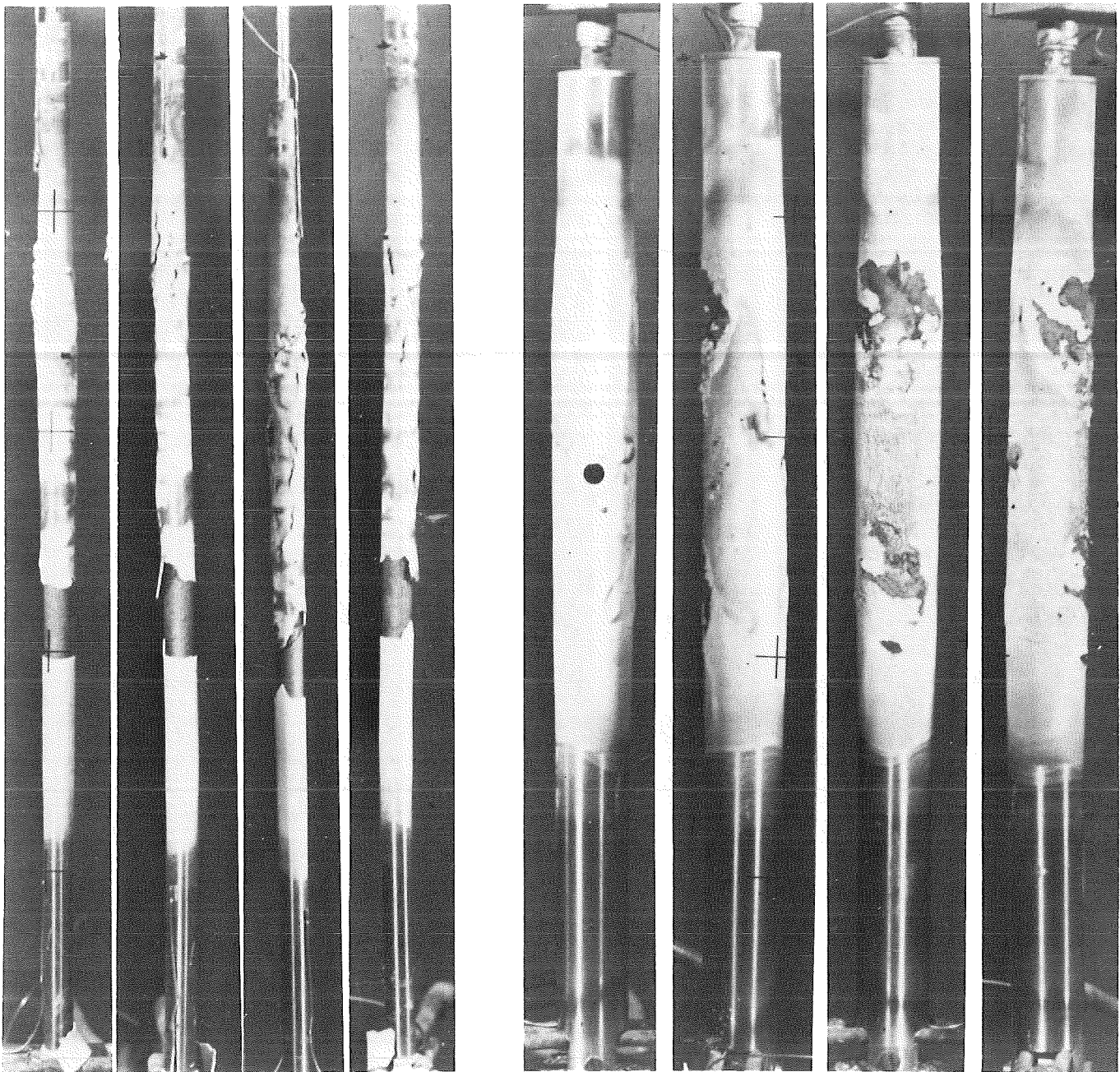


FIG.47 : POSTTEST APPEARANCE OF THE ESSI-5 FUEL ROD SIMULATOR AND SHROUD

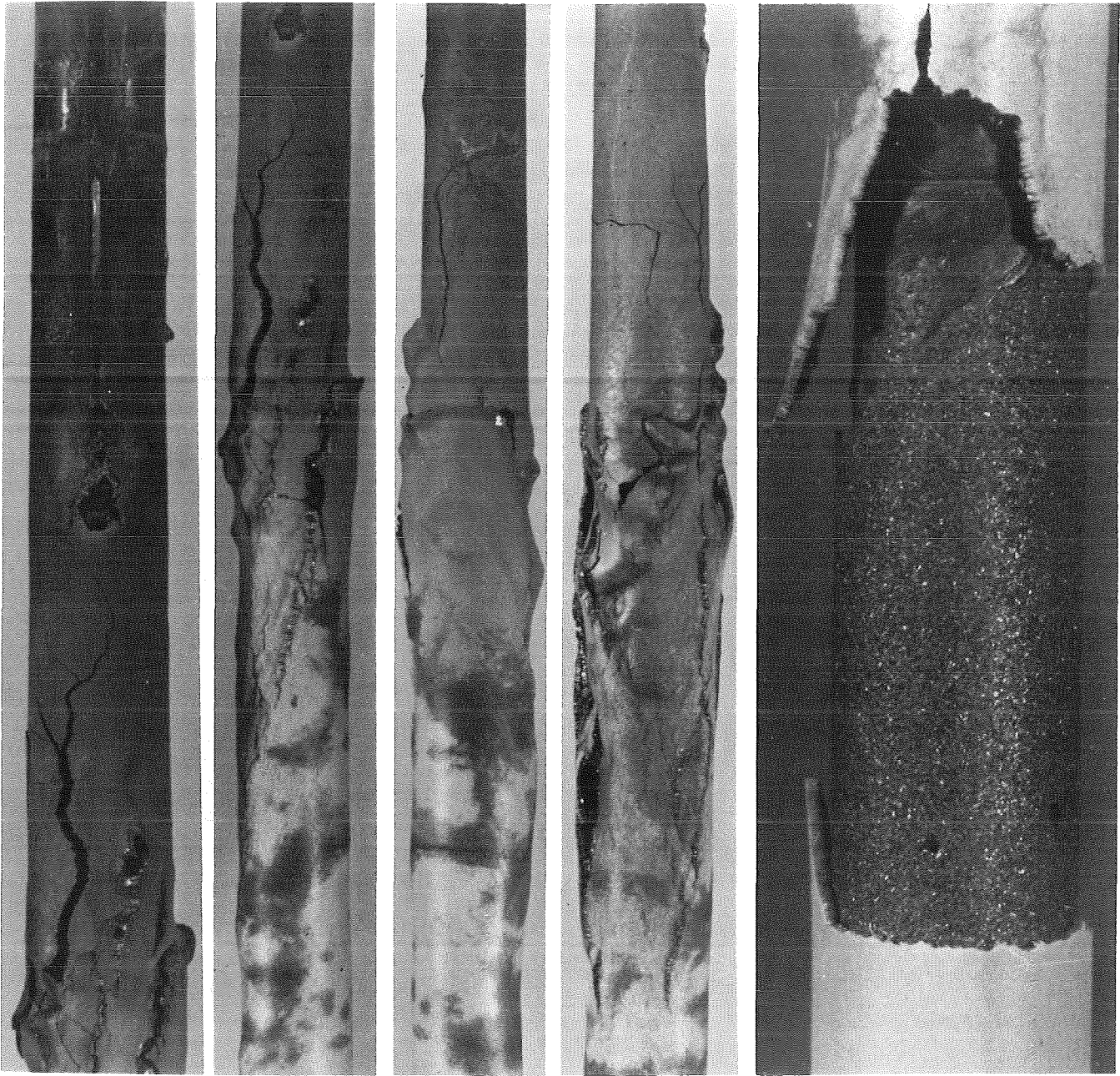


FIG.48 : DETAILS OF THE ESSI-5 POSTTEST APPEARANCE

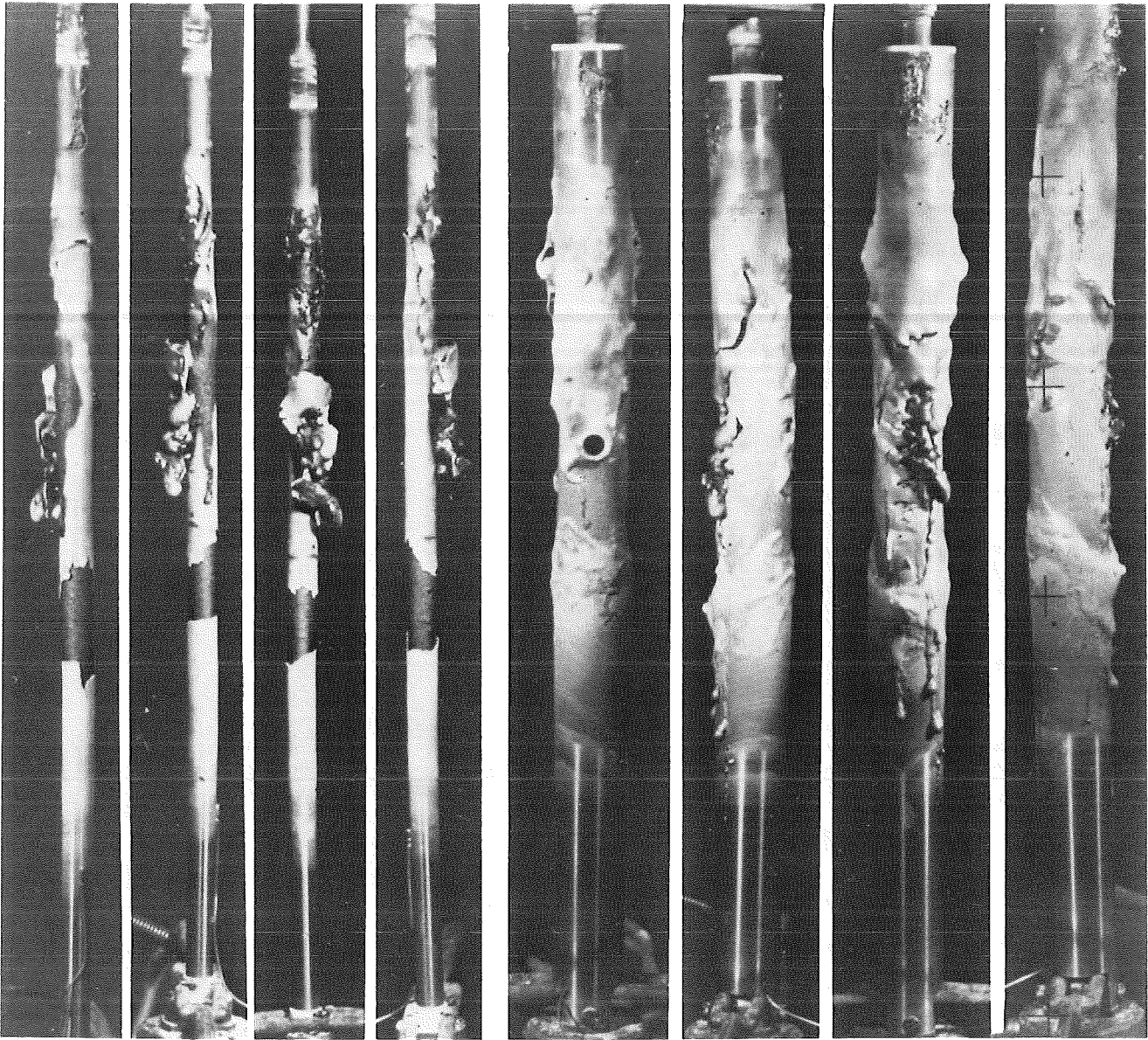


FIG.49 : POSTTEST APPEARANCE OF THE ESSI-6 FUEL ROD SIMULATOR AND SHROUD

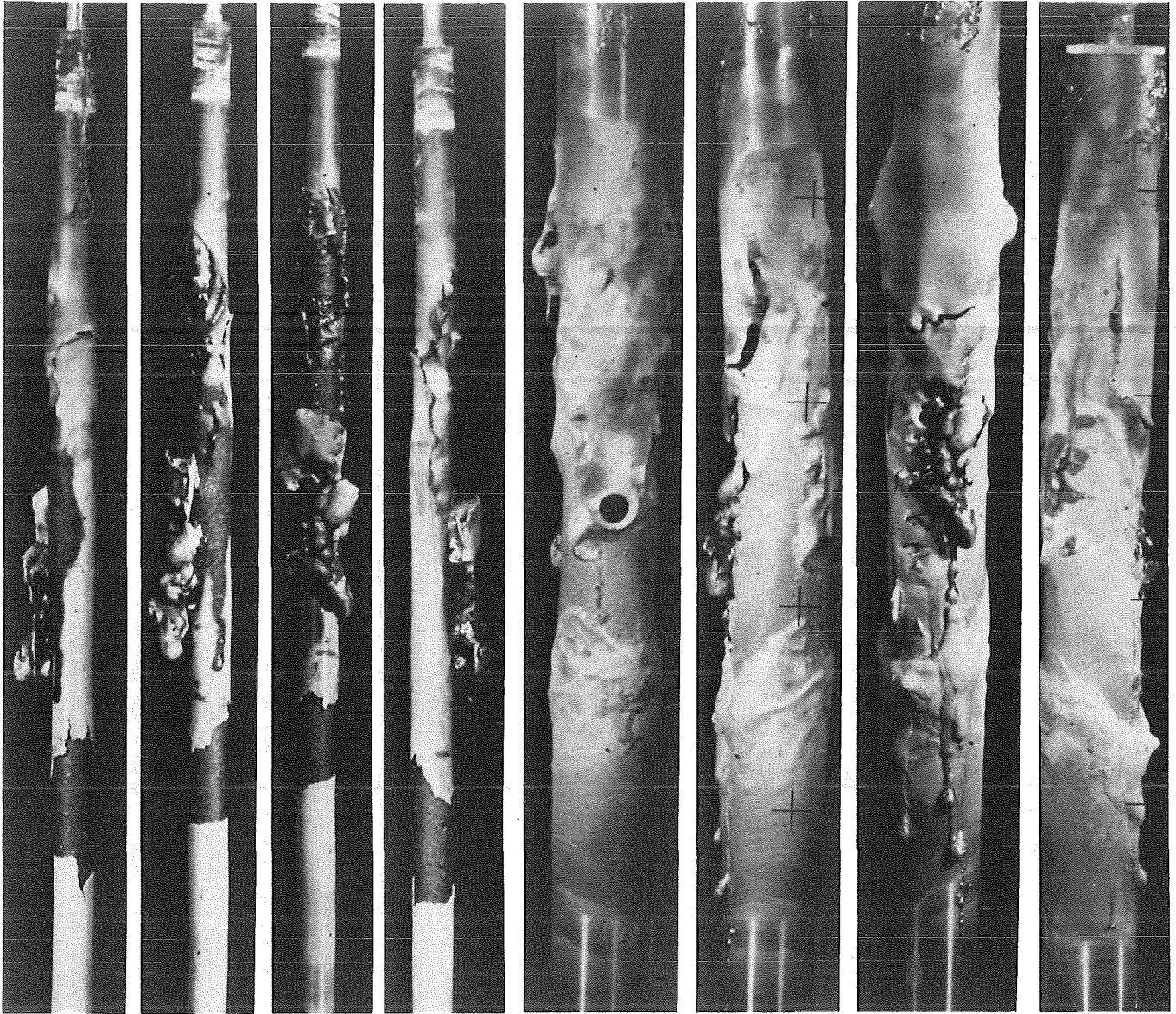


FIG.50 : DETAILS OF THE ESSI-6 FUEL ROD SIMULATOR AND SHROUD

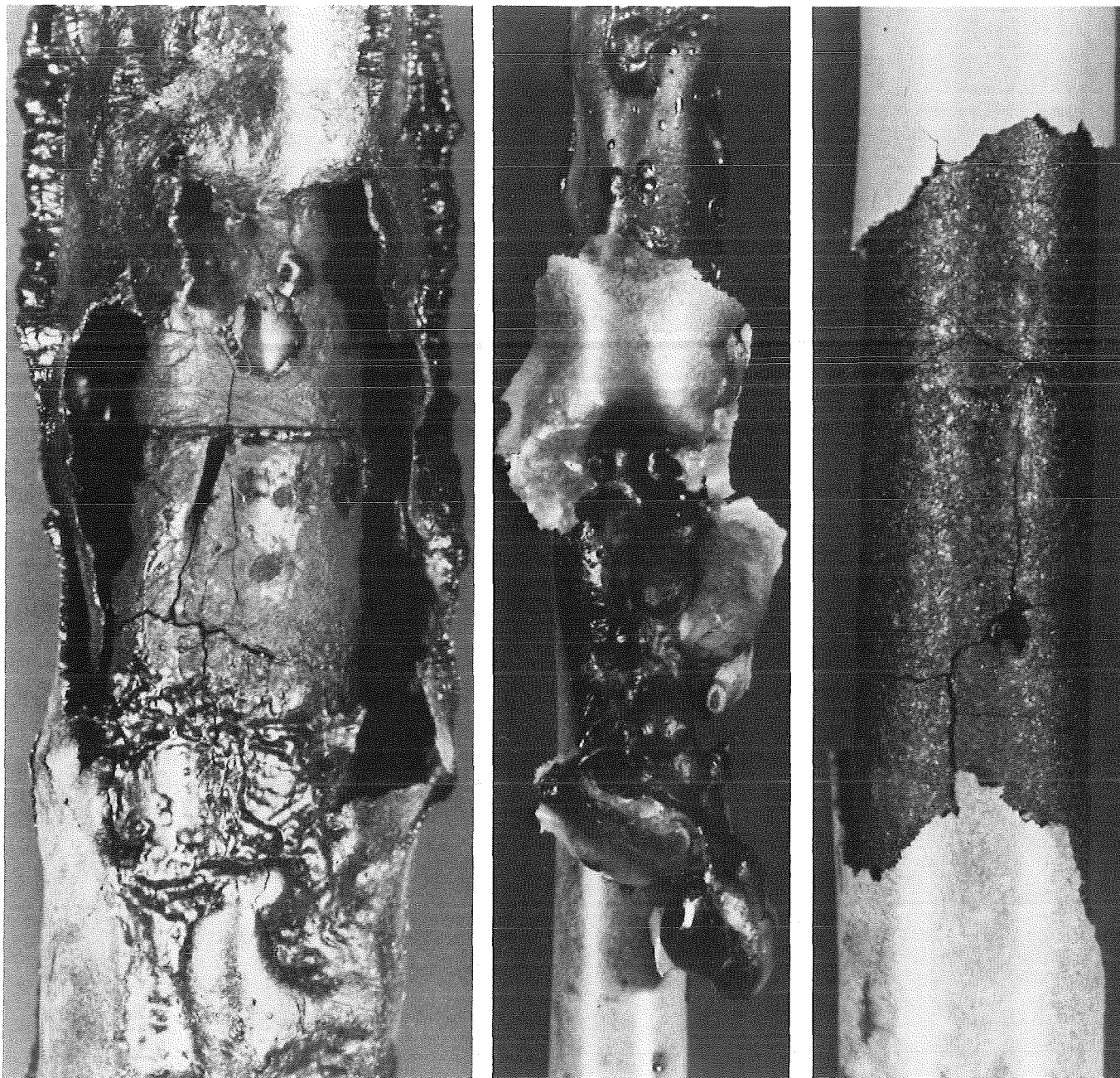


FIG.51 : ENLARGEMENT OF THE ESSI-6 FUEL ROD SIMULATOR

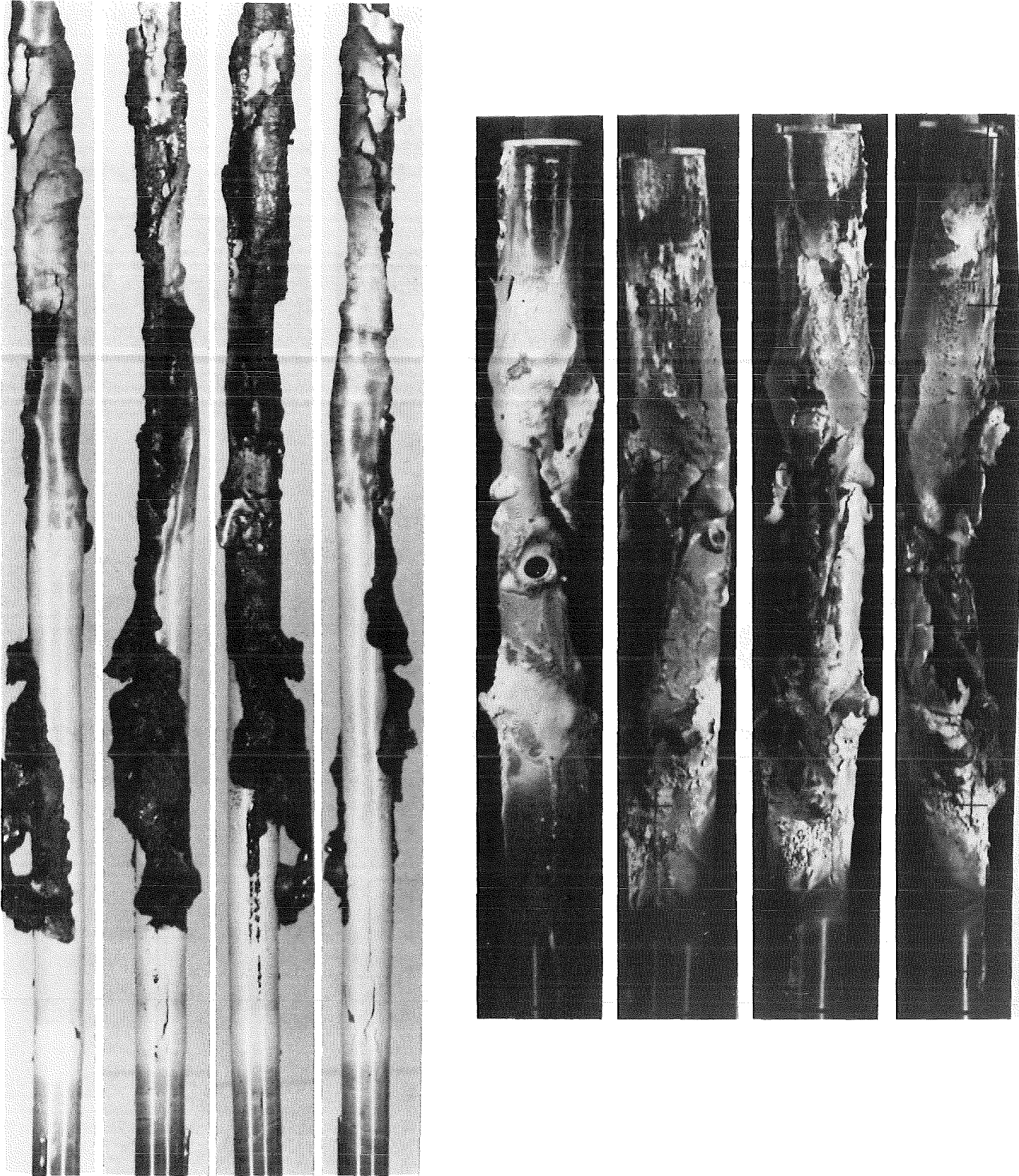


FIG. 52 : POSTTEST APPEARANCE OF THE ESSI-7 FUEL ROD SIMULATOR AND SHROUD



FIG. 53: DETAILS OF THE ESSI-7 FUEL ROD SIMULATOR AND SHROUD

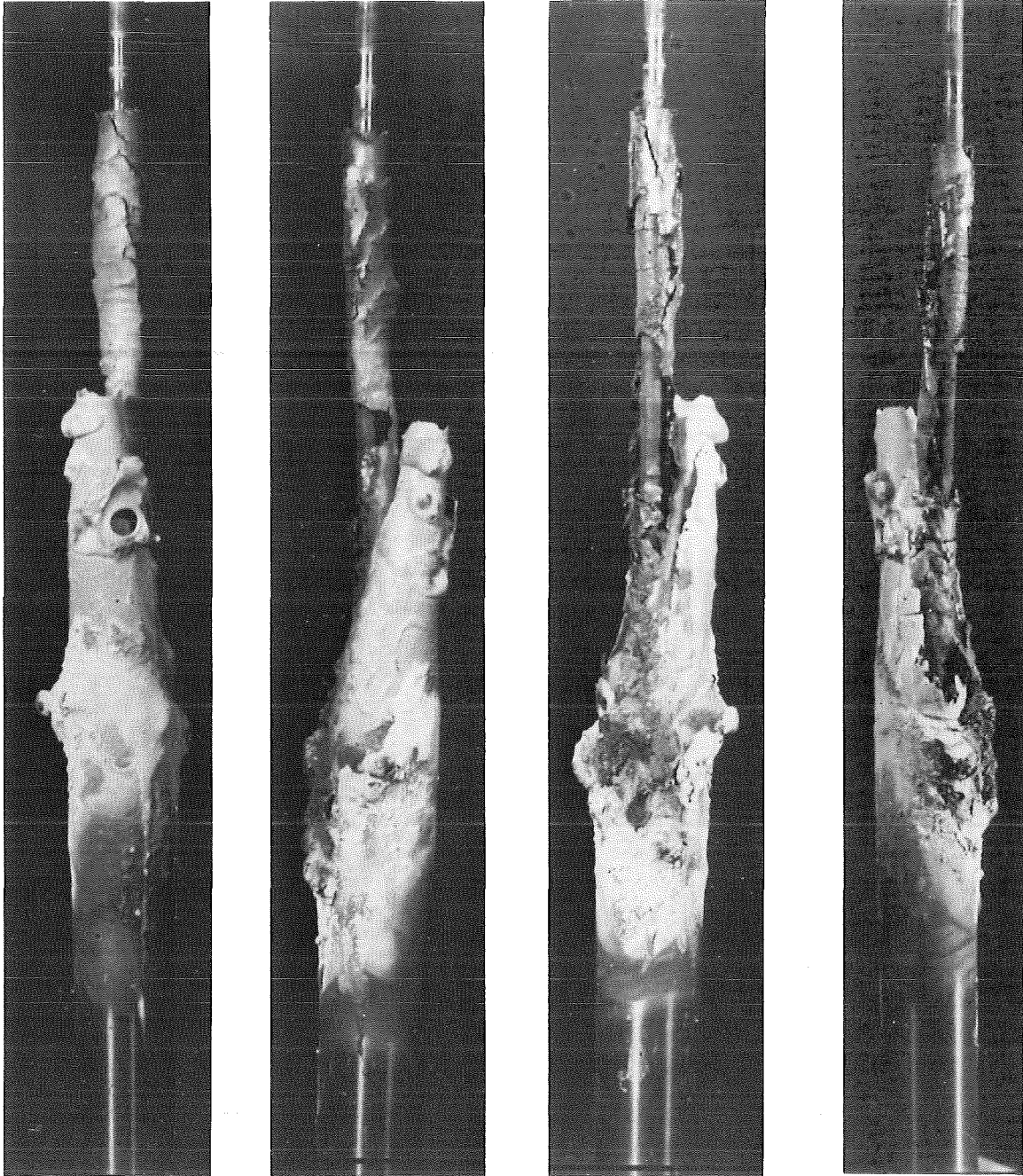


FIG.54: POSTTEST APPEARANCE OF THE ESSI-7 FUEL ROD SIMULATOR AFTER REMOVAL OF THE UPPER PART OF THE SHROUD

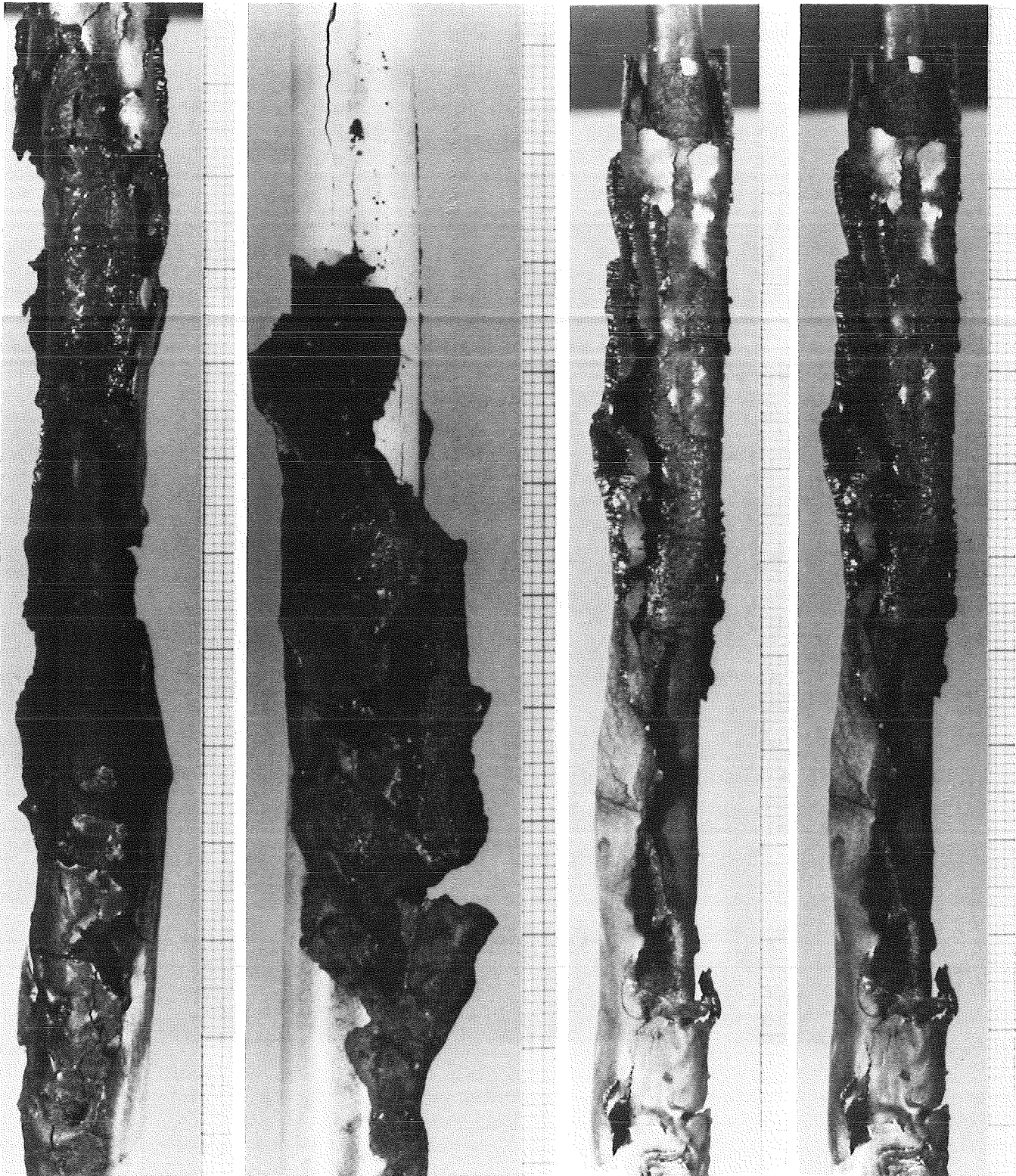


FIG.55 : DETAILS OF THE ESSI-7 FUEL ROD SIMULATOR

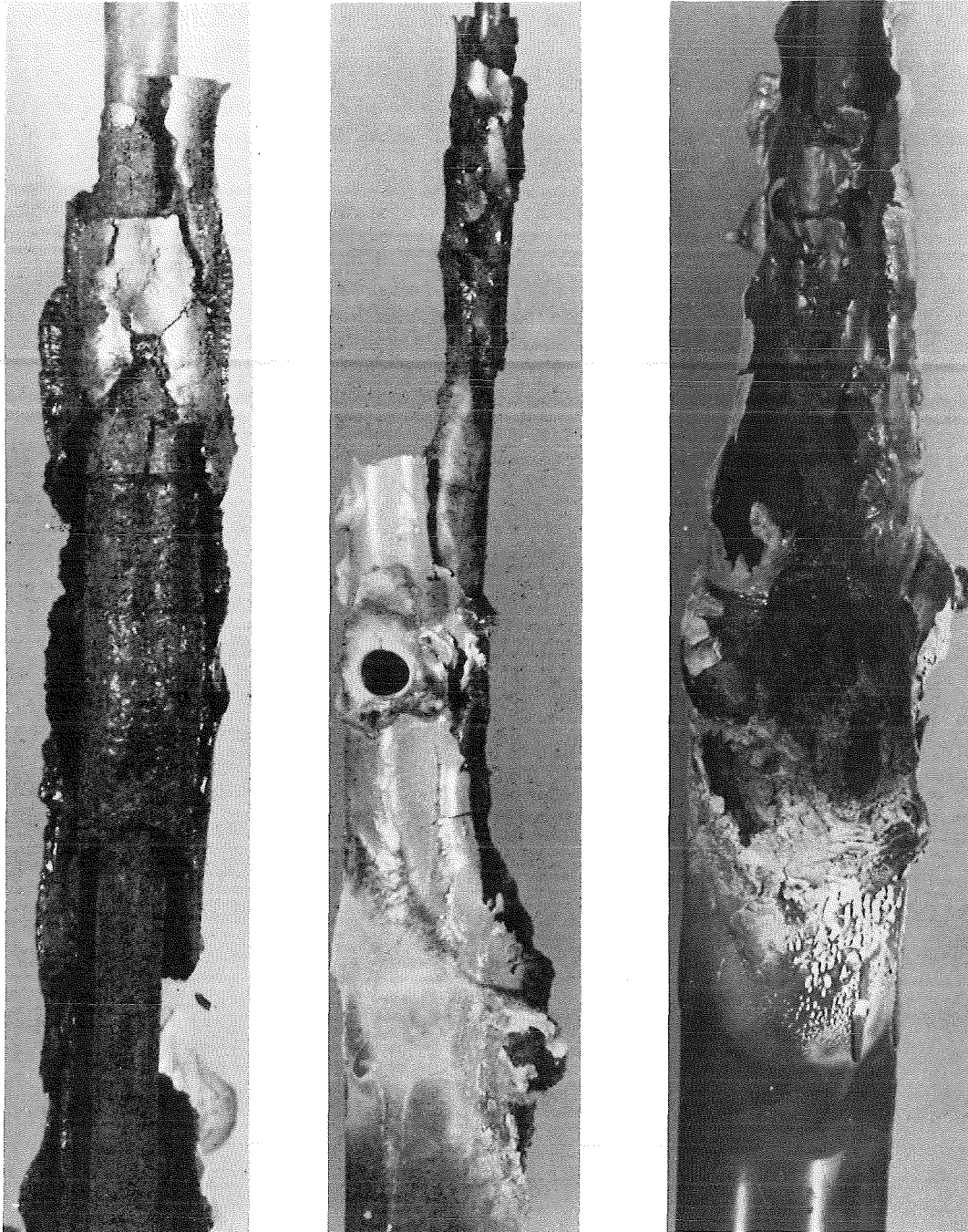


FIG.56: ENLARGEMENT OF THE ESSI-7 FUEL ROD SIMULATOR AND SHROUD

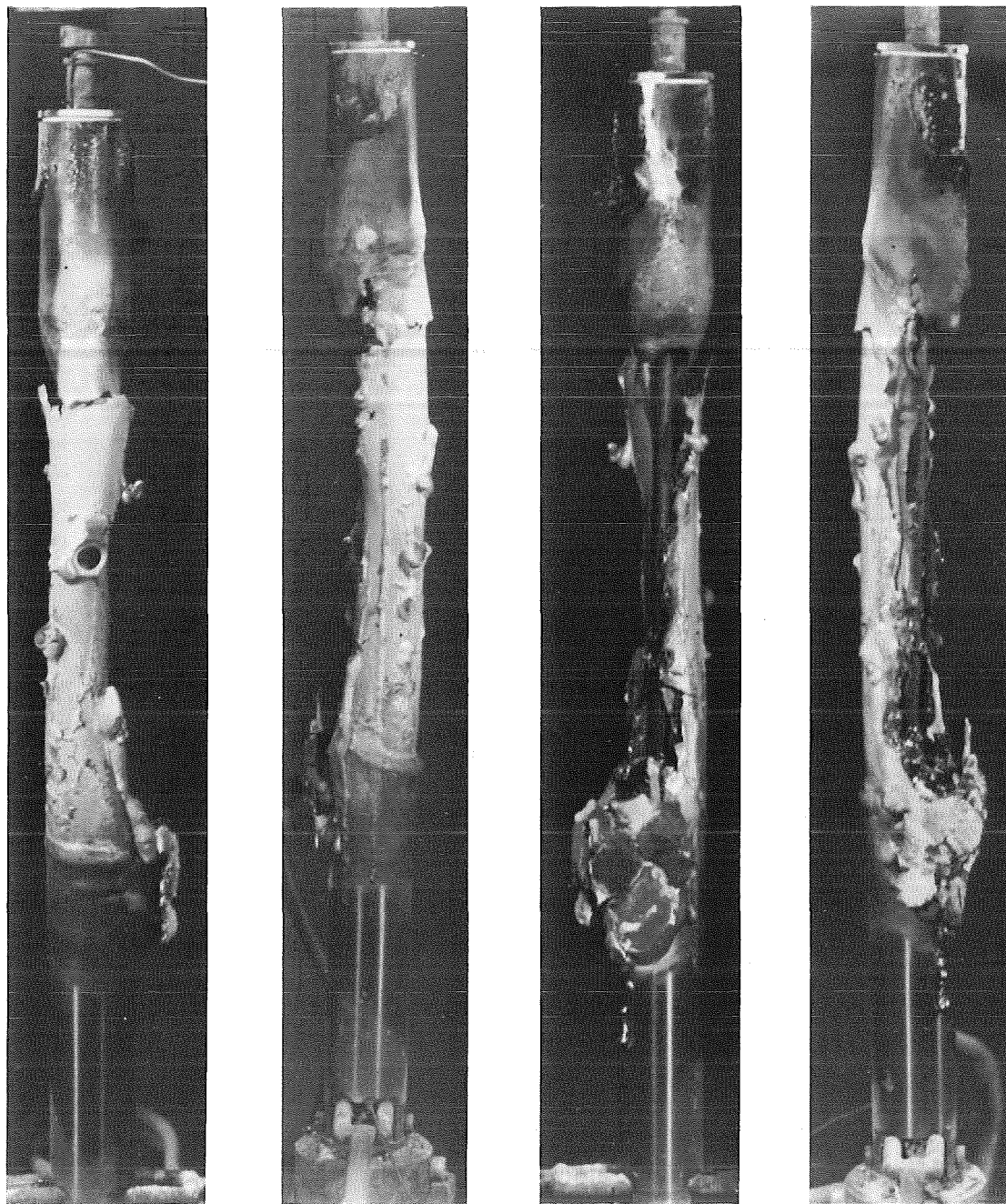


FIG. 57 : POSTTEST APPEARANCE OF THE ESSI-8 SHROUD

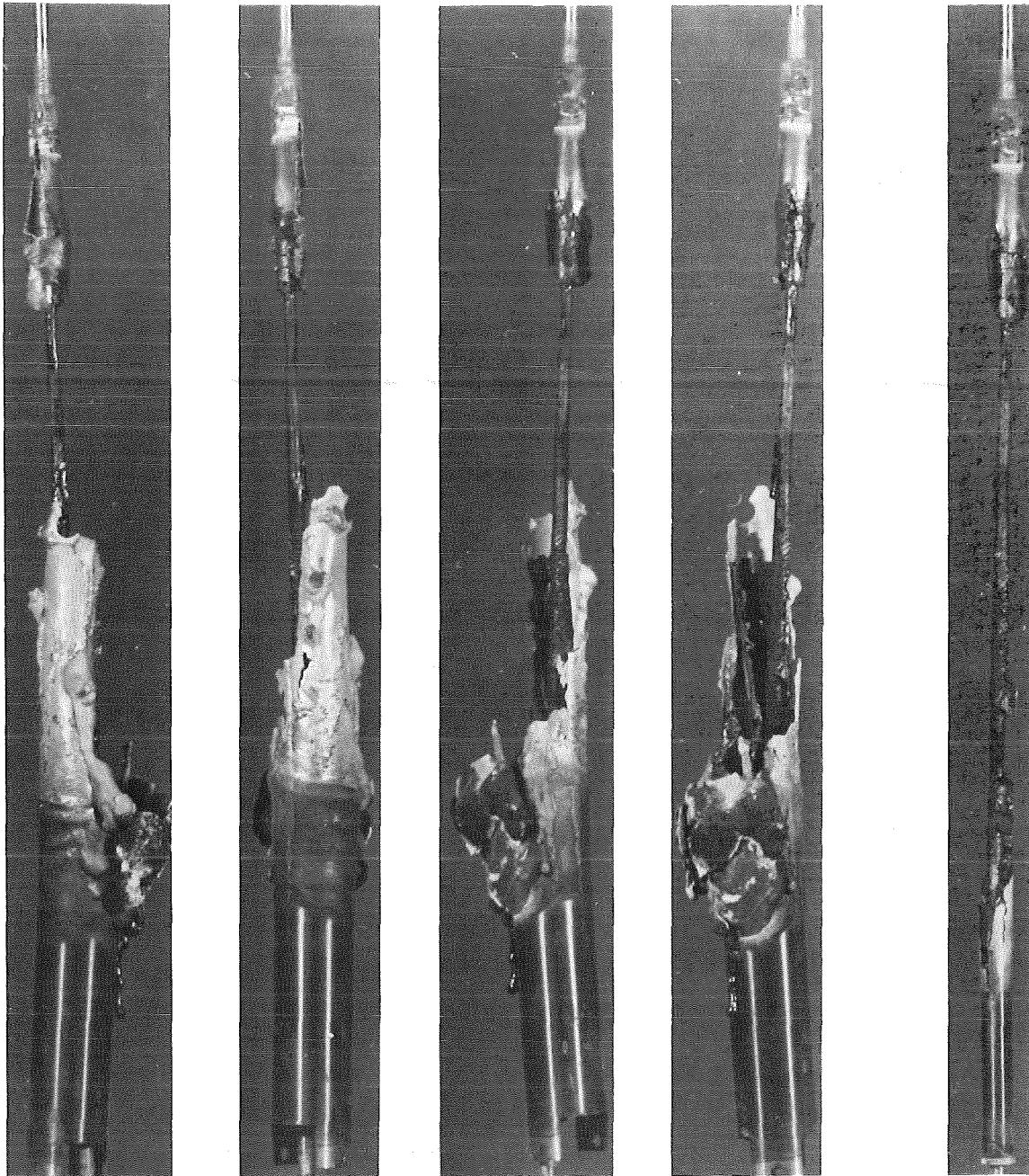


FIG. 58: POSTTEST APPEARANCE OF THE ESSI-8 FUEL ROD SIMULATOR
AFTER DISMANTLING

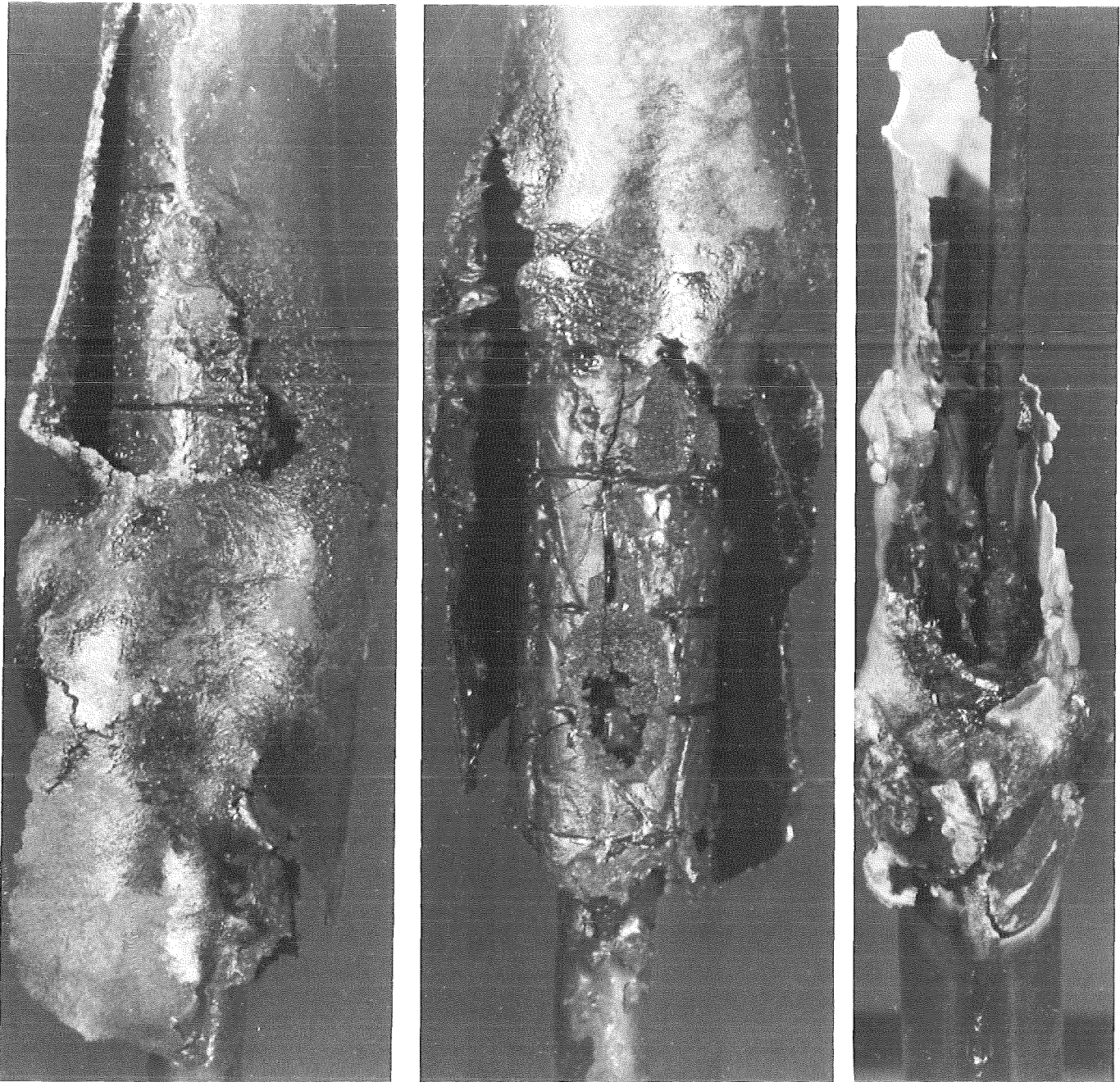


FIG.59 : DETAILS OF THE ESSI-8 FUEL ROD SIMULATOR AND SHROUD

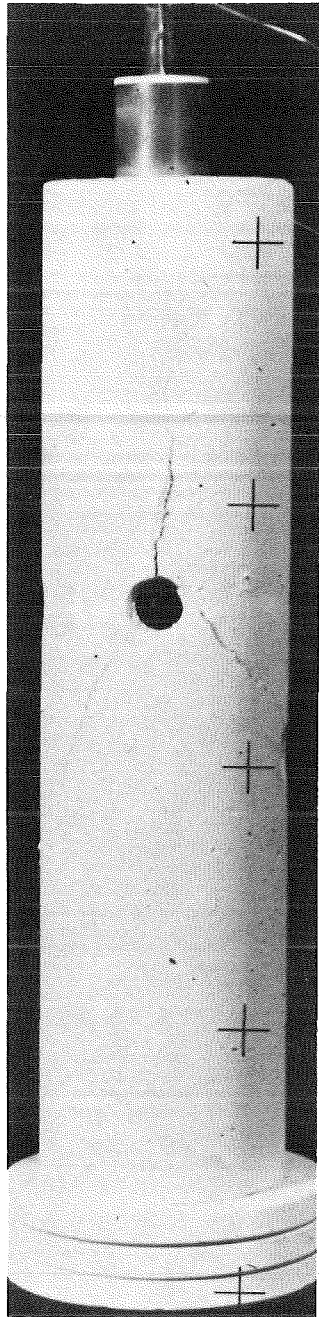


FIG.60 . 12 MM FIBER CERAMIC INSULATION IN ESSI-9

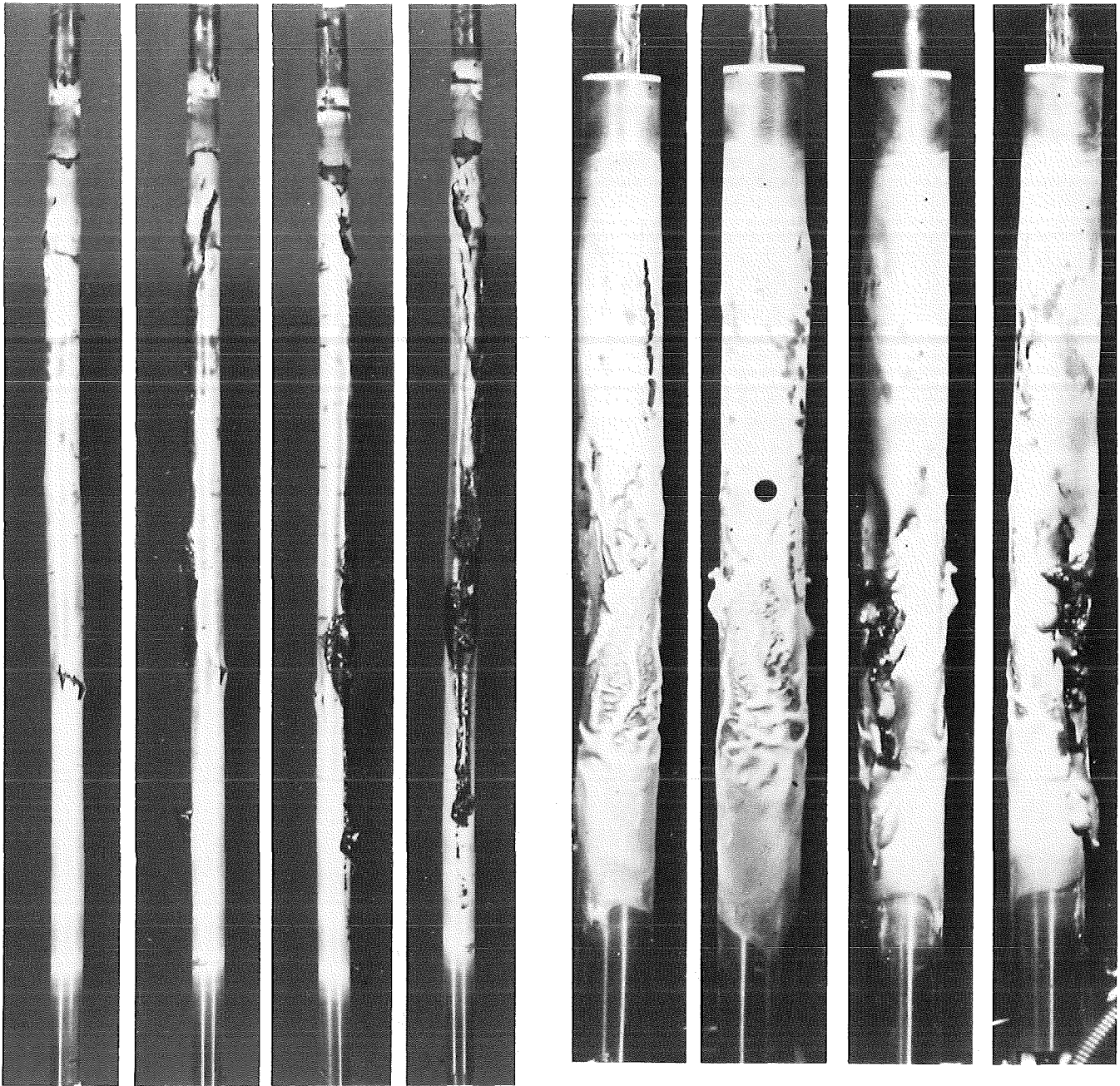


FIG.61 : POSTTEST APPEARANCE OF THE ESS1-9 FUEL ROD SIMULATOR AND SHROUD

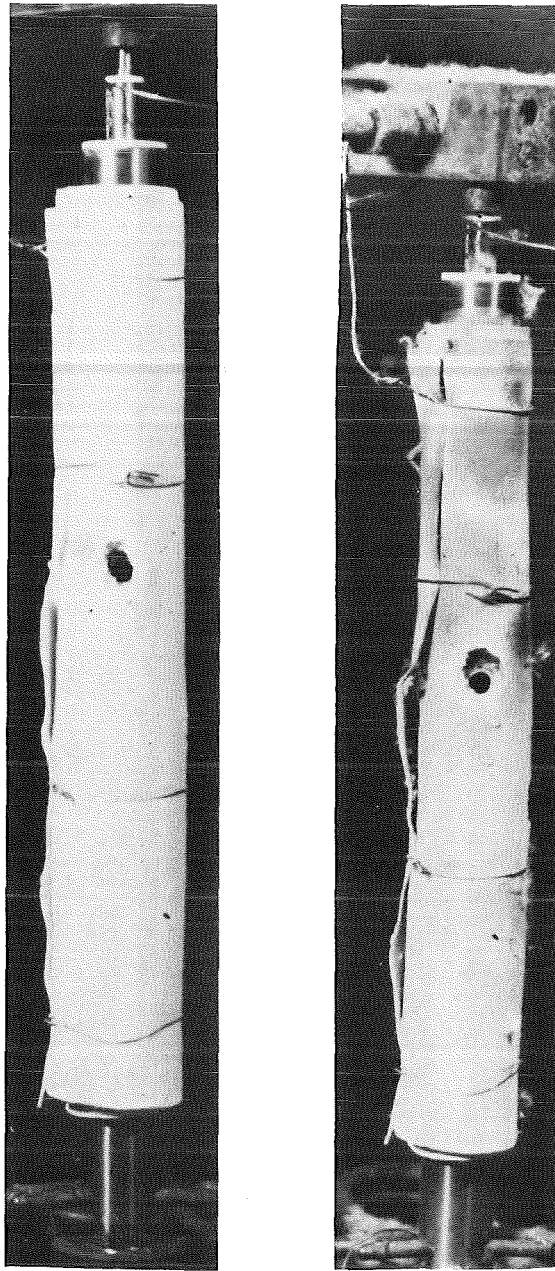


FIG.62: ESSI-10 FIBER CERAMIC INSULATION BEFORE AND AFTER THE TEST

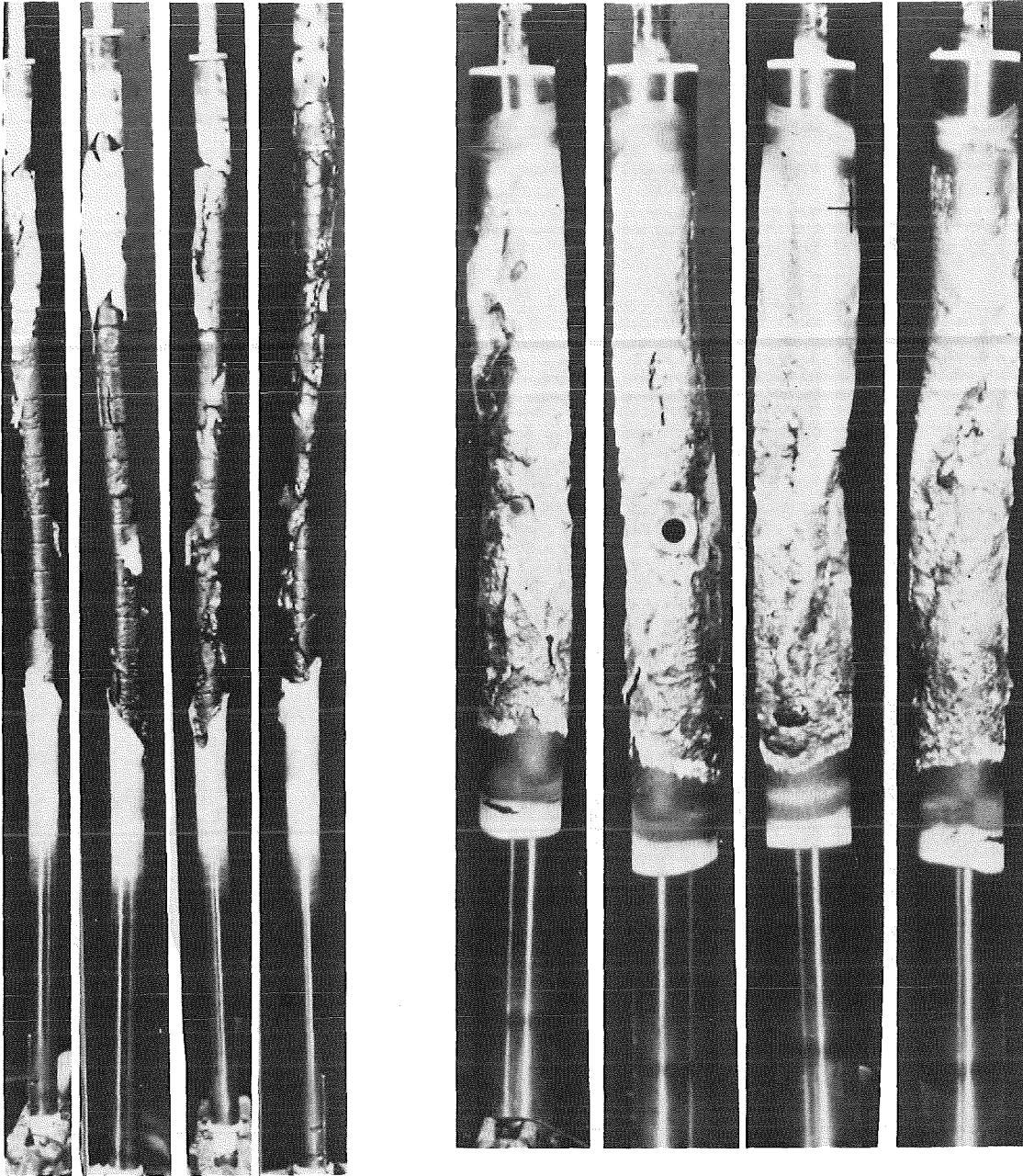


FIG.63 : POSTTEST APPEARANCE OF THE ESS1-10 FUEL ROD SIMULATOR AND SHROUD

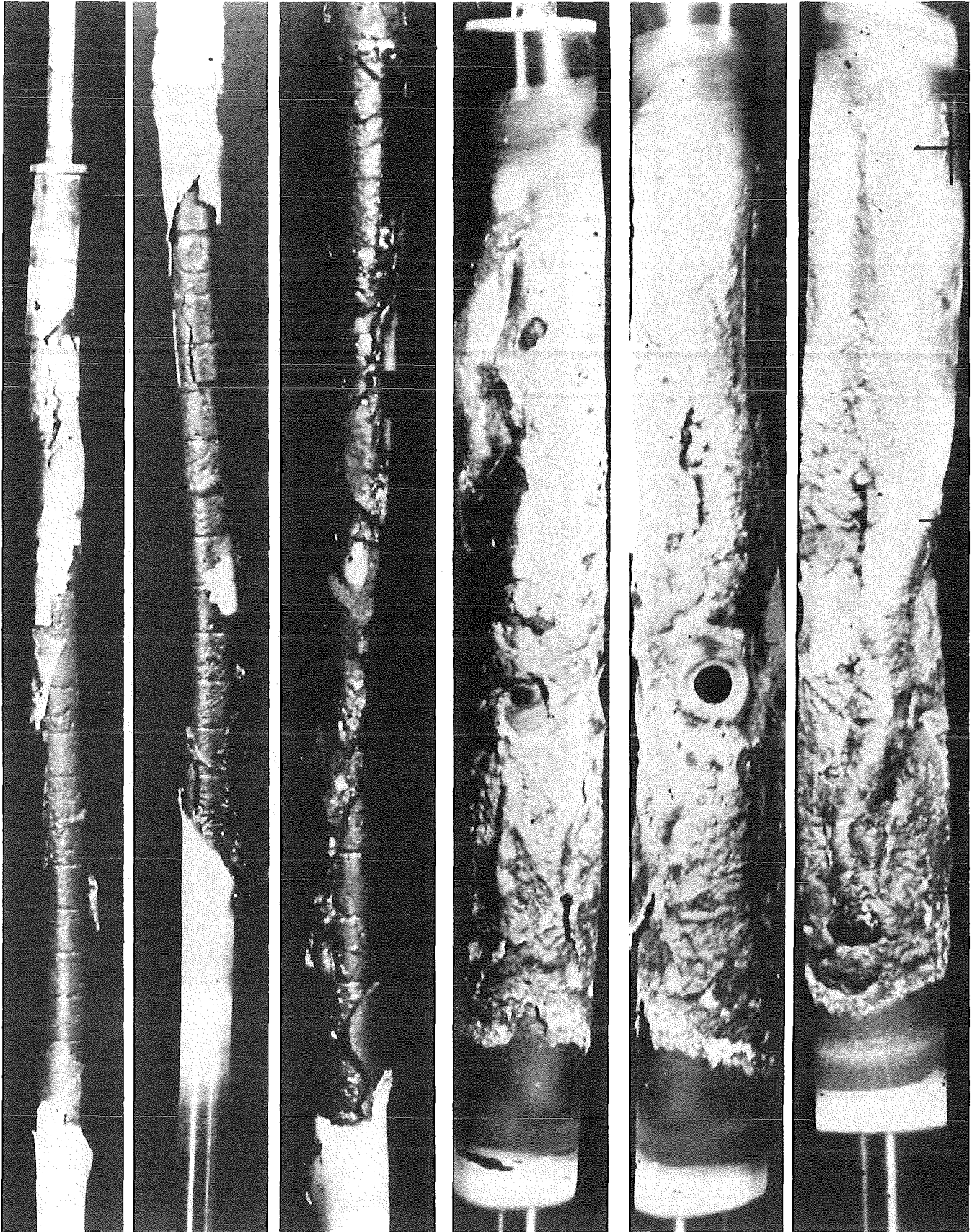


FIG.64 : DETAILS OF THE ESSI-10 FUEL ROD SIMULATOR AND SHROUD

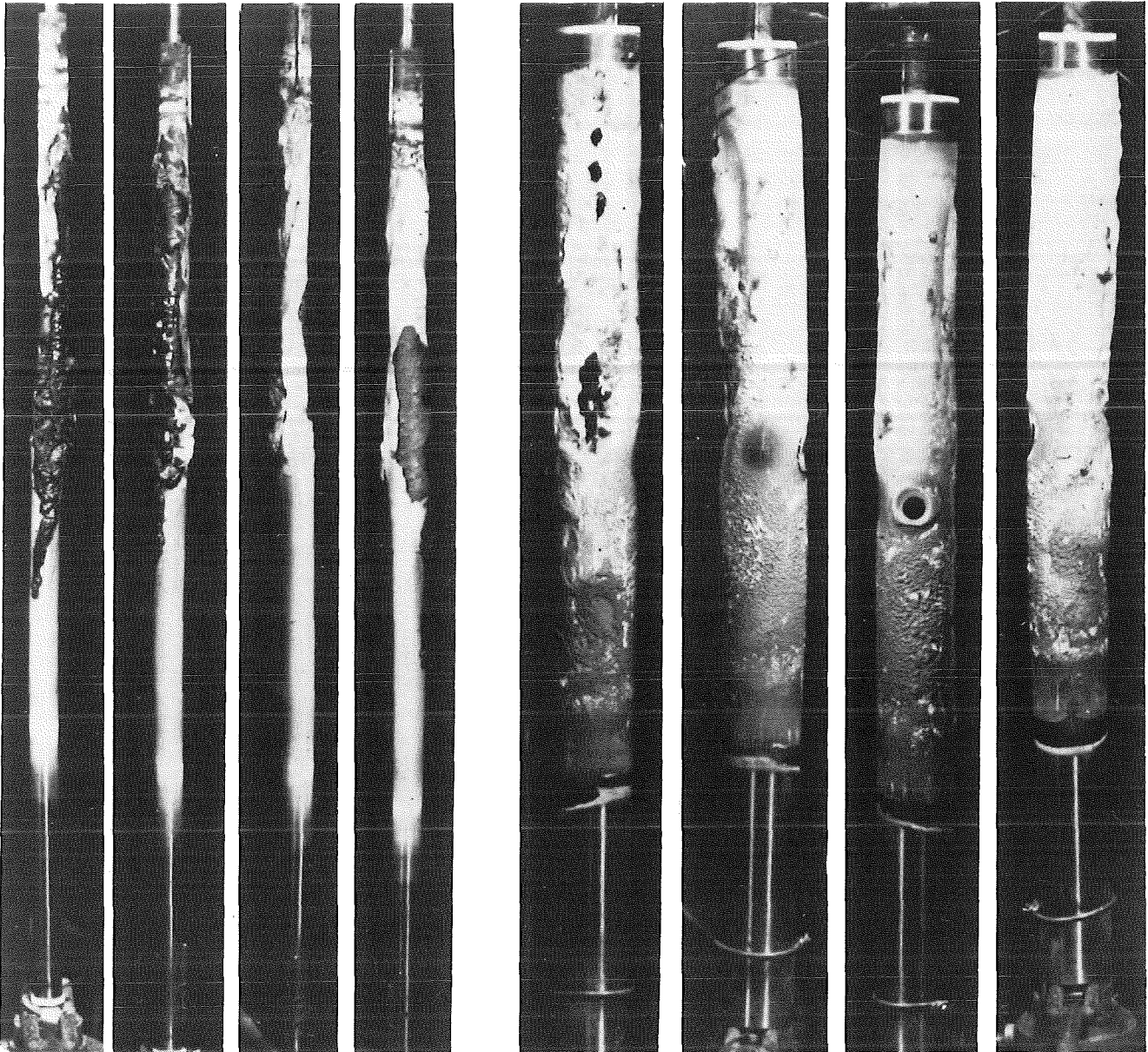


FIG.65 : POSTTEST APPEARANCE OF THE ESSI-11 FUEL ROD SIMULATOR AND SHROUD

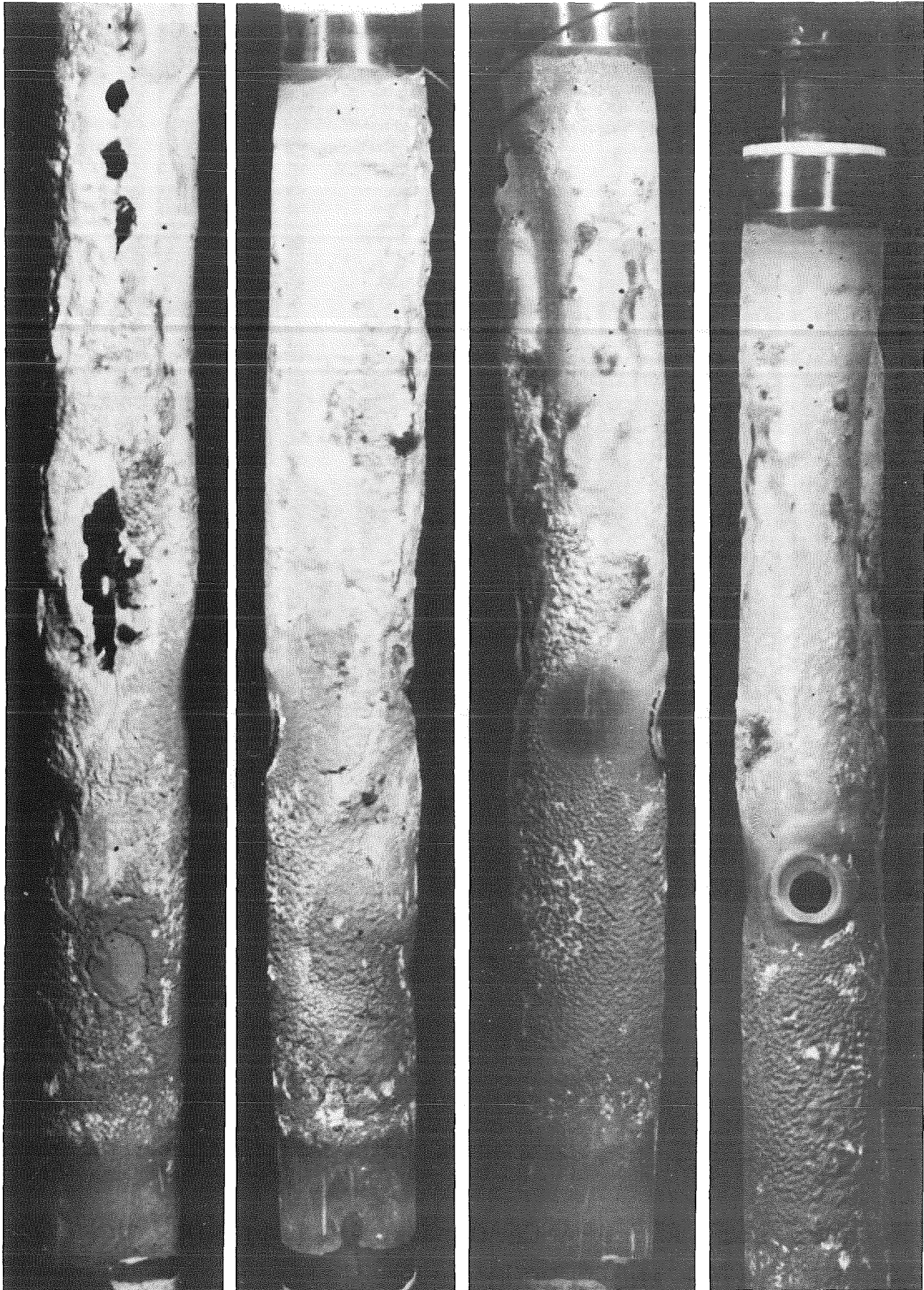


FIG. 66 : DETAILS OF THE ESSI-11 SHROUD